

The Influence of the Microbiome on Growth and Immune Development in Early-life
Undernutrition

Yadeliz Adlin Serrano Matos

San Juan, Puerto Rico

B.S., Molecular Biology, University of Puerto Rico – Rio Piedras Campus, 2020

A Dissertation presented to the Graduate Faculty of the University of Virginia in
Candidacy for the Degree of Doctor of Philosophy

Department of Microbiology, Immunology and Cancer Biology

University of Virginia

May 2025

Thesis Abstract

Linear growth stunting due to undernutrition affects 20% of children under the age of five with far-reaching consequences, including increased susceptibility to infection and altered cognitive development. Current nutritional interventions are largely ineffective in rescuing linear growth. A significant proportion of stunting originates *in utero*; however, the mechanisms by which maternal undernutrition is transmitted between generations remain poorly characterized. In this thesis, we utilized multiple gnotobiotic murine models of intergenerational undernutrition to investigate the contributions of (1) intergenerational microbial transmission, (2) maternal nutritional status, and (3) pre- and postnatal factors in the development of stunting. Offspring exposed to microbiota derived from children with growth stunting exhibited impaired linear growth and developed immune features characteristic of undernutrition and enteropathy, including intestinal villus blunting, reduced liver Insulin-like Growth Factor 1 (IGF-1), and increased accumulation of intraepithelial lymphocytes and plasma cells in the small intestine. In contrast, colonization after weaning mitigated host phenotypic changes driven by distinct microbial communities. Maternal undernutrition exacerbated offspring growth deficits in a microbiota-dependent manner, altering the offspring microbiota by increasing the abundance of *Enterococcus* species and *Escherichia coli*.

Our cross-fostering studies demonstrated that postnatal exposure to the stunted donor (SD) microbiota was sufficient to induce growth deficits, mirroring those observed in animals born to colonized dams. Furthermore, the ability of the SD microbiota to displace healthy donor (HD) microbes suggests that both pre- and postnatal interventions may be necessary to effectively restore growth in undernourished populations.

Additionally, we identified distinct microbial taxa targeted by Immunoglobulin A (IgA), a key regulator of gut homeostasis. These findings suggest that specific microbes may contribute to growth deficits, and future research will determine whether targeted microbial species independently drive stunting. This thesis findings highlight the critical role of the microbiota in shaping linear growth during gestation and early life, emphasizing the necessity of addressing both maternal and infant microbiota in the development of therapeutic interventions for undernutrition.

Acknowledgments

First and foremost, I would like to thank my mentor, Dr. Carrie Cowardin, who has been an incredible advisor throughout my Ph.D. journey. I am grateful for the opportunity to learn and grow as a scientist in your lab. Your guidance, support, and dedication have been invaluable in shaping my development, and I truly appreciate all that you have done for me.

I am thankful to all the members of the lab for their support and guidance in developing the projects discussed in this thesis. Their insights, collaboration, and encouragement have been invaluable throughout this journey. In particular, I would like to express my sincere appreciation to Jasmine Cano, with whom I worked closely during my early years as a Ph.D. student. Beyond being a research partner, Jasmine became a close friend, and her support made this experience all the more meaningful.

I would also like to sincerely thank my committee members, Drs. Isabelle Derré, Loren Erickson, Jason Papin, and Melanie Rutkowski, for their guidance and invaluable feedback throughout my Ph.D. Their expertise and advice have helped shape my research and scientific thinking, and I am truly grateful for their time and support.

I also want to extend my heartfelt thanks to my family, who have been cheering me on from Puerto Rico every step of the way. I am forever grateful to my grandmother, Isabel, and my aunt, Carmen, who raised me and provided the knowledge, wisdom, and guidance that have shaped my path. This thesis is dedicated to them. Without their unwavering love and support, I would not be where I am today. My aunt recognized my interest in science and encouraged me to attend a specialized school in the field. There, I discovered my passion for biology and gained the foundation to pursue higher education

at one of the top colleges in my country. I was fortunate to have this opportunity, as many young people in my country do not.

Lastly, I would like to thank William, who has been a tremendous source of strength throughout my Ph.D. journey. He has always believed in me, even when I struggled with self-doubt, and has supported me through my toughest moments. I would like to especially thank him for all those long nights we spent together at his or my work writing and practicing science communication. His unwavering encouragement and confidence in me have meant more than words can express.

Table of Contents

| | |
|---------------------------------|----|
| Thesis Abstract..... | ii |
| Acknowledgment..... | iv |
| Table of Contents..... | vi |
| List of Figures and Tables..... | 1 |
| List of Abbreviations..... | 4 |

Chapter 1: Introduction to Childhood Undernutrition and Stunting

| | |
|---|----|
| 1.1 Childhood Undernutrition & Stunting..... | 7 |
| 1.2 The microbiota..... | 11 |
| 1.3 Environmental Enteric Dysfunction (EED)..... | 14 |
| 1.4 Immune responses observed in stunted children..... | 21 |
| 1.5 Immunoglobulin A (IgA) as a tool to identify drivers of stunted growth..... | 23 |
| 1.6 The goal of this dissertation..... | 26 |

Chapter 2: Establishing a Mouse Model that Recapitulates Growth

Deficits & Immune Responses Observed in Stunted Children

| | |
|-----------------------|----|
| 2.1 Introduction..... | 31 |
| 2.2 Results..... | 33 |
| 2.3 Discussion..... | 50 |
| 2.4 Conclusions..... | 53 |
| 2.5 Methods..... | 54 |

Chapter 3: Maternal undernutrition exacerbates microbiota-driven growth stunting through pre and postnatal effects

| | |
|-----------------------|-----|
| 3.1 Introduction..... | 69 |
| 3.2 Results..... | 71 |
| 3.3 Discussion..... | 98 |
| 3.4 Conclusions..... | 101 |
| 3.5 Methods..... | 101 |

Chapter 4: Immunoglobulin A selectively targets specific microbes in the SD microbiota

| | |
|-----------------------|-----|
| 4.1 Introduction..... | 111 |
| 4.2 Results..... | 113 |
| 4.3 Discussion..... | 126 |
| 4.4 Conclusions..... | 127 |
| 4.5 Methods..... | 129 |

Chapter 5: General Discussion & Future Directions

| | |
|--|-----|
| 5.1 The microbiota shapes growth & immunity..... | 139 |
| 5.2 What about the maternal microbiome?..... | 142 |
| 5.3 Do immune responses regulate growth in our model?..... | 145 |
| 5.4 Which microbes are driving reduced linear growth?..... | 150 |
| 5.5 Pre- and post- natal factors influence in growth..... | 154 |
| 5.6 Implications of this dissertation work..... | 156 |
| References..... | 158 |

List of Figures and Tables

| Figures & Tables | Page |
|--|-------------|
| Figure 1.1. The intergenerational cycle of stunting and the consequences. | 9 |
| Figure 1.2. Small intestine structure and function. | 15 |
| Figure 1.3. Undernutrition and Environmental Enteric Dysfunction in the small intestine. | 17 |
| Figure 1.4. Immunoglobulin A (IgA) functions in the small intestine. | 25 |
| Figure 2.1. Development of a murine model of intergenerational undernutrition. | 36 |
| Figure 2.2. Intestinal morphology changes in IG mice at 8 weeks of age. | 38 |
| Figure 2.3. Microbial communities of recipient mice show distinct patterns of colonization. | 40 |
| Figure 2.4. Immune cell composition of the small intestinal epithelium in IG and PW colonized mice at 8 weeks of age. | 42 |
| Figure 2.5. Natural IELs are increased in the small intestine epithelium of SD-IG animals at 8 weeks. | 43 |
| Figure 2.6. Natural IELs isolated from SD-IG mice have increased intracellular levels of Granzyme A. | 45 |
| Figure 2.7. SD-IG animals exhibit an increase in microbiota-responsive T cells in the intestinal lamina propria. | 47 |
| Figure 2.8. Intergenerational colonization of SD microbiota increases plasma cells and CCL5 in the lamina propria. | 49 |
| Table 2.1. Flow cytometry gating strategy for cell types identified in the intestinal epithelium and lamina propria. | 63 |
| Table 2.2. Antibodies used for flow cytometry staining. | 64 |
| Figure 3.1. Maternal undernutrition exacerbates growth deficits in SD-MU mice. | 74 |
| Figure 3.2. Maternal undernutrition alters the SD microbiota at maturity. | 76 |
| Figure 3.3. Maternal undernutrition increases α -diversity and the total number of microbes in the microbiota of offspring at maturity. | 77 |
| Figure 3.4. SD-MU animals exhibit an increased relative abundance of <i>Enterococcus</i> sp. and <i>Escherichia coli</i> at maturity. | 79 |
| Figure 3.5. Microbiota composition in early life shapes physiological development. | 82 |
| Figure 3.6. Development of the microbiota in early life. | 85 |
| Figure 3.7. Postnatal exposure to SD microbiota is sufficient to drive long-term growth deficits. | 87 |

| | |
|---|------------|
| Figure 3.8. No exposure <i>in utero</i> to microbes leads to reduced levels <i>Bifidobacterium breve</i> at maturity. | 89 |
| Figure 3.9. Postnatal exposure to SD microbiota is insufficient to shape intestinal morphology at maturity. | 91 |
| Figure 3.10. Postnatal exposure to SD microbiota negatively impacts linear but not ponderal growth. | 93 |
| Figure 3.11. Postnatal exposure to SD microbiota displaces HD microbiota at maturity. | 95 |
| Figure 3.12. Postnatal exposure to SD microbiota negatively impacts muscularis thickness. | 97 |
| Figure 4.1. SD-MU mice develop an altered IgA response at maturity, similar to SD-NMU animals. | 114 |
| Figure 4.2. SD-MU animals have increased levels of total IgA soon after weaning. | 117 |
| Table 4.1. Metadata of MU animals selected for fecal and small intestine Bug-FACs. | 118 |
| Figure 4.3. Bug-FACS protocol and gating strategy to sort IgA+ and IgA- microbes. | 120 |
| Figure 4.4. Enriched taxa in fractions are different between HD-MU and SD-MU mice. | 122 |
| Figure 4.5 SD-MU animals have an increased likelihood of having <i>Enterococcus</i> sp. targeted by IgA in both feces and small intestine | 125 |
| Figure 5.1. Understanding <i>Bifidobacterium</i> sp. roles in growth. | 144 |
| Figure 5.2. Understanding the role of CCL5 in undernutrition and stunting. | 149 |
| Figure 5.3. Evaluating the impact of immunogenic bacteria on reduced linear growth | 153 |
| Figure 5.4. When is the critical window for nutritional interventions in stunted populations? | 157 |
| Table 3.1 PERMANOVA Analysis of NMU and MU animals at maturity | 179 |
| Table 3.2. Pairwise Comparisons between NMU and MU animals at maturity. | 179 |
| Table 3.3. PERMANOVA Analysis (SD-NMU and MU Animals 8W) | 180 |
| Table 3.4. PERMANOVA Analysis (HD- NMU and MU Animals 8W) | 180 |
| Table 3.5. PERMANOVA Analysis - Early Life Development - HD-MU | 180 |
| Table 3.6. Pairwise Comparisons - Early Life Development - HD-MU | 180 |
| Table 3.7. PERMANOVA Analysis - Early Life Development - SD-MU | 181 |
| Table 3.8. Pairwise Comparisons - Early Life Development - SD-MU | 181 |
| Table 3.9. PERMANOVA Analysis -HD-MU, SD-MU, GF-HD and GF-SD at maturity. | 181 |

| | |
|---|------------|
| Table 3.10. Pairwise Comparisons between HD-MU, SD-MU, GF-HD and GF-SD at maturity. | 182 |
| Table 3.11. Pairwise Comparisons between HD-MU, SD-MU, SD-HD and HD-SD at maturity. | 182 |
| Table 3.12. PERMANOVA Analysis - <i>In utero</i> vs Postnatal Cross-Fostering Groups HD-MU and SD-MU, HD-SD. SD-HD | 182 |
| Figure 4.1B. Gaussian mixture model analysis for IgA Probability Ratio Scores in HD animals. | 184 |
| Figure 4.2B. Gaussian mixture model analysis for IgA Probability Ratio Scores in SD animals. | 186 |
| Figure 4.3B. HD-MU animals have an increased likelihood of having <i>Escherichia coli</i> sp. targeted by IgA in both feces and small intestine | 188 |

List of Abbreviations

| Abbreviation | Meaning | Page |
|---------------------|---|-------------|
| WAZ | Weight-for-Age Z score | 7 |
| HAZ | Height-for-Age Z score | 7 |
| SDs | Standard Deviations | 7 |
| WHO | World Health Organization | 7 |
| LMCs | Low- and Middle-Income Countries | 7 |
| EED | Environmental Enteric Dysfunction | 8 |
| sp. | Species | 12 |
| SCFAS | Short Chain Fatty Acids | 13 |
| GH | Growth Hormone | 13 |
| IGF-1 | Insulin-like Growth Factor | 13 |
| SPF | Specific Pathogen Free mice | 13 |
| SEEM | Study of Environmental Enteropathy and Malnutrition in Pakistan | 19 |
| CCL5 | C-C chemokine ligand 5 | 19 |
| BEECH | Biomarkers of Environmental Enteropathy in Children cohort | 19 |
| BEED | Bangladesh Environmental Enteric Dysfunction cohort | 19 |
| SAM | Severe Acute Malnutrition | 19 |
| MAM | Moderate Acute Malnutrition | 19 |
| H&E | Hematoxylin and Eosin staining | 19 |
| CAL | Calprotectin | 20 |
| MPO | Myeloperoxidase | 20 |
| NEO | Neopterin | 20 |
| CD8 | Cluster of Differentiation 8 receptor | 22 |
| CD4 | Cluster of Differentiation 4 receptor | 22 |
| sIgA | Secretory Immunoglobulin A in the mucosa of small intestine | 23 |
| IgA | Immunoglobulin A found in small intestine tissue and serum | 23 |
| GALT | Gut associated lymphoid tissues | 24 |
| ILFs | Isolated lymphoid follicles in the small intestine | 24 |
| LP | Lamina propria of the small intestine | 24 |
| Tcl | T-cell independent mechanism | 24 |
| TcD | T-cell dependent mechanism | 24 |
| DCs | Dendritic cells | 24 |
| PPs | Peyer's Patches in the small intestine | 24 |

| | | |
|----------|---|------------|
| Tfh | T follicular helper cells | 24 |
| LNS | Lipid-based nutrient supplements | 27 |
| GF | Germ-free mice | 32 |
| IG | Intergenerational | 34 |
| HD | Healthy Donor | 34 |
| SD | Stunted Donor | 34 |
| PW | Post-Weaning | 34 |
| HD-IG | Mice colonized vertically with healthy donor microbiota | 34 |
| SD-IG | Mice colonized vertically with stunted donor microbiota | 34 |
| HD-PW | Mice colonized post-weaning with healthy donor microbiota | 34 |
| SD-PW | Mice colonized post-weaning with stunted donor microbiota | 34 |
| SD-4092 | Mice colonized with stunted donor microbiota #4092 | 35 |
| SD-3114 | Mice colonized with stunted donor microbiota #3114 | 35 |
| ELISA | Enzyme-Linked Immunosorbent Assay | 35 |
| ASV | Amplicon Sequence Variants | 41 |
| HD-NMU | Mice born to non-undernourished healthy dams | 71 |
| SD-NMU | Mice born to non-undernourished stunted dams | 71 |
| HD-MU | Mice born to undernourished healthy dams | 72 |
| SD-MU | Mice born to undernourished stunted dams | 72 |
| PCoA | Principal Component Analysis of distance matrices | 75 |
| GF-HD | Germ-free born neonate cross-fostered to HD dam | 86 |
| GF-SD | Germ-free born neonate cross-fostered to SD dam | 86 |
| HD-SD | HD born neonate cross-fostered to SD dam | 92 |
| SD-HD | SD born neonate cross-fostered to HD dam | 92 |
| SI | Small intestine | 112 |
| Bug-FACs | Bug Fluorescent Activated Cell Sorting | 112 |
| NMU | No maternal undernutrition model | 113 |
| MU | Maternal undernutrition model | 113 |

Chapter 1: Introduction to Childhood Undernutrition and Stunting

Yadeliz A. Serrano Matos & Carrie Cowardin

Author contributions:

Writing, Y.S.M., Editing, C.A.C.

1.1 Childhood Undernutrition & Stunting

Childhood undernutrition remains a significant global health challenge, contributing to nearly half of deaths in children under the age of five¹. Undernutrition often results from insufficient dietary intake or poor nutrient absorption due to poverty, food insecurity, diseases, and lack of nutritious food². Undernutrition has different manifestations, with stunting and wasting being the most studied forms. Stunting is caused by chronic nutritional deficits while wasting results from acute undernutrition³. Wasting is characterized as a child being underweight for their height. It is commonly assessed using a Weight-for-Length/Height Z-score which is then compared to the Child Growth Standards set by the World Health Organization (WHO)³. Stunting is defined as a child being short for their age⁴. This metric is frequently calculated using a Height-for-Age Z-score (or HAZ), which is then compared to the Child Growth Standards established by WHO. An HAZ less than two standard deviations (SDs) below the median indicates stunting, while an HAZ below three SDs is considered severe stunting⁵. Stunting is the most prevalent form of undernutrition today, with higher rates observed in Low- and Middle-Income Countries (LMICs) across Asia and Africa^{6,7}. Around 149 million children are stunted, compared to 49 million children wasted globally⁶. While both of these syndromes are important global health concerns, stunting in early life often leads to irreversible short-term and long-term consequences^{5,8}.

The short-term consequences of stunting can be described as the conditions or diseases (morbidity) these children often experience in early life⁹. These morbidities lower the quality of life and if severe, can lead to death⁸. In early life, stunted children frequently have repeated bouts of infections due to weakened immunity, develop

Environmental Enteric Dysfunction (EED), and have impaired brain development^{5,10,11}. EED is characterized by intestinal malabsorption and epithelial barrier disruption due to inflammation driven by changes in the gut microbiome and/or enteric infection^{10,12,13}. Despite (or because of) this inflammation, undernourished children exhibit lower vaccine-specific antibody titers, with oral rotavirus vaccine showing particularly low seroconversion efficiency among stunted children^{14,15}. EED is hypothesized to contribute to the reduced effectiveness of oral rotavirus vaccines in early life. Stunted children often display impaired behavioral development, are less likely to enroll in school, and tend to achieve lower grades⁵. The long-term irreversible consequences of stunting include reduced cognitive development, productivity, educational performance, and a higher risk for obesity, metabolic diseases, and diabetes in adulthood^{4,5}. All these factors collectively create a major barrier to human development in LMICs. This is one of the key reasons why it is critical to understand and prevent childhood stunting.

Stunting is a complex syndrome driven by multiple interrelated factors (**Figure 1.1**). Postnatal factors driving stunting include food insecurity, limited access to healthcare, low socioeconomic status, frequent infection, and disruption of the gut microbiota. However, additional prenatal factors are also linked to stunting, including birth practices, maternal nutrition, and genetics^{8,10}. Studies show shorter women may have a smaller pelvis, restricting fetal growth *in utero*^{16,17}. Maternal height is a significant predictor of growth, with shorter stature strongly associated with undernutrition and stunted growth in offspring¹⁸. These findings suggest that stunting is an intergenerational problem, meaning it occurs or exists between generations. There is a critical window for establishing immunity and healthy growth outcomes in children spanning the first 1,000

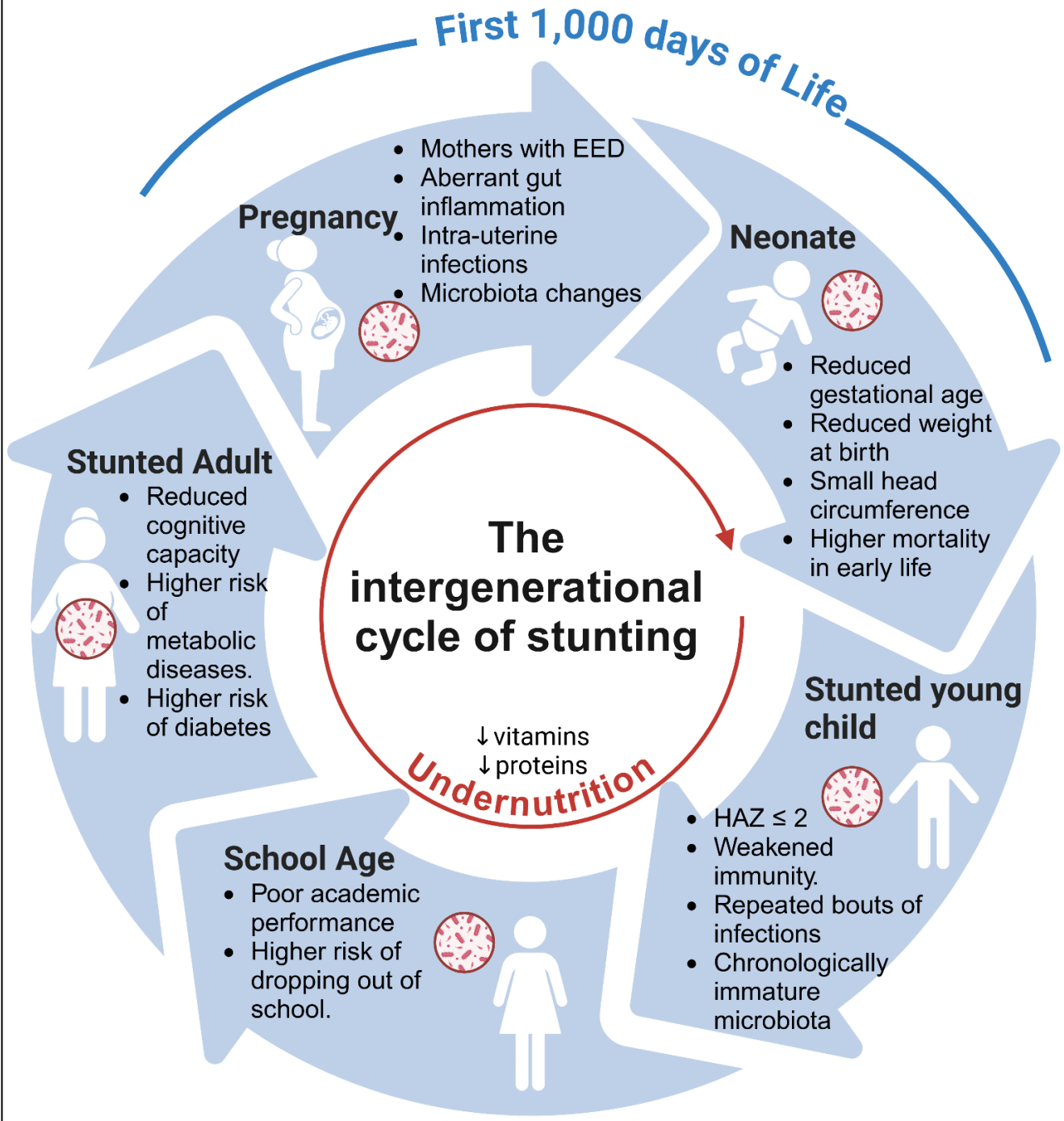


Figure 1.1. The intergenerational cycle of stunting and the consequences. This diagram illustrates the intergenerational cycle of stunting in humans, highlighting the short- and long-term consequences of this syndrome at various developmental stages. During pregnancy, maternal conditions such as Environmental Enteric Dysfunction (EED), gut inflammation, intrauterine infections, and microbiota can contribute negatively to fetal development. Soon after birth, infants born to undernourished mothers commonly have reduced gestational age, low birth weight, small head circumference, and an increased risk of mortality in early life. Children with stunted growth (typically around two years of age) commonly have a height-for-age Z-score (HAZ) of ≤ 2 , experience weakened immunity and recurrent infections and frequently have chronologically immature gut microbiota. Studies show that stunted children experience poor academic performance and have a higher risk of dropping out of school due to cognitive impairments. Stunted adults often have reduced cognitive capacity, a higher risk of metabolic diseases, and an increased likelihood of developing diabetes. The cycle perpetuates as stunted adults, specifically women, may give birth to undernourished neonates that become stunted soon after birth.

days of development from the time of conception¹⁹. Stunted mothers give birth to underweight neonates that become stunted in early life^{19,20}. This is problematic because longitudinal studies indicate that when stunting is present within the first three months of life, reversal is less likely^{7,21}.

The majority of nutritional interventions occur during the first 1,000 days of life, focusing on maternal nutrition during pregnancy and the child's nutrition during infancy, with the most common interventions taking place by the time the child reaches two years of age^{22–24}. However, micronutrient supplementation or lipid-based supplements with micronutrients have not been effective in limiting stunting^{22,23,25}. This observation and others showing that the onset of stunting happens soon after birth imply other factors beyond nutrient intake contribute to the development of stunting. These findings highlight the need to understand the early-life factors that contribute to the development of stunting and to determine when in early life interventions will be most effective.

1.2 The microbiota

The microbiota refers to the community of microorganisms—including bacteria, viruses, fungi, and archaea—that colonize various parts of the human body²⁶. Whereas the microbiome encompasses the complete collection of genomes from all microorganisms in a given environment²⁷. The microbiome includes not only the microbial community itself (the microbiota), but also their metabolites, structural components, and the surrounding environmental conditions that influence their activity²⁷. In the small intestine, the microbiota functions as a “metabolic organ” that breaks down complex carbohydrates and fibers that are sources of energy for the host²⁸. These digested

products cross-talk with the immune and metabolic systems of the host to influence overall physiology²⁹. At homeostasis, beneficial microbes in the small intestine help prevent infection by continuously competing for nutrients and attachment sites with harmful bacteria³⁰. Additionally, microbes help maintain the integrity of the epithelium by promoting the expression of tight junction genes in this barrier^{31,32}. Recent findings show that bacterial colonization in early life plays a crucial role in host development¹⁹. A homeostatic microbiome is essential for immune system development, and early-life disruptions to the microbiota in mice increase susceptibility to immunopathologies later in life^{33,34}. Due to the microbiota's critical role in maintaining host health, it has been proposed as a potential contributor to the development of stunting during early childhood¹⁹.

Disruption of the gut microbiome is commonly called dysbiosis³⁵. Microbiome dysbiosis is marked by a shift in the microbial community composition, characterized by an overgrowth of pathobionts and pathogens alongside a reduction in beneficial bacteria^{36,37}. Accumulating evidence shows that stunted children have distinct microbial communities when compared to non-stunted controls^{38–40}. This suggests that differences in the microbiota of stunted children may play a role in the development or persistence of stunting. Supporting this idea, Blanton et al demonstrated that the colonization of germ-free mice with microbiota from stunted children transmit growth deficits and metabolic abnormalities to the muscle, liver and brain of these animals⁴¹. This work also highlights the importance of microbiome-targeted interventions in addressing stunting.

Stunted children commonly have an increase in the relative abundance of *Proteobacteria*, *Bacteroidetes* sp., *Clostridium innocuum*, pathogenic *Escherichia coli*

and *Enterobacter* sp.^{40,42,43}. Additionally, a decrease in the relative abundance of *Prevotella* sp., *Bifidobacterium* sp., *Lactobacillus* sp., *Lactobacillus mucosae*, *Eubacterium* sp. has also been shown^{38,42}. Changes in the relative abundance of certain members of the microbiota are thought to impact on the metabolic functions of these communities and therefore impact host health. Surono et al demonstrated that a decrease in the relative abundance of *Prevotella* in stunted children from Indonesia leads to increased energy loss due to reduced digestion of macronutrients⁴⁴. The presence of pathogenic *Escherichia coli* in the feces of stunted children has been associated with the upregulation of pathways that enhance energy acquisition for bacterial colonization and virulence, reducing the availability of nutrients for host utilization⁴⁰. The increase in the relative abundance of *Enterobacteriaceae* is often associated with impaired digestion and localized gut inflammation⁴⁴.

Microbiota dysbiosis in stunted children has also been linked to a decrease in the abundance of fecal short-chain fatty acids (SCFAs)⁴². SCFAs serve as a major host energy source and are primarily produced by the gut microbiota⁴⁵. Ahn-Jarvis et al revealed that the microbiota of children with acute malnutrition is less efficient in the fermentation of inulin to SCFAs⁴⁶. Besides fermentation, SCFAs can also modulate immune responses in the host and help maintain gut barrier integrity⁴⁵⁻⁴⁹. The microbiota has also been shown to affect the production of Insulin-like Growth Factor 1 (IGF-1), a peptide hormone with a similar structure to insulin^{50,51}. IGF-1 is primarily produced in the liver in response to the growth hormone (GH) and its main function is to promote systemic growth^{50,52}. This peptide hormone is necessary for longitudinal skeletal and mass growth⁵³. In both human stunting and mouse models of undernutrition, low levels of IGF-

1 are associated with poor growth outcomes^{51,54–56}. Germ-free mice have reduced IGF-1 levels and reduced body and femur length compared to SPF-colonized mice⁵¹. Administration of *Lactobacillus plantarum* in a probiotic manner in a mouse model of undernutrition has been shown to improved growth⁵¹. Together, these findings highlight the need to understand how gut microbes alter metabolic functions and host growth to develop targeted microbiota-directed interventions for stunted children.

1.3 Environmental Enteric Dysfunction (EED)

The small intestine plays a crucial role in growth, developing alongside the microbiota in early-life⁵⁷. In early life, proper small intestine function is vital for nutrient absorption and host growth. Its main function alongside the microbiome is to completely digest foods and to absorb water and nutrients⁵⁸. The small intestine is composed of the duodenum, jejunum, and ileum and is covered by a layer of muscle called the muscularis (**Figure 1.2**). The muscularis layer's function is to contract and pass along the foods from the most proximal part of the small intestine to the colon (peristalsis)⁵⁸. The small intestine is composed of villi and microvilli, which are finger-like projections into the lumen that function to absorb nutrients. The small intestine is covered by a single layer of cells, the epithelium. Epithelial cells act as a protective barrier, reducing direct contact between the lamina propria, luminal contents, and microbes. The majority of the enzymatic digestion of food happens in the duodenum⁵⁸. Due to the large surface area of villi and microvilli in the jejunum, the majority of the nutrient absorption of digested carbohydrates and other molecules happens at this site. In the ileum, micronutrients (such as vitamins B and A) are primarily absorbed.

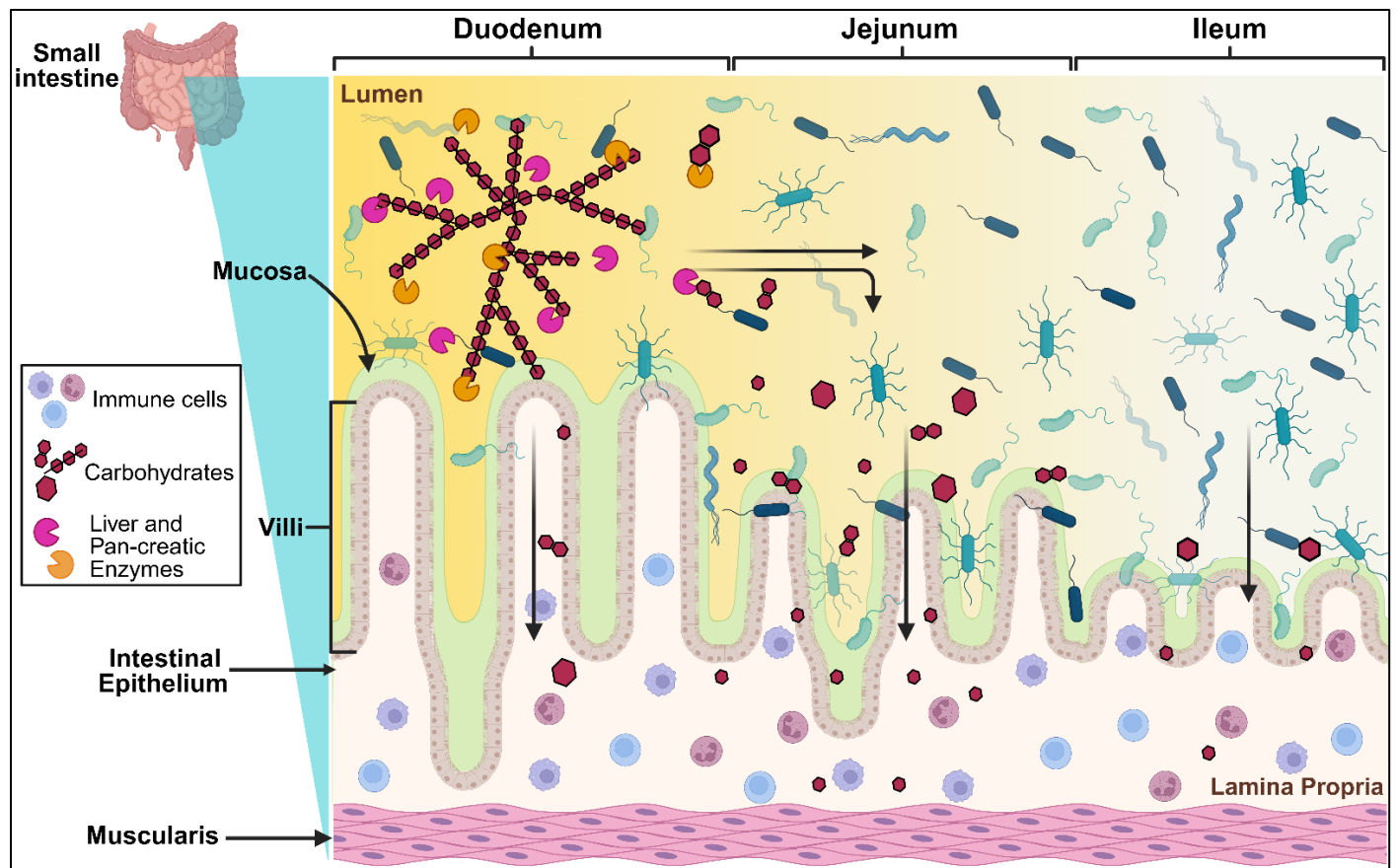
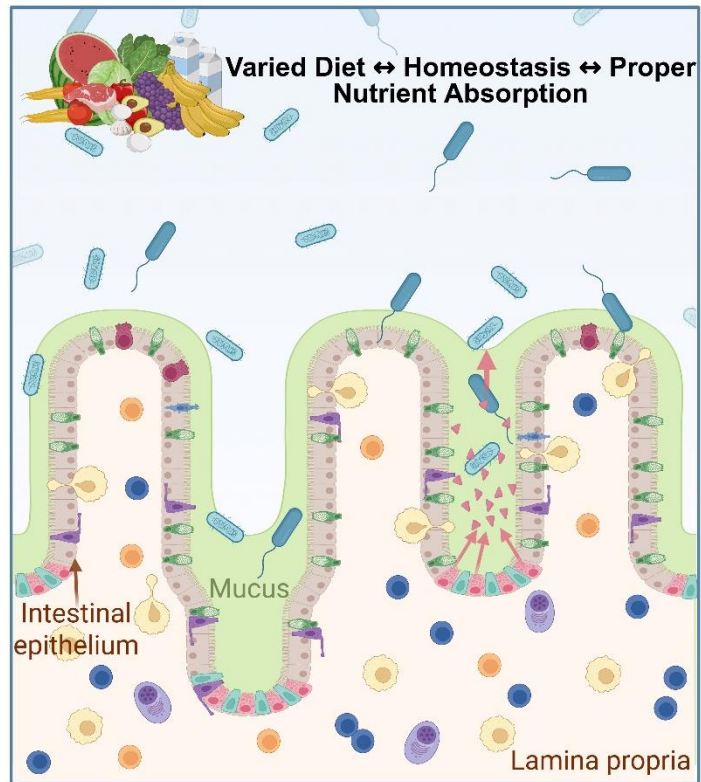


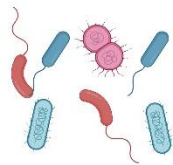
Figure 1.2. Small intestine structure and function. This figure illustrates the structural composition of the small intestine, a vital organ for growth in early life. The small intestine is divided into three major regions: duodenum, jejunum, and ileum. In a healthy individual, the mucosa (in green) contains a diverse microbial population (in different shades of teal), with increasing bacterial density from the duodenum to the ileum. In the duodenum, carbohydrates and other complex molecules are broken down by liver and pancreatic enzymes. This facilitates the absorption of nutrients in the jejunum and ileum. The lamina propria of the small intestine is protected from the lumen contents and microbes by an epithelial layer, which serves as a selective barrier for nutrient uptake and interactions with immune cells. The muscularis provides structural support, and its main function is peristalsis.

Stunted children living in LMICs with poor sanitation and hygiene have a high prevalence of Environmental enteric dysfunction (EED)⁵⁹. EED is a disorder of the small intestine characterized by nutrient malabsorption, villous blunting, and chronic inflammation^{10,60}. EED is thought to contribute to the persistence of stunting and lack of response to nutritional interventions by reducing the ability of the small intestine to absorb nutrients (**Figure 1.3**)^{10,61,62}. Several studies have demonstrated an association between the presence of pathogens (or perturbations of the microbiome) in the microbiota of undernourished children and altered absorptive function of the small intestine^{63,64}. The altered absorptive functions are thought to be caused by villus blunting, a reduction in the length of villi in the small intestine⁶². EED has no current treatment, and its etiology is not well-understood^{13,65}. Its diagnosis is performed via biopsy; therefore, accessibility to human samples, especially in children, makes the study of this disorder difficult.

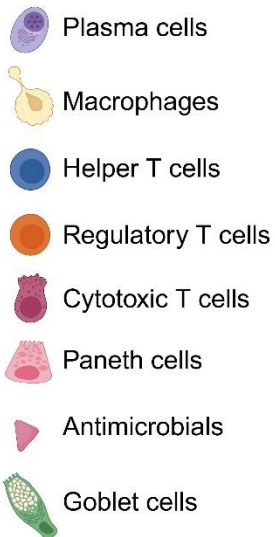
Healthy Gut



Microbiota



Immune cells



Undernutrition/EED

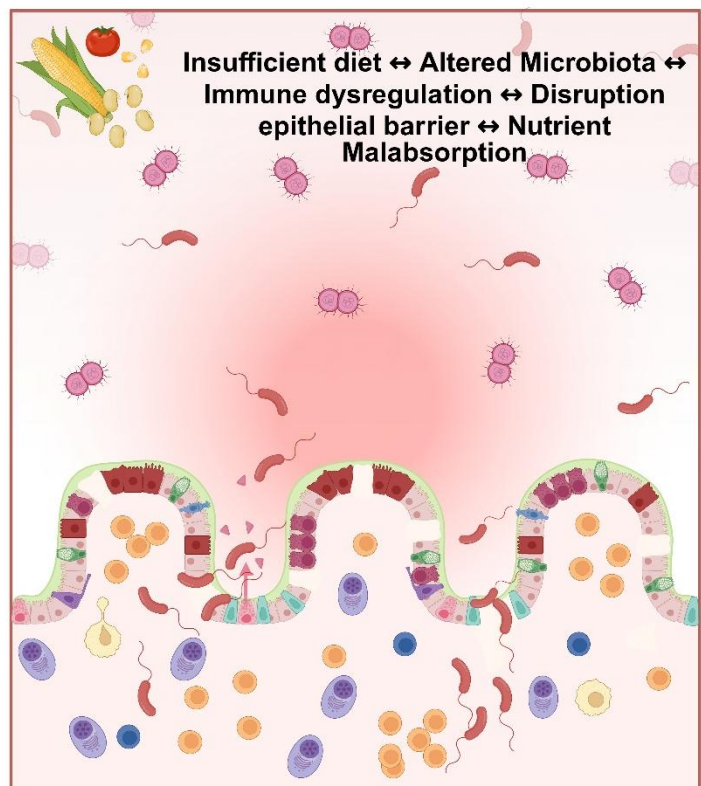


Figure 1.3. Undernutrition and Environmental Enteric Dysfunction in the small intestine.

This image illustrates the relationship between diet, gut microbiota, and the immune system. The top panel represents a healthy gut environment supported by a nutrient-sufficient diet. In a healthy small intestine, the epithelial barrier remains intact, lined with enterocytes, goblet cells, and other specialized immune cells, as shown on the left side of the figure. A thick mucus layer (in green) overlays the epithelium, providing a physical barrier between the epithelial cells and commensal (beneficial) bacteria, depicted as blue rod-shaped microbes. When we have a functional microbiota and immune system interaction, nutrient absorption occurs efficiently, and immune cells such as T cells and macrophages are present in controlled numbers within the lamina propria and epithelium, maintaining homeostasis. In contrast, the bottom panel depicts a dysfunctional gut environment. In EED, the intestinal mucus layer is reduced in thickness, and the epithelium barrier is disrupted, allowing the translocation of microbes (in red), to infiltrate the lamina propria. This leads to increased immune cell infiltration in the epithelium and lamina propria, signaling inflammation and leading to impaired nutrient absorption. This dysregulated environment highlights the reciprocal relationship between an insufficient diet, altered microbiota, immune dysfunction, and compromised barrier integrity.

Among the available human cohorts, the Study of Environmental Enteropathy and Malnutrition (SEEM) cohort in Pakistan has provided valuable information on pediatric EED⁶⁶. This study longitudinally tracked growth in children from birth until 2 years of age and characterized alterations in intestinal structure, function, and immune activation in children with EED who do not respond (non-responders) to nutritional interventions⁶⁶. The SEEM cohort is comprised of 350 malnourished children and 50 well-nourished healthy controls. Immunohistochemistry of duodenal biopsies from SEEM children with EED who did not respond to nutritional interventions showed an increase of intestinal intraepithelial lymphocytes is a strong predictor of chronic inflammation⁶⁷. Transcriptomic analysis of duodenal tissues of children from the SEEM cohort revealed an upregulation of pro-inflammatory cytokine genes encoding Lipocalin-2 and C-C chemokine ligand 5 (CCL5) compared to well-nourished controls⁶⁸.

Another relevant study is the Biomarkers of Environmental Enteropathy in Children (BEECH) cohort, which tracks longitudinal growth in over 100 children between 0 and 18 months of age with Moderate or Severe Acute Malnutrition (MAM or SAM) in Lusaka (a city with a high prevalence of stunting in Zambia)⁶⁹. Enrolled children were provided protein and micronutrient supplementation⁶⁹. A duodenal biopsy was collected from MAM and SAM non-responder children for characterization. Supporting the findings from the SEEM cohort, Hematoxylin and Eosin (H&E) staining of duodenal tissue showed hallmark features of EED in non-responders, such as villus blunting. Further characterization correlated a decrease in Paneth cells and Goblet density with villus blunting.

The Bangladesh Environmental Enteric Dysfunction (BEED) cohort contributes additional supporting data to the current understanding of EED. This study enrolled

wasted and stunted children to identify non-invasive biomarkers of EED⁷⁰. Like previous cohorts, a duodenal biopsy was collected in non-responders. Fecal samples were also collected before and after nutritional interventions. In this study, intraepithelial lymphocytosis as well as Goblet and Paneth cell depletion correlated with EED⁷¹. This study examined associations between hallmark features of EED and three hypothesized biomarkers: calprotectin (CAL), myeloperoxidase (MPO) and neopterin (NEO)⁷¹. CAL, an indirect measurement of neutrophil infiltration in the small intestine (and inflammation), was closely associated with intraepithelial lymphocytosis⁷¹. NEO, a marker of T cell immune activation, was shown to be associated with EED histology score and duodenal chronic inflammation⁷². MPO, an antimicrobial produced by macrophages, was increased in the duodenal sections collected from these children⁷¹. These findings suggest children with EED experience significant immune activation and inflammation in the small intestine.

Therefore, there has been a significant effort to develop mouse models capable of recapitulating EED. Bhattacharjee et al. demonstrated that malnourishment of Specific Pathogen Free (SPF) mice followed by infection with a pathogenic strain of *Escherichia coli* led to growth deficits, gut leakiness, and poor oral vaccine responses—hallmark features of EED⁷³. In another mouse model of EED, SPF mice fed a protein-deficient diet developed villus blunting, as well as reduced Paneth and Goblet cell density in both the ileum and duodenum⁷⁴. While murine models replicate some features of EED, most are conducted in mice with conventional murine intestinal microbial communities, limiting the ability to associate specific microbiota members with the phenotypes observed in children with EED. Furthermore, the murine models previously discussed demonstrate that the

observed features of EED are microbiota-dependent, resulting from diet-induced remodeling of the microbial community. Therefore, there is a need to develop gnotobiotic mouse models where we can dissect the specific contributions of human-derived microbes to the development of EED.

1.4 Immune responses observed in stunted children

The same factors that increase the risk of growth faltering in children also increase the risk of weakened immunity⁷⁵. Lack of absorption of macro- and micro-nutrients such as iron and antioxidant vitamins in early life can weaken the immune system leaving the body unable to defend itself against infections^{75,76}. On one hand, studies suggest undernutrition is a state of immunodeficiency⁶⁸, because a range of micronutrients and nutrient metabolites act as direct immune stimuli¹⁴. Therefore, the absence of specific nutrients can disrupt healthy immune system development. In rural Bangladesh, children with stunting born to undernourished mothers develop thymus atrophy (smaller thymus) in early life⁷⁷. The thymus is the organ primarily responsible for the production and maturation of lymphocytes, which help fight infections and protect against diseases⁷⁸. Moreover, maternal undernutrition has been shown to induce epigenetic alterations in offspring, potentially affecting long-term immune and metabolic outcomes^{79,80}.

On the other hand, immune dysregulation has been observed in undernutrition, although the directionality of this relationship remains unclear. Immune dysregulation is a condition in which the immune system functions abnormally, resulting in either excessive or insufficient immune responses¹⁴. Undernourished children often exhibit chronic inflammation in the small intestine—an example of immune dysregulation—

characterized by increased lymphocyte production^{59,64,76}. Since host sensing of the microbiome also shapes immunity in early life^{34,36}. Microbiome dysbiosis can lead to immune dysregulation as well¹⁴. Therefore, in stunting, both immunodeficiency and immune dysregulation are implicated. Maternal inflammation and early-life enteropathy in stunted children are associated with increased pro-inflammatory immune responses to bacterial antigens⁸¹. This suggests that early-life inflammatory signals (and intergenerational factors) shape the immune system of infants born to stunted mothers, potentially contributing to long-term immune dysregulation in stunted children. However, whether this shift towards an inflammatory profile in the gut of stunted children is beneficial or protective is still not well understood.

Single-cell transcriptomics from small intestinal biopsies of patients with EED revealed a strong association between increased numbers of Cluster of Differentiation 8 (CD8)+ T cells expressing *Ccl5*, and decreased numbers of Cluster of Differentiation 4 (CD4)+ T cells with EED severity⁸². This decrease in CD4+ T cells is thought to have functional consequences for host protection. In the previously mentioned mouse model of EED using a malnourished diet and *Escherichia coli* infection, reduced antigen-specific CD4+ T cells and increased regulatory T cells drove the observed failure of oral vaccine responses⁷³. CD4+ T cells are also known as helper cells and are part of the adaptive immune system, where they play a crucial role in maintaining gut homeostasis by activating other immune cells to defend against pathogens⁸³. Regulatory T cells play an essential role in maintaining tolerance to commensal bacteria while balancing defense against pathobionts via anti-inflammatory pathways⁸⁴. This suggests that the immune

environment in the small intestine of these mice may be skewed toward immune suppression, potentially limiting the effectiveness of oral vaccines.

Similarly, undernourished/stunted children exhibit poor responses to oral vaccines, particularly against rotavirus^{85,86}. This suggests that immune dysregulation observed in Environmental Enteric Dysfunction (EED) may also contribute to vaccine failure in human populations. EED is highly prevalent in stunted children⁸⁷. This is alarming because rotavirus infection is one of the leading causes of acute diarrhea in children under five living in LCMs¹⁵. The mechanism resulting in reduced effectiveness of the rotavirus vaccine in these populations is not well understood. Furthermore, poor oral vaccine protection in undernourished populations is not restricted to rotavirus infection⁶². It is essential to understand why this occurs, as a Peruvian study found a modest positive link between rotavirus vaccination and improved growth outcomes in children with mild stunting¹⁵.

Studies have shown that children with gastroenteritis due to active rotavirus infection (inflammation in the stomach and small intestine), do not mount proper secretory Immunoglobulin A (sIgA) responses against the rotavirus vaccine⁸⁸. This has raised questions about the role of sIgA protection in stunted/EED children. Understanding how EED and stunting contribute to impaired immune responses to vaccines is crucial for addressing this challenge effectively.

1.5 Immunoglobulin A (IgA) as a tool to identify drivers of stunted growth

Humans possess two Immunoglobulin IgA (IgA) subclasses, IgA1 and IgA2, while mice produce only one type⁸⁹. However, both species produce two different forms of IgA:

monomeric (serum IgA) and dimeric secretory IgA (sIgA)⁹⁰. The summarized functions of secretory IgA in the small intestine are described in **Figure 1.4**. Monomeric IgA is produced by plasma cells in the bone marrow and secreted into the serum^{89,91}. At mucosal sites, sIgA is produced by plasma cells in gut associated lymphoid tissues (GALT) and isolated lymphoid follicles (ILFs) located in the lamina propria (LP)⁹². The synthesis of sIgA can be T cell-independent (Tcl) or dependent (TcD)^{93,94}. Tcl sIgA synthesis occurs in IgA+ Plasma Cells derived from B1b cells located in ILFs and is induced by dendritic cells (DCs) that constantly sample luminal bacteria transported into the LP through M cells, goblet cells and macrophages⁹⁵. Tcl sIgA is usually low-affinity or polyreactive and is called homeostatic sIgA because it targets and binds conserved patterns across different commensal bacteria⁹⁴. T cell-dependent IgA synthesis occurs mainly in follicular B2 cells that reside in germinal centers of Peyer's Patches (PPs) in the GALT⁹⁵. DCs sample microbes transported into the LP upon activation, migrate into T cell zones in germinal centers (GCs). There, they prime naïve T cells which differentiate into T follicular helper cells (Tfh). These Tfh cells induce follicular B cell transformation into IgA+ plasma cells⁹⁵. T cell-dependent sIgA has high affinity, is antigen-specific, and mainly produced against enteric microbes including pathogens⁹⁵.

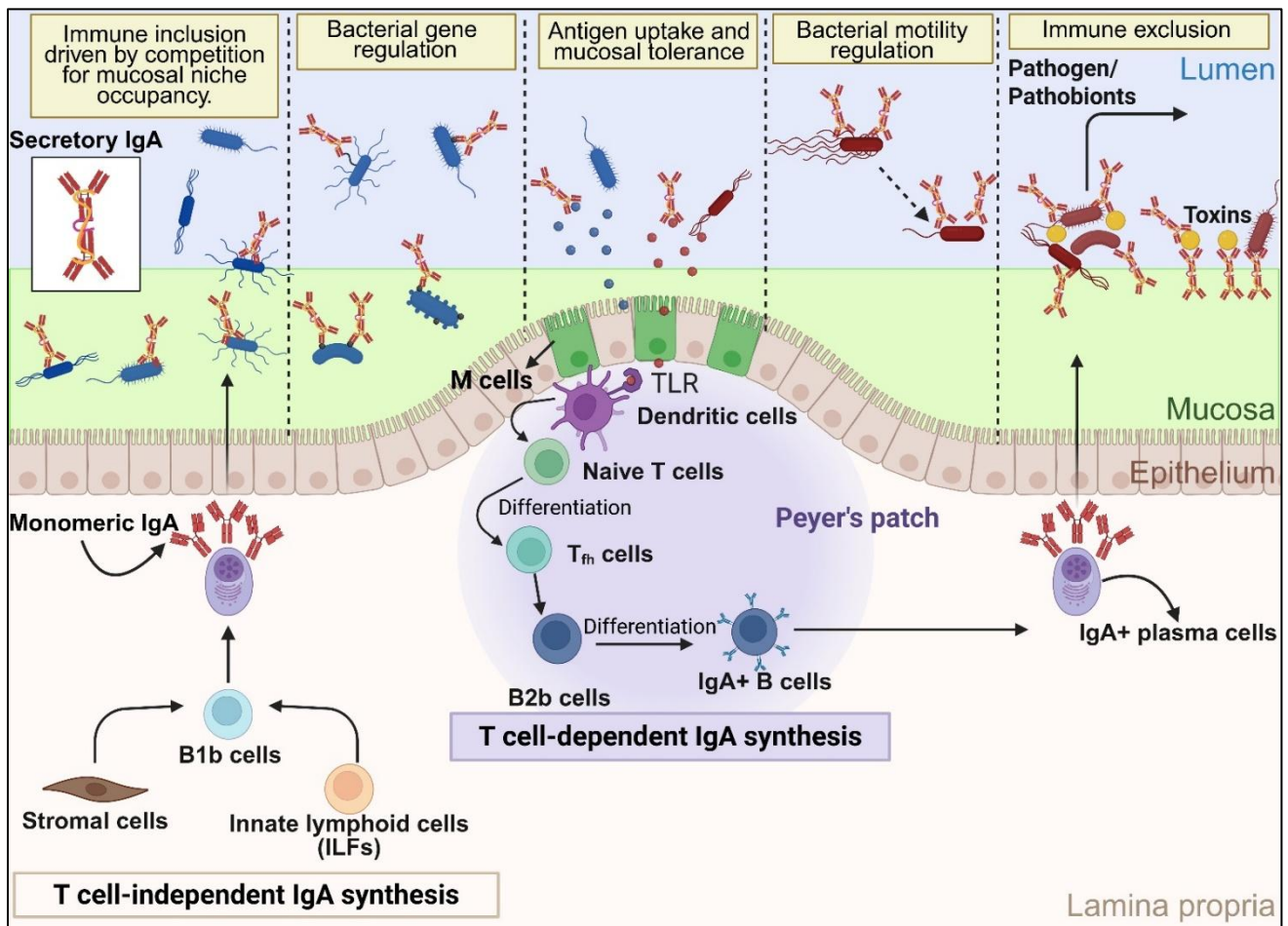


Figure 1.4. Immunoglobulin A (IgA) functions in the small intestine. This illustration depicts T cell-dependent and -independent pathways for IgA production in the small intestine. In the T cell-dependent pathway, dendritic cells sample antigens via M cells and activate naïve T cells in Peyer's patches, leading to the differentiation of T follicular helper (T_{fh}) cells. T_{fh} cells drive class switching in B2b cells, generating antigen-specific IgA+ B cells that differentiate into plasma cells. In the T cell-independent pathway, stromal cells and innate lymphoid cells (ILFs) stimulate B1b cells to produce IgA without T cell involvement. Monomeric IgA is transported across the epithelium, where it becomes dimeric and is secreted into the lumen. Secretory IgA maintains intestinal homeostasis by promoting immune inclusion through niche competition, modulating bacterial gene expression, facilitating antigen uptake and tolerance, suppressing bacterial motility, and excluding pathogens and toxins.

Undernourished children have elevated levels of sIgA in the feces compared to healthy individuals^{96,97}. Stunted children also have a higher proportion of their fecal microbiota targeted by IgA³⁹, suggesting these children have a dysregulated humoral immune response. sIgA is an important contributor to gut barrier function and homeostasis and helps maintain a balanced microbiota^{92,93}. To do so, IgA functions in pathogen/antigen neutralization and excretion, promotion of commensal bacterial colonization and reduction of colonization with pathogens/fast growing bacteria in the intestine^{16,24}. sIgA achieves gut homeostasis by being hypo-responsive against commensals and hyper-responsive against pathogens⁹⁸. Recent work shows IgA targeting in inflammatory bowel diseases can identify colitogenic bacteria⁹⁹. Similarly, IgA-targeted bacteria isolated from undernourished children and used to colonize 4-week-old germ-free mice caused diet-dependent weight loss and enteropathy⁹⁶. These findings suggest IgA targeted microbes in undernourished children can contribute to impaired nutrient absorption. Thus, the discriminatory functions of IgA could serve to identify immunogenic bacteria that cause reduced linear growth and altered immunity in early life.

1.6 The goal of this dissertation

Taken together, there is a body of literature demonstrating that other factors besides dietary insufficiency contributes to the development of stunting. Evidence shows stunted children have alterations in the composition of their microbiome and immune system. However, little is known about how these microbes contribute to stunting and associated comorbidities or the functional consequences of altered immunity. There is also a lack of understanding of how immune alterations in stunted children influence

growth regulation. It has been shown that children inherit a significant portion of their microbiota from their mothers¹⁹. Due to stunting's intergenerational nature, stunted children may be more likely to receive microbes that promote EED. Therefore, there is a need for murine models of undernutrition to investigate the effects of vertically transmitted microbes in growth and immunity, in a controlled and ethical manner. Microbes may negatively impact growth outcomes by interrupting gut homeostasis, impairing intestinal digestion and nutrient absorption soon after birth during a vital period for growth⁶². Furthermore, current mouse models of undernutrition do not characterize linear growth and have not been used to determine optimal windows of development for interventions. These models also fail to dissect the contributions of the diet or the microbiome into the phenotypes that develop.

The purpose of this dissertation is to address these gaps of knowledge in the field by establishing a gnotobiotic mouse model of intergenerational undernutrition for the mechanistic study of stunting in early life. To do so, we developed a model in which germ-free mice were colonized after weaning with the microbiota from four human infant donors from Malawi, including two healthy and two stunted (with HAZ scores below 2 SDs) donors. The infant donors selected for this thesis work come from the iLiNS-DYAD-M study (NCT01239693). This cohort study enrolled pregnant women in Malawi to evaluate the effectiveness of lipid-based nutrient supplements (LNS) during pregnancy and child growth development. In this study, infants did not receive nutritional supplementation until after six months of age. Fecal microbiota samples collected at this time were used to colonize germ-free breeders, as maternal supplementation did not impact the microbiota composition of human infant donors^{100,101}.

To dissect the direct contributions of the microbiome in growth and immunity, we created two distinct models of undernutrition using a humanized undernourished Malawi-8 (M8) diet. This diet is low in both protein and micronutrients and is representative of what the infant donors consume daily after weaning¹⁰². In these models, we address the importance of the microbiota at distinct time points during development. The first model represented “intergenerational” undernutrition by first colonizing sires and exposing them to the malnourished diet during early life. These mice were then bred, and transmitted distinct microbial communities to their offspring.

We also designed a second model of post-weaning undernutrition. In this model, instead of colonizing sires (and offspring acquiring microbiota vertically), 4-week-old germ-free female and male mice were colonized with donor microbiota directly and started in the M8 diet until maturity. We hypothesized that only intergenerational colonization of microbes from a stunted infant donor will cause reduced linear growth, changes in intestinal morphology (recapitulating EED), and immunity in the offspring.

In another arm of this dissertation, we aimed to investigate the role of maternal undernutrition in perpetuating the cycle of stunting. To address this, we modified our murine model of intergenerational undernutrition to include maternal diet and microbiome exposure in early life. Both the dams and sires underwent a four-week period of undernutrition assault before setting up breeding. We hypothesized that maternal undernutrition would exacerbate stunting-like features in offspring already exhibiting growth deficits, while also inducing growth-related effects in offspring without preexisting stunting-like features, better recapitulating human stunting. The establishment of this

model allows for the mechanistic study of maternal contributing factors in the development of stunting.

Another aspect investigated in our models of intergenerational undernutrition is when in early life growth deficits and changes in immunity happen. Specifically, we investigate the relative contributions of *in utero* and post-natal factors in the development of stunting. We employed cross-fostering approaches to answer this question. Finally, we assess the hypothesis of whether immune recognition of specific microbes can help us identify drivers of stunted growth in our model and dive into understanding how accurate or representative IgA targeting in the fecal microbiome is compared to what is happening in the small intestine.

This thesis presents innovative findings integrating diverse murine models and techniques that enable the mechanistic study of how microbes, maternal nutritional status, and intestinal immune responses influence EED and stunting.

Chapter 2: Establishing a Mouse Model that Recapitulates Growth Deficits & Immune Responses Observed in Stunted Children

Part of this chapter has been adapted from “Colonization during a key developmental window reveals microbiota-dependent shifts in growth and immunity during undernutrition.”

Yadeliz A. Serrano Matos¹, Jasmine Cano¹, Hamna Shafiq, Claire Williams, Julee Sunny, Carrie A. Cowardin. 2024. *Microbiome* April 09;12(1)

¹These authors contributed equally to this work

Author Contributions:

Conceptualization, Y.S.M and C.A.C.; Sample collection, Y.S.M, J.C., H.S., C.W., J.S. and C.A.C.; Investigation, Y.S.M, J.C., H.S., C.W., J.S. and C.A.C.; Analysis; Y.S.M, J.C., H.S., J.S. and C.A.C.; Visualization, Y.S.M, J.C., H.S., J.S. and C.A.C.; Resources, J.C., Y.S.M and C.A.C; Funding, Y.S.M. and C.A.C, Supervision, C.A.C; Writing, Y.S.M, J.C. and C.A.C.

2.1 Introduction

Childhood undernutrition is a formidable global health challenge, contributing to nearly half of all deaths in children under the age of five^{9,103}. The first 1,000 days of life, spanning from conception to age two, are widely recognized as critical in determining developmental outcomes, and undernutrition during this period can have devastating consequences^{104,105}. Linear growth stunting (length-for-age Z score ≤ 2 standard deviations below the WHO median) is a major complication of undernutrition impacting 149.2 million children globally in 2020^{103,106}. Mothers who experience growth stunting as children are more likely to give birth to stunted children later in life, leading to a cycle of intergenerational transmission that has proven difficult to disrupt^{107,108}. Supporting this observation, among of the best predictors of attained height in children are the child's weight and length at birth and mother's attained height, emphasizing the importance of development *in utero* and in early life^{17,109–112}. The negative consequences of growth stunting persist into adulthood and include poor cognitive development, reduced educational attainment, and increased risk of metabolic and infectious disease^{105,113}. This syndrome is multifactorial and driven by inadequate nutrition, altered gut microbial communities, intestinal inflammation and pervasive pathogen colonization^{72,114}. These combined insults can drive a subclinical syndrome of intestinal epithelial derangement, inflammation, and barrier dysfunction known as Environmental Enteric Dysfunction (EED), which is prevalent in areas with high rates of undernutrition. EED is thought to limit the efficacy of therapeutic foods by decreasing the absorptive capacity of the small intestine^{62,87,115}. Hallmark features of EED include epithelial remodeling and immune activation, with increased numbers of small intestinal antibody-

producing plasma cells, regulatory and cytotoxic T cells, and reductions in intestinal macrophages^{68,82,116}. Despite measurable progress in reducing stunting due to undernutrition, many of its long term consequences have proven resistant to pharmaceutical and nutritional therapies, highlighting the need to further understand the underlying etiology and mechanisms driving pathology^{24,117}.

The gut microbiome plays a critical role in shaping both local and systemic immunity, and children with undernutrition are known to have altered gut microbial communities^{12,41,118}. Transplantation of microbes from undernourished human donors to recipient germ-free animals (GF) suggests these community alterations are causally linked to deficits in growth and alterations in metabolism^{12,119}. Murine models have likewise highlighted early life as a critical window in which the immune system develops in reaction to the gastrointestinal microbiome^{34,120}. Indeed, GF mice that are colonized after the weaning period display heightened susceptibility to inflammatory pathologies³⁴. Thus, the timing of colonization can dictate later immune outcomes, with significant implications for the long-term sequelae of undernutrition, many of which can be linked to immune dysfunction. These findings also raise the question of whether immunity differs depending on the composition of the microbiota that is present during critical periods of development.

To address these questions, we designed a murine model of early life undernutrition using human gut microbiota transmitted vertically from parents to offspring. In this “intergenerational” model, GF breeding mice were colonized with microbiota obtained from human infants with healthy or stunted growth trajectories. Offspring born to these mice inherited distinct microbial communities and were weaned onto a nutrient-

deficient diet, capturing a critical window of early life development. We compared these mice to animals born GF but colonized directly after the weaning period. We demonstrate that intergenerational colonization with gut microbiota from human infant donors with linear growth stunting leads to reduced growth, small intestinal villous shortening, and significant intestinal immune alterations. These changes arise when animals are born to colonized parents, but not when colonized directly after weaning. We suggest that this model may serve as a useful tool with which to delineate the role of specific microbiota-dependent immune changes and their functional consequences during early life undernutrition.

2.2 Results

Establishing an intergenerational model of undernutrition

In order to determine whether immune developmental outcomes would differ depending on the composition of the gut microbiota during early life, we colonized young (4 week-old) GF C57Bl/6 mice with fecal microbiota sampled from one of four donors: two healthy (height-for-age Z score (HAZ) = 1.12 and 1.74) or two stunted (HAZ = -3.35 and -2.33) six-month-old Malawian infants^{41,121}. Mice were fed low in protein and micro-nutrient deficient diet composed of foods commonly consumed by the donor population (Malawi-8 or M8⁴¹). In one arm of the experiment, male and female GF mice were colonized at 4 weeks of age and maintained on the M8 diet until 8 weeks, when microbiota composition and immune phenotypes were assessed. These animals represent the “Post-Weaning” (PW) model of colonization (**Fig. 2.1A**). In a second arm of the experiment, male mice were similarly colonized and maintained on M8 from 4 to 8 weeks of age. At 8

weeks, age-matched GF females were introduced, breeding pairs were cohoused and maintained thereafter on a nutrient-sufficient diet. Male and female offspring from these breeding pairs were weaned onto the M8 diet from 3 to 8 weeks of age. These animals represent the “Intergenerational” (IG) model of colonization (**Fig. 2.1A**). To identify phenotypes that differed based on donor growth status, we assessed results by combining data from both stunted donors (SD) and comparing against combined data from both healthy donors (HD).

Intergenerational colonization with SD microbiota reduces linear growth

We next assessed growth phenotypes in both IG and PW animals at 8 weeks of age. We found no difference in overall weight between HD and SD animals colonized either intergenerationally or post-weaning (**Fig. 2.1B**); however, both groups weighed significantly more when colonized after weaning, possibly due to an additional week of undernutrition in the IG groups. Consistent with these results, we found no significant differences in weight between groups of IG dams and sires after colonization, or between SD-PW and HD-PW mice in the first two weeks after colonization¹²². In contrast, we noted a significant reduction in tail length, a surrogate for linear growth, in SD-IG relative to HD-IG mice (**Fig. 2.1C**). No difference in tail length was detected between SD-PW and HD-PW groups. Overall, both IG groups had significantly shorter tails than their PW counterparts, consistent with the finding of reduced body weight. As a second measure of linear growth, we also assessed femur length, which showed similar outcomes, although differences between SD-IG and HD-IG groups did not reach statistical significance (**Fig. 2.1D**). Interestingly, reductions in femur length appeared more severe

in SD-4092 animals compared to the SD-3114 animals, suggesting differences in community composition between the two stunted donors are likely involved. These trends were evident when comparing between IG and PW mice in each individual donor group and were not sex-dependent¹²². In human cohorts and other mouse models of undernutrition, levels of Insulin-like Growth Factor-1 (IGF-1) correlate strongly with linear growth^{56,123}. We next assessed levels of IGF-1 in the liver by ELISA, and found a significant reduction in IGF-1 in SD-IG animals relative to the HD-IG group (**Fig. 2.1E**), with no significant difference identified between SD-PW and HD-PW mice. Over the course of the experiment, we did not find significant differences in litter size between IG groups colonized with distinct donor microbiota¹²². Because all four IG groups showed reduced growth compared to PW animals, these differences could reflect either paternal or early life M8 diet exposure in addition to earlier microbial colonization. These findings also suggest that intergenerational but not post-weaning colonization with SD microbiota negatively influences linear growth and liver IGF-1 relative to HD microbial communities.

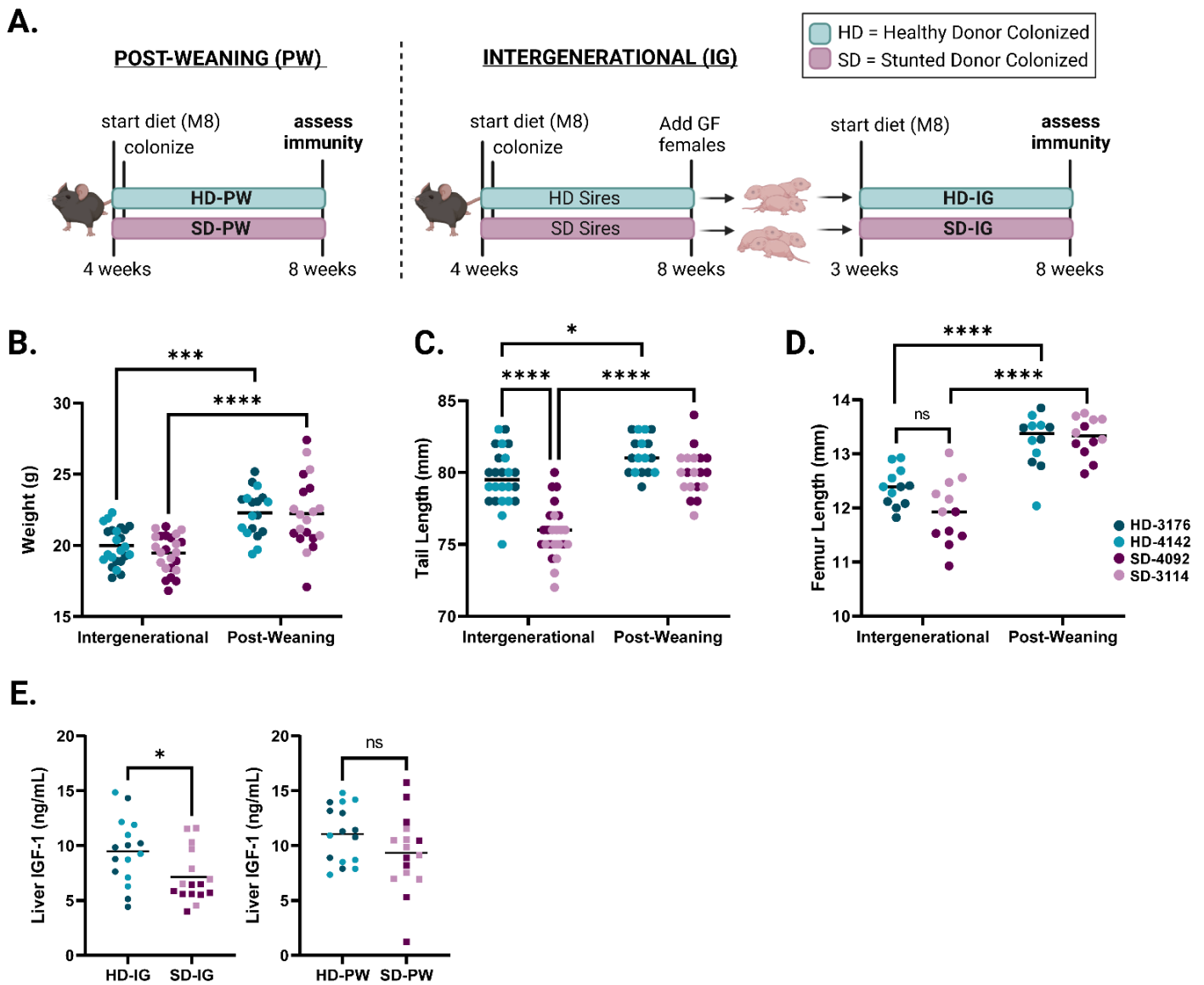


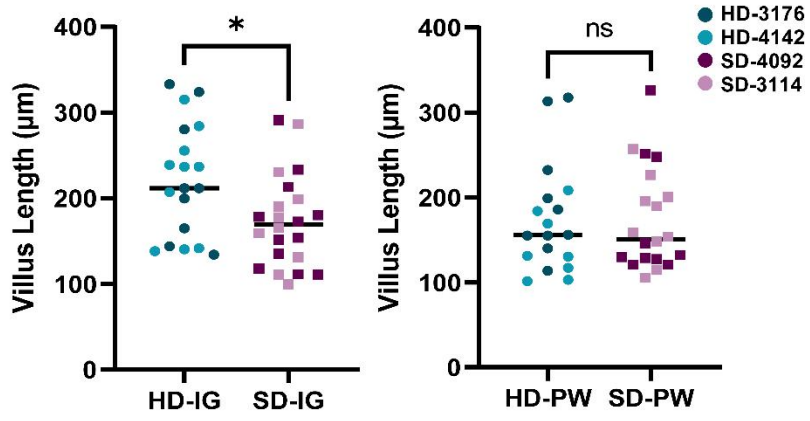
Figure 2.1. Development of a murine model of intergenerational undernutrition. (A) Schematic of experimental design (created with Biorender.com). Both HD and SD pups in the PW model are maintained on the M8 diet from 4-8 weeks of age. HD and SD pups in the IG model are likewise weaned onto the M8 diet at 3 weeks of age. HD and SD pups in the IG model are likewise weaned onto the M8 diet at 3 weeks of age. **(B)** Absolute weight of animals at the time of euthanasia. **(C)** Tail length. **(D)** Femur length. **(E)** Measurement of IGF-1 in liver tissue of IG and PW mice. Data shown pooled between healthy donor colonized mice (3176 and 4142) and stunted donor colonized mice (4092 and 3114) at 8 weeks of age. Each point represents an individual animal. **(B-D)** * $p \leq 0.05$, **** $p \leq 0.0001$ by Two-Way ANOVA with Šídák's multiple

comparisons test. **(B-C)** n = 24/group [12 per donor] for IG groups, n=18-20/group [8-10 per donor] for PW groups. **(D)** n = 12/group [6 per donor] for all groups in all conditions **(E)** n = 16/group [8 per donor] for all groups

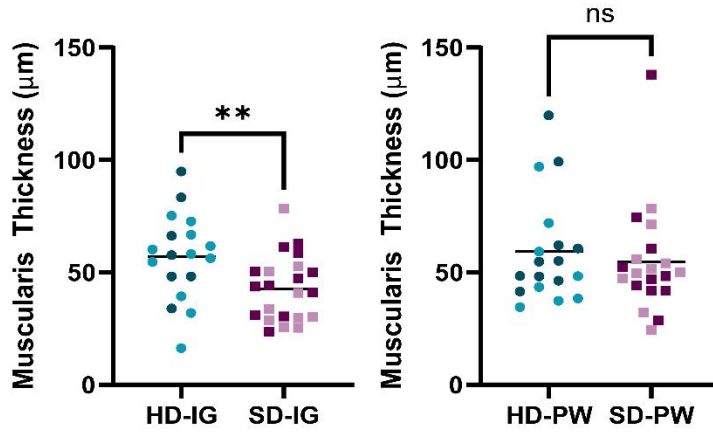
SD microbial communities influence intestinal histopathology

To begin to characterize underlying differences between SD-IG and HD-IG offspring that could explain the observed reductions in linear growth, we next examined small intestine histopathology. Blinded scoring of hematoxylin and eosin-stained ileal tissue sections from all four donor groups revealed significant reductions in quantitative measurements of villus length and muscularis thickness in SD-IG relative to HD-IG mice (**Fig. 2.2A-B**). Interestingly, these changes were not present when comparing HD-PW to SD-PW groups, suggesting that the reduction in villus length was not a general consequence of the presence of specific microbes, but depended on when these microbes were encountered. In addition to these quantitative measures, we also subjected sections to blinded scoring using three subjective parameters commonly observed in human intestinal biopsies from patients with undernutrition and EED¹²⁴⁻¹²⁶, including immune cell infiltration, villous architecture and enterocyte injury. Surprisingly, we did not identify significant differences in these parameters, which may depend on additional environmental, or pathogen exposures not replicated in our model¹²².

A.



B.



C.

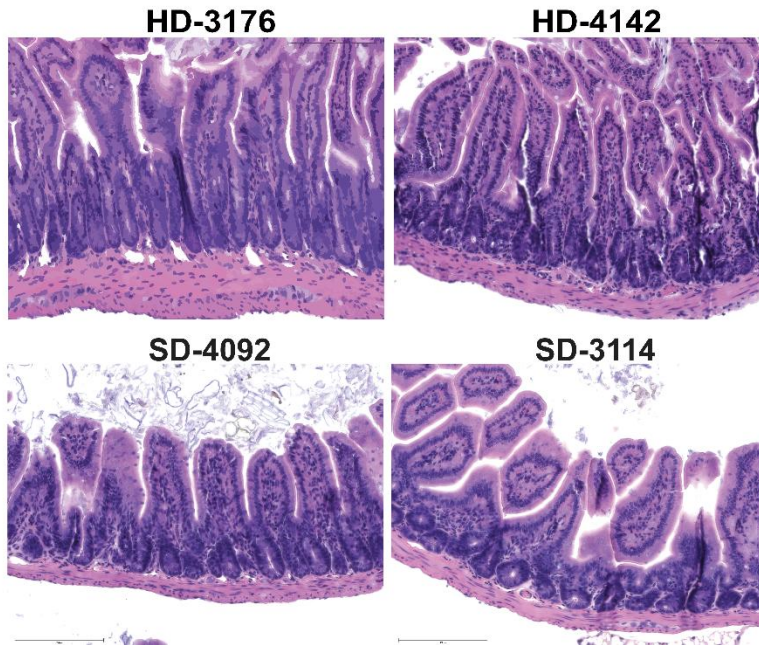


Figure 2.2. Intestinal morphology changes in IG mice at 8 weeks of age. (A-B) Quantification of villus length and muscularis thickness in IG and PW mice. **(C)** Representative histological images of H&E stained ileal tissue from IG mice. Data shown pooled between healthy donor colonized mice (3176 and 4142) and stunted donor colonized mice (4092 and 3114) at 8 weeks of age. Each point represents an individual animal. **(A-B)** n = 18-22/group [7-12 per donor] for IG groups, n = 18-20/group [8-10 per donor] for PW groups. **(A-B)** * p ≤ 0.05, ** p ≤ 0.01 by Mann-Whitney U test.

Distinct microbial communities colonize all four donor groups

In order to define the microbial communities mediating these effects, we next performed V4 16s rRNA sequencing of the fecal microbiota from mice in all four donor groups. Analysis of samples from IG animals at maturity revealed distinct community configurations for each donor (**Fig. 2.3A**), with a modest number of shared taxa¹²². Analysis of UniFrac distances demonstrated that the composition of the fecal microbiota was similar between PW and IG samples within each individual donor, with the greatest variability present in donor 3114, and to a lesser extent, donor 4092 (**Fig. 2.3B**). Direct comparisons of PW to IG samples for each donor by weighted (**Fig. 2.3C**) and unweighted¹²² UniFrac demonstrated significant differences in community structure between PW and IG mice colonized with the two stunted donor communities. Because PW mice were colonized directly while IG mice received vertically transmitted microbes, these results suggest the HD communities may be more efficiently passed from parents to offspring. In contrast, SD microbiota appeared to be surprisingly dependent on the mode of colonization (**Fig. 2.3D**). Whether these divergent patterns represent poor intergenerational transmission by the SD communities, more efficient engraftment by

direct oral gavage, or shaping of the community by differential host immune responses warrants further investigation.

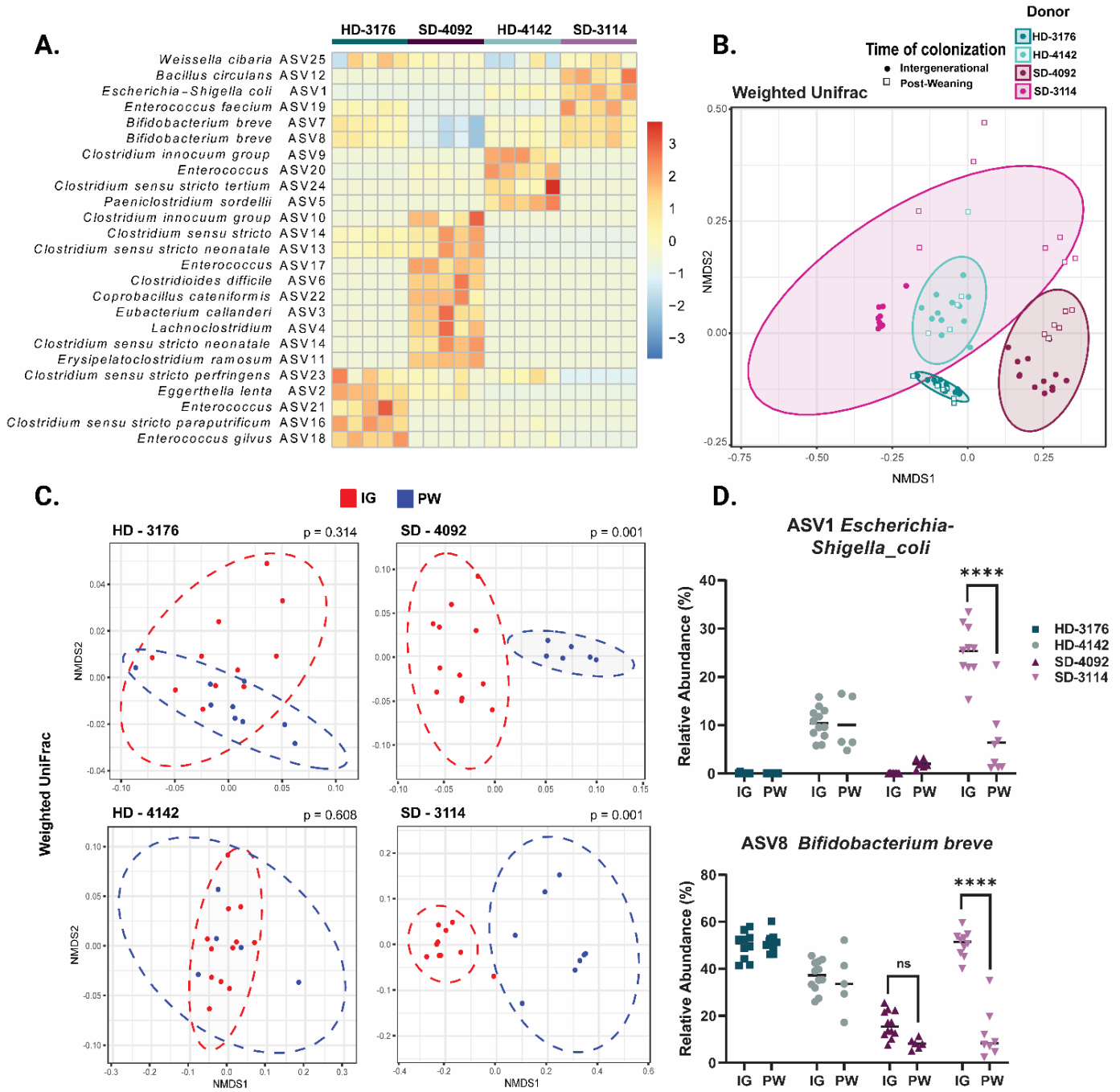


Figure 2.3. Microbial communities of recipient mice show distinct patterns of colonization.

(A) Row-normalized heatmap of the top 25 ASVs by relative abundance for all four IG donor groups in fecal samples at 8 weeks of age. n=5/group. **(B)** NMDS plot of weighted UniFrac distances of IG and PW fecal samples at 8 weeks of age by donor colonization. n=5-12/group. **(C)** NMDS plot of weighted UniFrac distances of IG versus PW fecal samples at 8 weeks of age by individual donor. n=5-11 mice/group with p value calculated by PERMANOVA. **(D)** Relative abundances of ASV1 *Escherichia-Shigella coli* and ASV 8 *Bifidobacterium breve* for all four IG and PW donor-colonized groups at 8 weeks of age. n = 5-12/group, * p ≤ 0.05, ** p ≤ 0.01, **** p ≤ 0.0001 for comparisons between IG and PW samples within each donor by Two-Way ANOVA with Šídák's multiple comparisons test.

Intergenerational colonization shapes small intestinal Intraepithelial Lymphocytes

Based on differences in linear growth and intestinal histopathology between SD-IG and HD-IG mice, we next sought to determine whether these microbial communities influenced immune cell composition in the small intestine epithelium. We first identified significantly elevated TCRβ⁺ cells in SD-IG relative to HD-IG mice (**Fig. 2.4A**), a difference that was not observed in HD-PW and SD-PW groups. Within this compartment, SD-IG mice had a significantly greater proportion of CD8α⁺ TCRβ⁺ cells and a significantly reduced proportion of CD4⁺ TCRβ⁺ T cells in the epithelium, whereas SD-PW and HD-PW mice did not (**Fig. 2.4B-C**). These results pointed towards potential differences in populations of intraepithelial lymphocytes (IELs), a heterogeneous group of microbiota-responsive immune cells located within the intestinal epithelium with diverse regulatory and inflammatory functions^{127–130}.

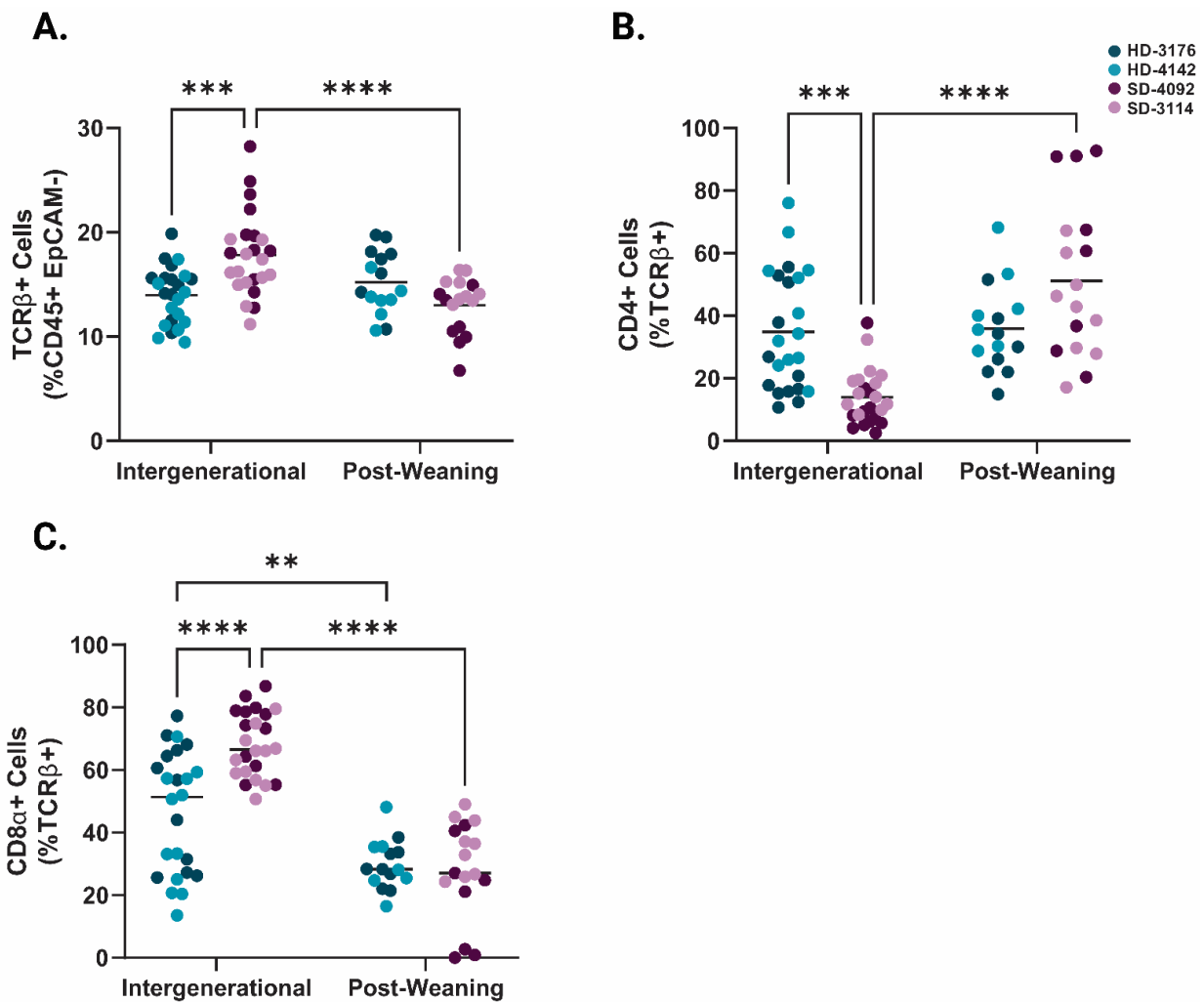


Figure 2.4. Immune cell composition of the small intestinal epithelium in IG and PW colonized mice at 8 weeks of age. (A) TCR β + cells shown as a percentage of CD45+ EpCAM- Live cells. **(B)** CD4+ cells shown as a percentage of TCR β + CD45+ EpCAM- Live cells. **(C)** CD8+ cells shown as a percentage of TCR β + CD45+ EpCAM- Live cells. **(A-C)** n = 24/group [12 per donor] for IG groups, n=18-20/group [7-10 per donor] for PW groups. * p \leq 0.05, ** p \leq 0.01, *** p \leq 0.001, **** p \leq 0.0001 by Two-Way ANOVA with Šídák's multiple comparisons test.

Natural IELs are increased in the small epithelium of SD-IG animals

IELs exist as two major subsets, including 'natural' IELs that are activated within the thymus, and 'induced' IELs that derive from conventional T cells activated peripherally⁴³. Intriguingly, SD-IG mice showed a significant increase in two subsets of natural IELs. CD8 $\alpha\alpha$ + TCR β + and CD8 $\alpha\alpha$ + TCR $\gamma\delta$ + IELs were both significantly more abundant in SD-IG mice relative to HD-IG animals, but neither cell type differed between the PW groups (Fig. 2.5A-B). In contrast, induced CD8 $\alpha\beta$ + TCR β + IELs did not significantly differ between groups (Fig. 2.5C).

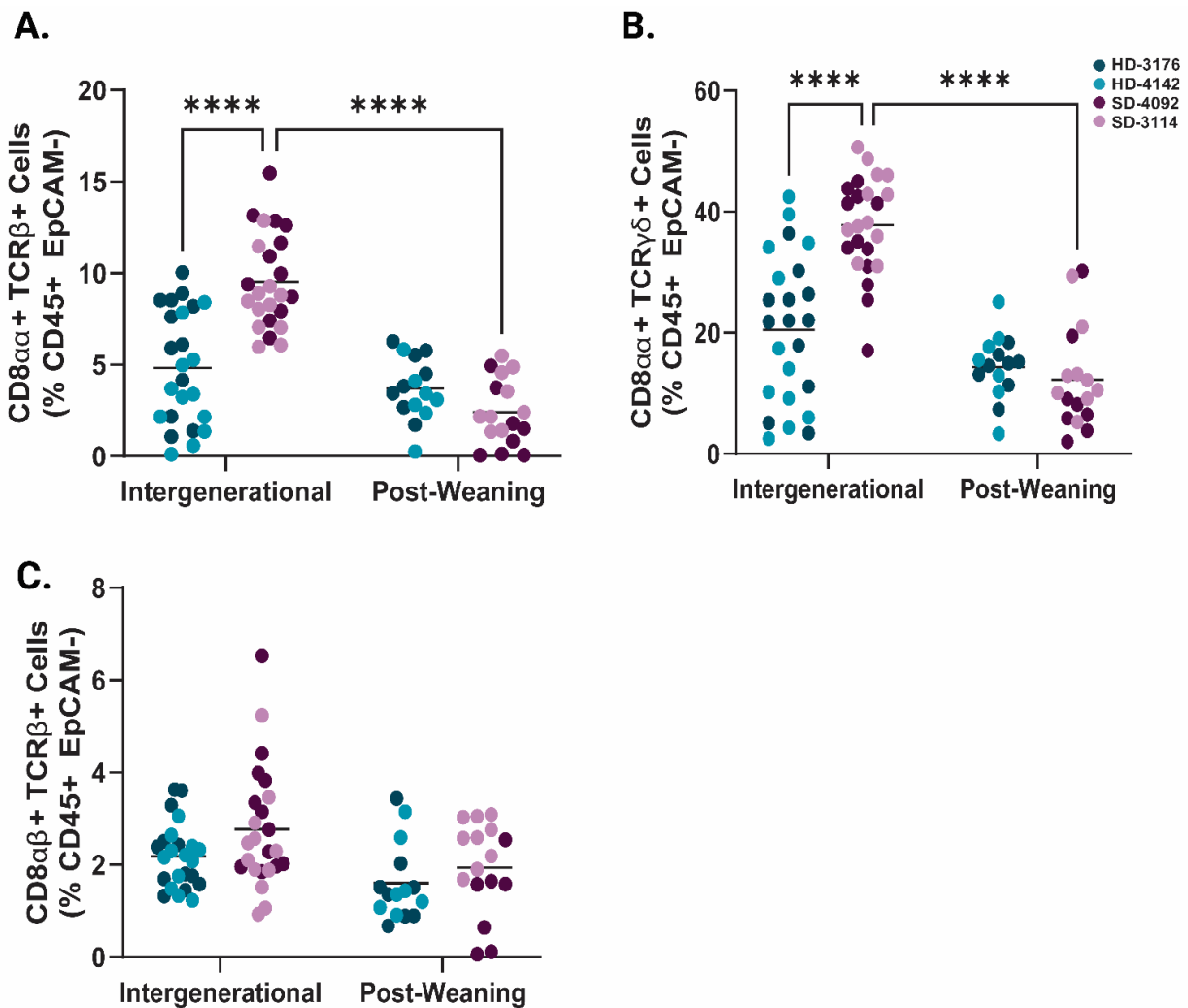


Figure 2.5. Natural IELs are increased in the small intestine epithelium of SD-IG animals at 8 weeks. (A) CD8 $\alpha\alpha$ + TCR $\alpha\beta$ Natural IELS (gated as CD8 α + CD8 β - TCR β + cells as a percentage of CD45+ EpCAM- Live) **(B)** CD8 $\alpha\alpha$ + TCR $\gamma\delta$ Natural IELs (gated as CD8 α + CD8 β -CD4- TCR $\gamma\delta$ + cells as a percentage of CD45+ EpCAM- Live). **(C)** CD8 $\alpha\beta$ + TCR $\alpha\beta$ Induced IELs (gated as CD8 α + CD8 β + TCR β + cells as a percentage of CD45+ EpCAM- Live). Data shown pooled between healthy donor colonized mice (3176 and 4142) and stunted donor colonized mice (4092 and 3114). Each point represents an individual animal. **(A-C)** n = 24/group [12 per donor] for IG groups, n=18-20/group [7-10 per donor] for PW groups. * p \leq 0.05, ** p \leq 0.01, *** p \leq 0.001, **** p \leq 0.0001 by Two-Way ANOVA with Šídák's multiple comparisons test.

A significantly greater proportion of CD8 $\alpha\alpha$ + TCR $\gamma\delta$ + IELs in SD-IG mice were also positive for Granzyme A, a cytotoxic mediator found in T lymphocytes (**Fig. 2.6A-B**)²¹. Based on these results, we concluded that differences in the proportions and function of natural IEL subsets were influenced by the composition of the microbiota when colonized intergenerationally, but not when colonized after weaning.

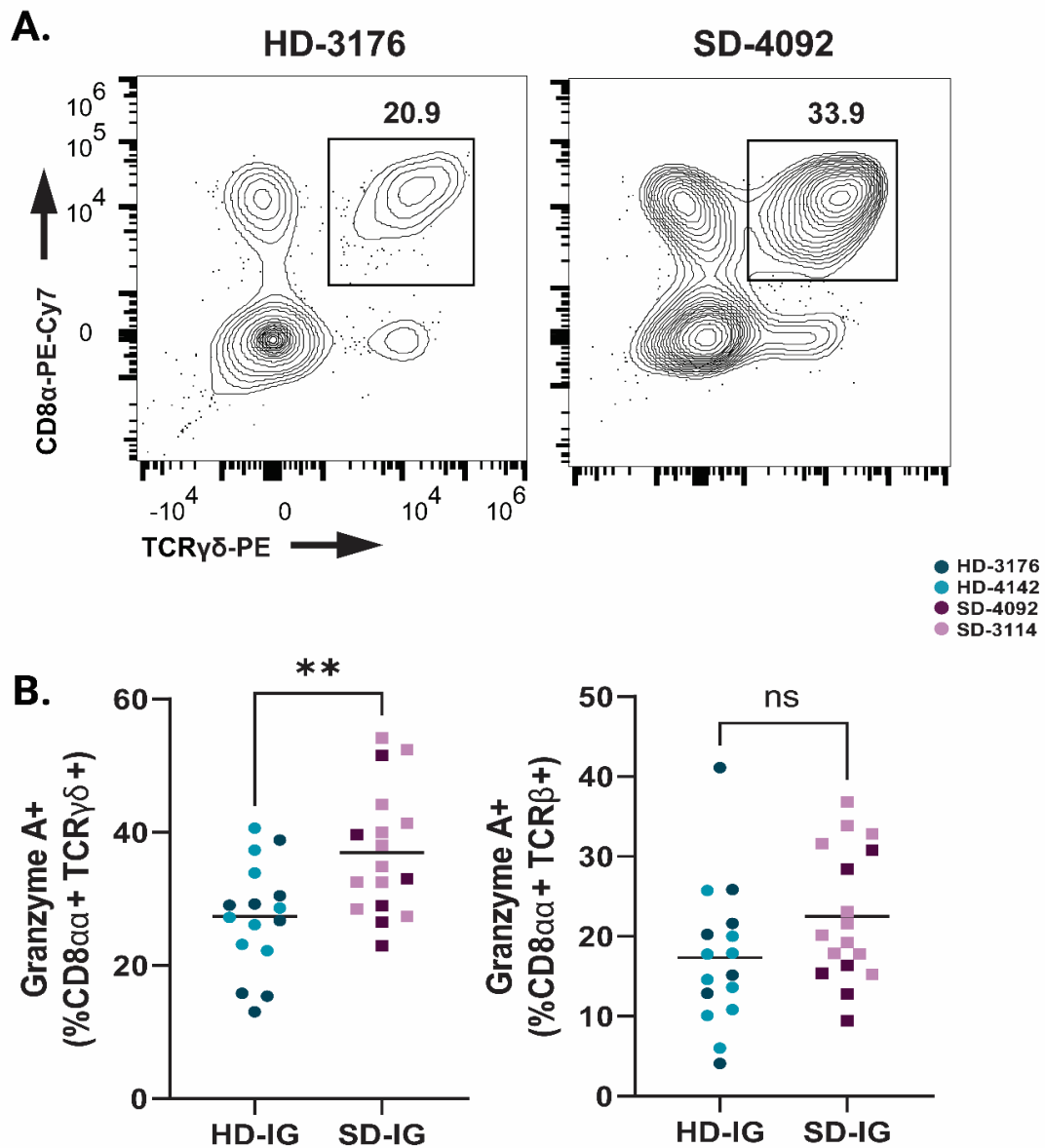


Figure 2.6. Natural IELs isolated from SD-IG mice have increased intracellular levels of Granzyme A. (A) Representative flow plots of TCR $\gamma\delta$ + Natural IELs in HD and SD IG mice. Cells were gated on the Live CD45+ EpCAM- population. (B) Granzyme A+ cells shown as a percentage of CD8 α + CD8 β - CD4- TCR $\gamma\delta$ + CD45+ EpCAM- Live cells (left) or CD8 α + CD8 β - TCR β + CD45+ EpCAM- Live cells (right) within IG colonized mice. Data shown pooled between healthy donor colonized mice (3176 and 4142) and stunted donor colonized mice (4092 and

3114). Each point represents an individual animal. (A-B) n =16-17/group [6-11 per donor], ** p ≤ 0.01 by Mann-Whitney U test.

Roryt+ T regulatory cells are increased in SD-IG mice

We next investigated changes to innate and adaptive immune populations within the small intestine lamina propria. Overall, cellular changes in this compartment were less marked than those in the epithelium. However, we did note an overall increase in the proportions of Roryt+ CD4+ T cells in the lamina propria of SD-IG mice (**Fig. 2.7A**). Recent findings from a murine model of undernutrition and EED induced by malnourished diet and adherent invasive *Escherichia coli* infection likewise reported increased microbiota-directed T regulatory cells, and increased numbers of these cells have also been reported in human cohorts and other murine models of undernutrition^{73,116}. Consistent with these findings, we found increased numbers of Roryt+ FoxP3 regulatory T cells in the lamina propria of SD-IG mice relative to HD-IG animals (**Fig. 2.7B**). While the majority of innate immune cells were unchanged between groups, we did observe a reduction in lamina propria macrophages in SD-IG groups (**Fig. 2.7C**), again consistent with data from human cohorts with EED²¹. Interestingly, the reduction in macrophages appeared to be driven by donor 4092 to a greater extent than donor 3114. Finally, we also noted increased numbers of IgA+ Plasma Cells in the lamina propria of SD-IG mice relative to HD-IG mice (**Fig. 2.8A-B**). These cells were also significantly increased in HD-PW mice relative to HD-IG mice. Because the microbial communities of HD mice were similar between IG and PW groups, these results support the idea that the timing of exposure to the microbiota can play a major role in shaping the subsequent host immune response.

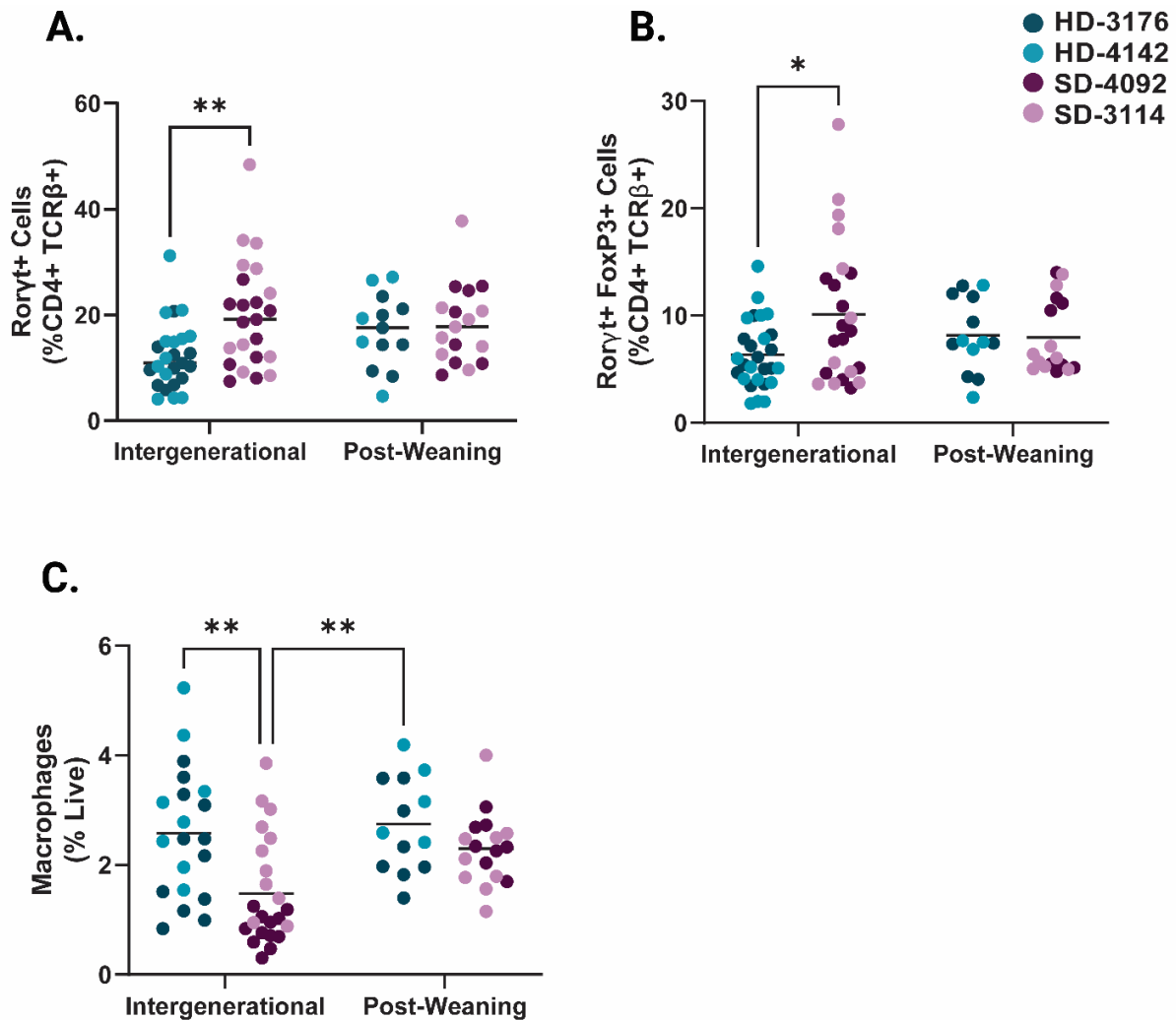


Figure 2.7. SD-IG animals exhibit an increase in microbiota-responsive T cells in the intestinal lamina propria. (A) Roryt+ cells in the small intestine lamina propria shown as a percentage of CD4+ TCRβ+ live cells. **(B)** Roryt+ Regulatory T cells (gated as Roryt+ FoxP3+ CD4+ TCRβ+ live cells) in the small intestine lamina propria shown as a percentage of CD4+ TCRβ+ live cells. **(C)** Macrophages (gated as F4/80+ CD11b+ CD45+ live cells) in the small intestine lamina propria shown as a percentage of live cells. Data shown pooled between healthy donor colonized mice (3176 and 4142) and stunted donor colonized mice (4092 and 3114). Each point represents an individual animal. **(A-C)** n = 20-24/group [10-12 per donor] for IG groups, n=14-17/group [5-9 per donor] for PW groups. * p ≤ 0.05, ** p ≤ 0.01, *** p ≤ 0.001, **** p ≤ 0.0001 by Two-Way ANOVA with Šídák's multiple comparisons test.

SD-IG mice show elevated CCL5 and IL-1 β in the small intestine

To investigate immune signals underlying the observed changes in cell composition in these groups, we next measured changes in small intestinal tissue chemokines and cytokines at the protein level. In ileum tissue lysates, we identified a significant increase in CCL5 (also known as regulated on activation, normal T cell expressed and secreted [RANTES]) protein by ELISA in SD-IG mice relative to HD-IG mice (**Fig. 2.8C**). CCL5 production can be induced by the microbiota in other murine models, notably exacerbating inflammation during DSS colitis¹³¹. *CCL5* gene expression was also upregulated in duodenal biopsies obtained from a cohort of Pakistani patients with EED compared to healthy US controls or patients with celiac disease⁶⁸. Similarly, there was also a trend towards higher Interleukin-1 β (IL-1 β) in the SD-IG group. IL-1 β is an acute phase protein whose secretion is triggered by activation of the inflammasome^{131,132} (**Fig. 2.8D**). Overall, levels of these immune signaling molecules were markedly higher in both PW groups relative to both IG groups (**Fig.2.8D**).

To further explore potential immune signaling differences between IG and PW colonization, we next performed multiplex bead-based analysis on a subset of ileal tissue lysate samples. Of the detectable cytokines and chemokines included in this analysis, we did not identify any additional significant differences between SD and HD groups in either the IG or PW samples. However, several were significantly elevated in both PW groups compared to both IG groups. These included IL-7, IL-10 and IL-17, among others¹²². Overall, these results provide further insight into immune outcomes shaped by recognition of the microbiota in early life and support the idea that the timing of exposure to microbial communities plays a critical role in shaping immunity.

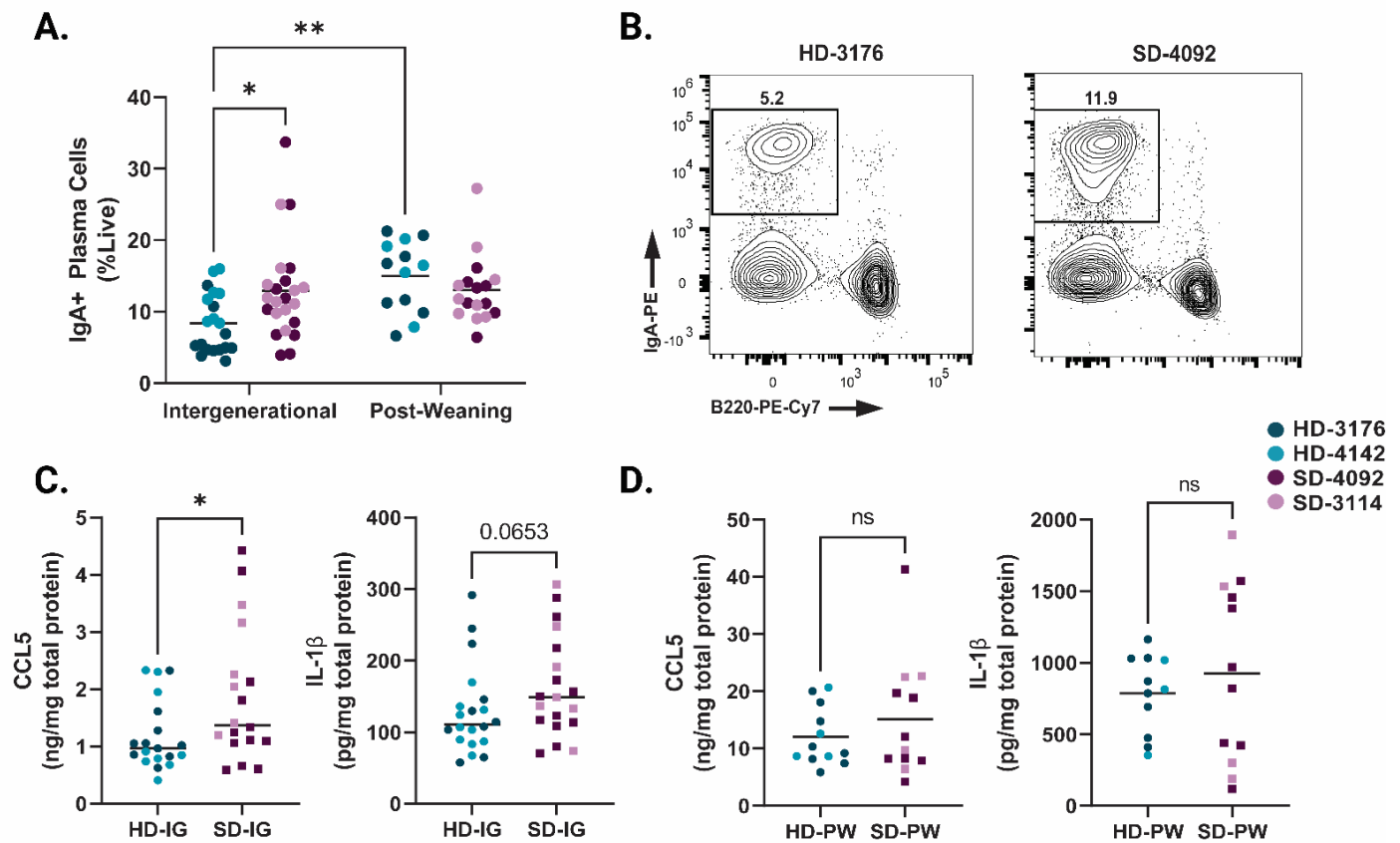


Figure 2.8. Intergenerational colonization of SD microbiota increases plasma cells and CCL5 in the lamina propria. (A) IgA+ Plasma Cells (gated as Lin- [CD3-TCRβ-CD4-CD11c-NK1.1-F4/80-] IgA+ B220- live cells) in the small intestine lamina propria shown as a percentage of live cells. (B) Representative flow plots of IgA+ Plasma Cells (gated on live Lin- cells) in HD and SD IG groups. (C) Levels of CCL5 and IL-1β in ileal tissue lysates from IG mice as measured by ELISA. (D) Levels of CCL5 and IL-1β in ileal tissue lysates from PW mice as measured by ELISA. Data shown pooled between healthy donor colonized mice (3176 and 4142) and stunted donor colonized mice (4092 and 3114). Each point represents an individual animal. (D) n = 20-24/group [10-12 per donor] for IG groups, n=14-17/group [5-9 per donor] for PW groups. * p ≤ 0.05, ** p ≤ 0.01, *** p ≤ 0.001, **** p ≤ 0.0001 by Two-Way ANOVA with Šídák's multiple comparisons test. (C-D) n =18-20/group [6-13 per donor], * p ≤ 0.05 by Mann-Whitney U test.

2.3 Discussion

Maternal and child undernutrition have increasingly been recognized as intergenerational challenges^{105,133,134}. Altered gut microbial communities contribute to undernutrition, and infants inherit a significant portion of their microbiota from maternal sources¹³⁵. Despite important observations in human cohorts, murine models of undernutrition that incorporate and investigate intergenerational exposures are lacking. Preclinical models are important in understanding the biological underpinnings and immune consequences of undernutrition in early life. Recent work has shown that targeting the gut microbiota via therapeutic foods can improve child weight gain¹³⁶. This approach was developed based on extensive testing in gnotobiotic animal models, highlighting the important role that preclinical investigation can play in the development of therapies to treat this complex disorder¹²³.

Here we demonstrate that microbiota from two human infant donors with growth stunting can mediate reductions in linear growth and intestinal villus length as well as alterations in small intestinal immune cell populations relative to microbiota from healthy children. While pooling donors into HD and SD groups allowed us to look for shared phenotypes, differences in the microbial communities between donors also drove variation in certain host phenotypes, including femur length and small intestinal macrophage populations. High levels of inter-individual variation in microbiota composition are frequently observed in human cohorts¹³⁷. Our results support the idea that variation between human microbial communities can be informative for understanding specific microbial functions that influence host biology¹³⁸.

Immune and epithelial changes in the small intestine are characteristic of EED and undernutrition, although the functional consequences of these changes are not well understood^{87,116}. Recent work describing intestinal abnormalities in patients with EED at the single cell level showed intriguing similarities to changes identified in this model, including increases in Granzyme A+ TCR $\gamma\delta$ + IELs, antibody-producing plasma cells, and reductions in intestinal macrophages⁸². While our model was not originally designed to reflect enteropathy, the areas of overlap in immune consequences between these studies suggest this approach may be useful in delineating beneficial or deleterious functions of specific immune populations during undernutrition.

Our results are also broadly consistent with previous work demonstrating that exposure of the immune system to microbial products during the weaning phase is a critical determinant of later life immune function^{34,120}. Germ-free mice are known to have altered immune development that can be partially but not entirely restored after exposure to microbes in adulthood^{12,139}. We observed that differences between animals colonized with microbiota from HD and SD donors were evident when animals are born to colonized parents but are less apparent when animals were directly colonized after weaning. Our results suggest that immune outcomes differ based not only on the presence of a microbiota during early life but also on which microbes are present.

These studies raise questions about the critical time points in early life that shape growth and immunity. While the current body of evidence suggests the weaning phase is one critical time period, many children who develop stunting show reduced linear growth at birth, and our results do not rule out a potential role for the maternal gut microbiome during development *in utero*¹¹¹. Furthermore, a weaning reaction to the microbiota has

not been demonstrated in humans, so it is unclear how these findings translate to children with undernutrition. However, data from human studies do support an important role for the gut microbiota during early life development^{56–58}. Despite these differences, we identified immune alterations in this model (increased IELs, regulatory T cells and plasma cells and reduced macrophages) that have also been shown in patients with EED^{68,82,116}, suggesting certain features of the immune response to the microbiota may be shared between mice and humans.

Limitations of our study

There are several important caveats to the current study. First, due to the complexity and length of the experimental design employed, we were unable to investigate more than four total microbiota donors. While several of our findings show similarities to human studies in patients with undernutrition, the small number of donors employed limits the overall generalizability of our results. We likewise restricted our investigation to microbiota samples from one specific age group (six-month-old infants), and it is unclear how later diversification of the microbiome in children with varied environmental exposures could impact immune composition and function at maturity. Similarly, without having undergone intestinal biopsy, we are unable to determine whether the stunted donors used in this study showed similar intestinal alterations to those observed in gnotobiotic recipients. Additional studies employing intergenerational colonization with an expanded sample size of human donors are necessary to further investigate the link between gut microbial community composition and intestinal physiology, growth, and host immunity in early life.

Another challenge in interpreting our results is the finding that colonization of the two SD microbiota groups differed significantly between PW and IG mice. While interesting, this finding does suggest that observed differences in these groups may be driven by changes in community composition rather than timing of colonization. Finally, it also remains to be determined whether this model can recapitulate other long-term sequelae of undernutrition, including oral vaccine failure, increased susceptibility to infectious disease, and cognitive developmental changes. These possibilities likewise warrant further investigation.

2.4 Conclusions

Maternal and child undernutrition are major global health challenges that current therapies do not adequately address. Mechanistic insight into growth and immune pathways regulating development in adverse environments will facilitate the development of targeted therapies to improve global child health. Here we report that intergenerational colonization of gnotobiotic mice with distinct microbial communities leads to altered growth and immune outcomes at maturity. Relative to microbiota from children with healthy growth, microbiota from two donors with linear growth stunting recapitulated several host phenotypes associated with undernutrition (including villous shortening, decreased liver IGF-1, and increased small intestinal IELs and plasma cells). In contrast, colonization of mice after the weaning phase reduced phenotypic differences in recipients harboring microbiota from healthy or stunted donors. In summary, we suggest that intergenerational colonization may be a useful approach with which to elucidate the functional role of microbial and immune alterations during undernutrition in early life.

2.5 Methods

Donor microbiota and study protocol

Details of enrollment for the iLiNS-DYAD-M study were described in an earlier publication⁴¹. Briefly, enrollment was open to consenting women over the age of 15 years with ultrasound confirmation of pregnancy of <20 weeks gestation in the Mangochi District of southern Malawi. The randomized controlled clinical trial [clinicaltrials.gov #NCT01239693] tested the effects of providing small quantity Lipid-based Nutrient Supplements (SQ-LNS) to pregnant and lactating women through 6 months postpartum and to their children through 6-18 months of age¹²¹. During pregnancy and 6 months thereafter, women received one daily capsule of iron-folic acid supplement (IFA group), one capsule containing 18 micronutrients (MMN group), or one 20-g sachet of SQ-LNS [lipid-based nutrient supplements (LNS), containing 21 micronutrients, protein, carbohydrates, essential fatty acids, and 118 kcal]. Children in the IFA and MMN groups received no supplementation; children in the LNS group received SQ-LNSs from 6 to 18 months²³. Donors used in this study were selected from samples collected at the six month time point (prior to supplementation) from a broader subset of donors based on their ability to colonize recipient gnotobiotic mice at an efficiency of >50% (more than half of taxa present in the original donor sample were identified in initial experiments⁴¹). No significant differences in infant microbiota composition based on maternal supplementation at this time point were identified^{100,101}.

Gnotobiotic Mice

All gnotobiotic mouse experiments were performed using protocols approved by the University of Virginia Institutional Animal Care and Use Committee. All gnotobiotic animals used in this publication were germ-free C57BL/6NTac mice obtained from Taconic Biosciences. Upon arrival, germ-free status was verified by quantitative PCR. Mice were housed in plastic flexible film gnotobiotic isolators (Class Biologically Clean Ltd.) under a 12-hour light cycle. Animals received *ad libitum* access to food and water throughout the experiment, and were euthanized at the conclusion of the experiment using AVMA approved procedures. For Post-Weaning experiments, male and female mice were obtained from Taconic Biosciences at 4 weeks of age, and were immediately transitioned to the M8 diet upon arrival. Three days later, they were colonized with donor microbiota and maintained thereafter on M8 until the time of euthanasia at 8 weeks of age. For Intergenerational experiments, male mice were obtained from Taconic Biosciences at 4 weeks of age and were immediately transitioned to the M8 diet upon arrival. Three days later, they were colonized with donor microbiota and maintained on M8 diet until 8 weeks of age. At this point, 8 week old germ-free females were introduced into the donor isolators. Males and females were co-housed and switched to an autoclaved nutrient-sufficient breeder chow (LabDiet 5021 Autoclavable Mouse Breeder Diet, LabDiet Inc.). Breeding animals were maintained on this diet thereafter. Offspring of these breeders (both HD and SD) were weaned at 21 days of life onto the M8 diet, and maintained on this diet until euthanasia at 8 weeks of age. Breeding mice were refreshed after six months, and offspring used in these experiments were derived from breeders from two separate rounds of colonization (total of 4 males and 6 females per breeding

isolator). All data shown represent results from a minimum of two separate litters. Weight and tail length measurements were collected after euthanasia at 8 weeks of age. Tails were measured using a standard laboratory ruler from the base of the tail to the tip along a straight line. Fecal samples were collected at the indicated time points and immediately frozen. Samples were stored at -80°C until use.

Colonization and Diets

To prepare infant fecal samples for colonization of germ-free mice, aliquots of each sample were removed from storage at -80°C, weighed and immediately transferred into anaerobic conditions (atmosphere of 75% N₂, 20% CO₂ and 5% H₂; vinyl anaerobic chambers from Coy Laboratory Products). Samples were subsequently resuspended in pre-reduced PBS containing 0.05% L-Cysteine Hydrochloride at a concentration of 10 mg/mL. Samples were vortexed for one minute and allowed to clarify by gravity for 5 minutes. The supernatant was removed to a fresh anaerobic tube and combined with an equal volume of sterile, pre-reduced PBS containing 0.05% L-Cysteine HCL and 30% glycerol. Gavage mixtures were aliquoted into sterile 2 mL screw cap tubes (Axygen) and frozen at -80°C until use. To colonize recipient mice, pools of gavage mixtures were sterilized externally with ionized hydrogen peroxide (STERAMIST System, TOMI Inc.) and passed into each isolator after appropriate exposure time (20 minutes). Animals were colonized via a single oral gavage with a 200 µl volume of gavage mixture.

The micro and macro-nutrient deficient Malawi-8 diet was prepared as previously described^{41,140} and obtained from Dyets, Inc. Briefly, ingredients (corn flour, mustard greens, onions, tomatoes, ground peanuts, red kidney beans, canned pumpkin and

peeled bananas) were cooked and combined in an industrial mixer. Dry pellets of the M8 diet were extruded, vacuum-sealed and double bagged prior to sterilization by irradiation (Steris Co). The nutritional content of the cooked and irradiated diet was assessed by N.P. Analytical Laboratories as described in Blanton et al⁴¹. LabDiet 5021 was sterilized by autoclaving at 129°C and 13.2 PSI for 15 minutes. Sterility of both diets was routinely assessed by culturing pellets in Brain Heart Infusion (BHI) broth (Millipore), Nutrient broth (Millipore), and Sabouraud-Dextrose (Millipore) broth for five days at 37 °C under aerobic conditions, and in BHI broth and Thioglycolate broth (Difco) supplemented with 0.05% L-Cysteine Hydrochloride (Sigma) under anaerobic conditions. After the five-day liquid culture, cultures of all diets were plated on BHI agar supplemented with sheep blood (Thermo Scientific). All diets were stored at -20 °C prior to use.

Histopathology and Anthropometry

At the time of euthanasia, a 1 cm section of the proximal ileum was dissected from each mouse and fixed in 10% neutral-buffered formalin overnight at room temperature before being transferred to 70% Ethanol. Tissue processing and H&E staining were performed by the University of Virginia's Research Histology Core. Samples were paraffin embedded and sectioned before mounting. Slides were stained with hematoxylin & eosin prior to imaging at a 20x magnification using an EVOS M7000 microscope. To assess the histopathological features of the ileum, the stained tissues were scored in a blinded manner by two independent observers. Resulting scores were then averaged. Scores were assigned using a scoring system based off published findings in human intestinal biopsies¹²⁵. Scoring parameters consisted of three qualitative features: immune cell

infiltration (0, no visible increase in tissue area; 1, increase in immune cells present in < 50% of tissue area; 2, increase in immune cells present in > 50% of tissue area), villous architecture (0, majority of villi are >3 crypt lengths long; 1, majority of villi are <3 but >1 crypt length long, with abnormality; 2, majority of villi are absent or <1 crypt length long, with abnormality) and enterocyte injury (0, majority of enterocytes show tall columnar morphology; 1, < 50% of enterocytes show low columnar, cuboidal, or flat morphology; 2, > 50% of enterocytes show low columnar, cuboidal, or flat morphology). Cumulative scores were calculated as the sum of the averaged score for all three parameters. ImageJ was used to obtain two quantitative parameters consisting of ileum villus height (μm) and ileum muscularis thickness (μm). Two measurements were obtained for each parameter and averaged.

To measure femur length, the femur and tibia were harvested from the right rear leg of each animal and cleaned of muscle and connective tissue. Femurs were fixed for ≥ 48 hours in 70% ethanol. The femur was isolated via gentle disarticulation from the patella. Measurements were taken using digital calipers (Fisherbrand) at the longest points of the bone by a blinded observer.

Microbial Sequencing

DNA was prepared from fecal samples by bead beating (BioSpec Products) in a solution containing 500 μL of extraction buffer [200 mM Tris (pH 8.0), 200 mM NaCl, 20 mM EDTA], 210 μL of 20% SDS, 500 μL phenol:chloroform:isoamyl alcohol (pH 7.9, 25:24:1, Calbiochem), and 500 μL of 0.1-mm diameter zirconia/silica beads. The aqueous phase was removed and DNA purified by PCR Purification Kit (Qiagen). Pure DNA was

quantified by Qubit dsDNA BR assay (Invitrogen). DNA was normalized to a 2 ng/ μ l concentration and 15 ng total DNA was used as template for subsequent PCR reactions. Bacterial V4 16S rRNA gene amplicons were generated using barcoded primers 515F-806R¹⁴¹. PCR was performed with Invitrogen High Fidelity Platinum Taq using the manufacturer's suggested cycling conditions. No-template controls were run with every sample plate to ensure there was no contamination of the barcoded primers or reagents. Amplicons were purified using Qiagen Qiaquick Purification Kit following the manufacturer's protocol. To confirm the presence of targeted amplicons, PCR products were subjected to gel electrophoresis followed by quantification using the Qubit dsDNA Assay (Invitrogen). Barcoded amplicons were pooled to a concentration of 4 nM then sequenced using the Miseq Reagent Kit v3 and Miseq platform (Illumina) following the manufacturer's recommended protocols.

Sequencing Quality Control & Data Analysis

Sequence reads were demultiplexed using Illumina Miseq Reporter Software. Quality checks were performed using fastqc version 0.11.5 before and after trimming. Samples with less than 5,000 reads were excluded from downstream analysis. Remaining reads were trimmed using the Bbduk tool from BBMap (<https://sourceforge.net/projects/bbmap/>) to 150 base pairs (bp) and with sequence quality qc ≥ 10 . ASVs were generated using the DADA2 pipeline (version 1.26.0) in R (version 4.2.3). Taxonomic assignments were performed using the SILVA ribosomal RNA gene database (v138.1). ASVs were filtered based on abundance ($>0.1\%$ across all samples) and prevalence ($>2\%$ across all samples¹⁴²). Ordination plots showing UniFrac

distances were produced using the phyloseq package (version 1.42.0) in R¹⁴³. The heatmap shown in Fig. 2A was created using the pheatmap package in R (version 1.0.12) with row normalization using the 'scale' function to center and scale the data. Stacked bar plots were generated using the miaViz package (version 1.9.0).

Flow Cytometry

Tissue Harvest and Cell Isolation

The entire small intestine was dissected from each mouse and placed onto a moist piece of gauze soaked in HBSS with 10 mM HEPES (Gibco) to prevent drying. The intestine was separated into duodenum, jejunum, and ileum, and a small portion (~1 cm) of the proximal end of each section was removed for histological analysis. Intestinal contents were then gently squeezed out of each section. Peyer's Patches and any fat were removed from the small intestine exterior, then the tissue was sliced lengthwise to expose the lumen, and samples were placed in 10ml of HBSS with 10 mM HEPES on ice. Intestines were then transferred to 20ml of room temperature epithelial removal buffer (1x HBSS with 20% FBS (Gibco), 7.5 mM HEPES (Invitrogen), and 2.5 mM EDTA (Invitrogen)) and rotated on a tube rotator for 20 minutes at room temperature, then vortexed for 20 seconds. Intestines and buffer were then poured over a 100 µm filter and the collected cell suspension containing intestinal epithelial cells was spun at 500xg for 5 minutes at 4°C, resuspended in 5ml FACS buffer (1x DPBS with 2% FBS), and reserved for flow cytometric staining and analysis. This process was repeated once more with each intestine sample and the remaining intact tissue at this point consisted of small intestine lamina propria. Tissue was then rinsed in 1x HBSS with 10 mM HEPES to remove

residual epithelial removal buffer, and finely chopped with scissors, then resuspended in 10ml of warmed complete RPMI (Gibco) and 100ul of 100 U/mL collagenase IV (Millipore Sigma). Samples were incubated at 37°C on a shaker at 180rpm for 45 minutes. The resulting mixture was poured over a 40 µm filter and tissue mashed through the filter with the end of a syringe plunger. Plunger, filter, and original digestion tube were rinsed with up to 5ml of FACS buffer to ensure maximum cell yield. Resulting cell suspension was spun at 500xg for 5 minutes at 4°C, then the supernatant was decanted, and the cell pellet was resuspended in 4mls of 40% Percoll (Cytiva) in HBSS in a 15ml conical tube. This Percoll layer was gently underlaid with 3ml of 70% Percoll in HBSS to create two distinct layers. Tubes were spun at 850xg for 20 minutes at 4°C with the centrifuge brake turned off to prevent mixing of the Percoll layers. After spin, the interface of cells between the two Percoll layers was collected and added to 10ml of HBSS with 10 mM HEPES. Tubes were spun at 500xg for 5 minutes at 4°C, then supernatant was aspirated off and cell pellets were resuspended in 500ul of FACS buffer.

Surface and Intracellular Staining for Flow Cytometry

Epithelium and lamina propria cell suspensions were plated in 96 well round bottom plates, spun at 500xg at 4°C for 5 minutes, supernatant decanted, and 50ul of surface stain mixture (fluorescent antibodies for surface markers, TruStain FcX PLUS [Biolegend], and Zombie Aqua Fixable Viability dye [Biolegend]) in FACS buffer was applied to each well and incubated for 20 minutes at room temperature in the dark. Plates were then spun at 500xg at 4°C for 5 minutes, and supernatant decanted. If cells were receiving no intracellular stains, cells were resuspended in 100ul of 1x Fixation Buffer (BD

Biosciences) for 20 minutes in the dark at 4°C. They were then spun at 500xg at 4°C for 5 minutes, supernatant was decanted, and they were resuspended in 200ul of FACS buffer and allowed to sit at 4°C overnight in the dark. On the day of analysis, cells were spun at 500xg at 4°C for 5 minutes, supernatant decanted, and resuspended in 200ul FACS buffer plus 5ul of CountBright Absolute Counting Beads (Thermo Fisher). For intracellular staining, cells were fixed in 100ul FoxP3 Fix/Perm Buffer (Invitrogen) for 20 minutes at 4°C in the dark, then spun at 500xg at 4°C for 5 minutes, supernatant was decanted, and cells were resuspended in 100ul of intracellular antibodies diluted in 1x permeabilization buffer (Invitrogen) with 2% rat serum (Invitrogen) and incubated overnight at 4°C in the dark. On the day of analysis, cells were spun at 500xg at 4°C for 5 minutes, supernatant decanted, resuspended in 200ul of 1x permeabilization buffer and allowed to sit at room temperature for 5 minutes. Cells were then spun again, decanted, and resuspended in 200ul FACS buffer plus 5ul of CountBright Absolute Counting Beads (Thermo Fisher).

Analysis and Gating

Samples were run on the Attune NxT Acoustic Focusing Cytometer with CytKick Auto Sampler and analyzed using FlowJo software. All cell types were first gated as live, single cells. Subsequent gating was performed as follows:

| Tissue Type | Cell Type | Markers |
|----------------------------------|--|--|
| Epithelium | $\alpha\beta$ T Cells | CD45+ EpCAM- TCR β + |
| Epithelium | CD4+ T Cells | CD45+ EpCAM- TCR β + CD4+ |
| Epithelium | CD8+ T cells | CD45+ EpCAM- TCR β + CD8+ |
| Epithelium | $\gamma\delta$ T Cells | CD45+ EpCAM- TCR $\gamma\delta$ + |
| Epithelium | CD8 $\alpha\alpha$ + TCR $\alpha\beta$ Natural IEL | CD45+ EpCAM- TCR β + CD8 α + CD8 β - |
| Epithelium | CD8 $\alpha\alpha$ + TCR $\gamma\delta$ Natural IEL | CD45+ EpCAM- TCR $\gamma\delta$ + CD4- CD8 β - CD8 α + |
| Epithelium | CD8 $\alpha\beta$ + TCR $\alpha\beta$ Induced IEL | CD45+ EpCAM- TCR β + CD8 α + CD8 β + |
| Lamina Propria/Epithelium | Eosinophils | CD45+ CD11b+ Ly6G- SiglecF+ SSC high |
| Lamina Propria/Epithelium | Monocytes | CD45+ CD11b+ Ly6C+ Ly6G- |
| Lamina Propria/Epithelium | Neutrophils | CD45+ CD11b+ Ly6C+/- Ly6G+ |
| Lamina Propria/Epithelium | Macrophages | CD45+ CD11b+ F4/80+ SiglecF- |
| Lamina Propria | $\alpha\beta$ T Cells | TCR β + |
| Lamina Propria | $\gamma\delta$ T Cells | TCR $\gamma\delta$ + |
| Lamina Propria | CD4+ T Cells | TCR β + CD4+ CD8- |
| Lamina Propria | CD8+ T cells | TCR β + CD4- CD8+ |
| Lamina Propria | Roryt+ | TCR β + CD4+ CD8- Roryt+ |
| Lamina Propria | Treg | TCR β + CD4+ CD8- FoxP3+ |
| Lamina Propria | Roryt+ Treg | TCR β + CD4+ CD8- FoxP3+ Roryt+ |
| Lamina Propria | CD44+ T cells | TCR β + CD44+ |
| Lamina Propria | B Cells | B220+ CD19+ |
| Lamina Propria | IgA+ Plasma Cells | Lin- (CD3-TCR β -CD4-CD11c-NK1.1-F4/80-) B220- IgA+ |

Table 2.1. Flow cytometry gating strategy for cell types identified in the intestinal epithelium and lamina propria.

| Target | Fluorophore | Clone | Vendor | Catalog # |
|-------------------------------------|----------------------|--------------|----------------|------------------|
| B220 | PE-Cy7 | RA3-6B2 | Biologend | 103222 |
| CD11b | PerCP-Cy5.5 | M1/70 | Biologend | 101228 |
| CD11c | Brilliant Violet 421 | N418 | Biologend | 117330 |
| CD19 | Brilliant Violet 421 | 6D5 | Biologend | 115538 |
| CD4 | FITC | RM4-5 | Biologend | 100510 |
| CD4 | APC | RM4-5 | Biologend | 100516 |
| CD44 | APC-Cy7 | IM7 | Biologend | 103028 |
| CD45 | APC eFluor780 | 30-F11 | eBioscience | 47-0451-82 |
| CD8α | PE-Cy7 | 53-6.7 | Biologend | 100722 |
| CD8β | FITC | YTS156.7.7 | Biologend | 126605 |
| EpCAM | Brilliant Violet 421 | G8.8 | Biologend | 118225 |
| F4/80 | APC | BM8 | Biologend | 123116 |
| FoxP3 | APC | FJK-16s | eBioscience | 17-5773-82 |
| Granzyme A | PE | 3G8.5 | Biologend | 149704 |
| IgA | PE | mA-6E1 | eBioscience | 12-4204-83 |
| LY6C | FITC | AL-21 | BD Biosciences | 553104 |
| LY6G | PE-Cy7 | 1A8 | Biologend | 127618 |
| PD1 | APC-Cy7 | 29F.1A12 | Biologend | 135224 |
| Roryt | PE | B2D | eBioscience | 12-6981-82 |
| SiglecF | PE | E50-2440 | BD Biosciences | 552128 |
| TCRβ | PerCP-Cy5.5 | H57-597 | Biologend | 109228 |
| TCR$\gamma\delta$ | Brilliant Violet 421 | GL3 | Biologend | 118120 |
| TCR$\gamma\delta$ | PE | GL3 | Biologend | 118108 |
| CD3 | PerCP-Cy5.5 | 145-2C11 | Biologend | 1000328 |
| CD4 | PerCP-Cy5.5 | RM4-5 | Biologend | 100539 |
| CD11c | PerCP-Cy5.5 | N418 | Biologend | 117327 |
| NK1.1 | PerCP-Cy5.5 | PK136 | Biologend | 108728 |
| F4/80 | PerCP-Cy5.5 | BM8 | Biologend | 123127 |
| Live dead | Aqua | -- | Biologend | 423101 |

Table 2.2. Antibodies used for flow cytometry staining.

Protein Quantification

Liver and ileum tissue were collected at the time of euthanasia and flash frozen in liquid nitrogen. Liver and ileum samples were homogenized in Lysing Matrix F (MP Biomedicals, ref. 6540440) and 500uL of 1x HALT (Thermo Scientific, ref. 78429) in T-PER (Thermo Scientific, ref. 78510). Homogenates were centrifuged at 4 °C and 10,000 xg for 5 minutes. Protein concentration was determined by BCA assay (Thermo Scientific, ref. 23227) using the manufacturer's protocol. Lysates were normalized and stored at -80 °C until analysis. Ileum samples were sent to UVA's Flow Cytometry Core Facility where the Luminex assay (MILLIPLEX MAP Mouse Cytokine/Chemokine 32-Plex Magnetic Bead Panel) was performed according to the manufacturer's protocol, which is as follows: 200uL of Wash Buffer (room-temperature 1x Wash Buffer in deionized water) was added to each well of a clean plate and sealed. Plate was mixed for 10 minutes on a plate shaker at 20-25 °C. After removing the wash buffer, 25uL of standard or control was added to the corresponding wells. 25uL of assay buffer were added to background and sample wells. 25uL of previously mentioned lysis buffer was added to the background, standards, and control wells. After vortexing the mixing bottle, 25uL of the mixed or premixed beads were added to each well. The plate was sealed, covered with foil, and incubated overnight at 2-8 °C with agitation. After removing the well contents and washing the plate twice, 25uL of detection antibody was added to each well. The plate was sealed, covered with foil, and incubated for 1 hour at 20-25 °C with agitation. 25uL of Streptavidin-Phycoerythrin was added to the wells containing detection antibody. The plate was sealed, covered with foil, and incubated for 30 minutes at 20-25 °C with agitation. After removing the well contents and washing the plate twice, 150uL of Sheath Fluid PLUS was

added to all wells. The beads were resuspended on a plate shaker for 5 minutes and the plate was measured on the Luminex xMAP Intelliflex. Sample analyte concentration was calculated by fitting the median fluorescence intensity (MFI) data to that of a standard curve, validated by lot-matched quality controls using the Milliplex Analyst software.

CCL5 and IL-1 β in ileum lysates and IGF-1 in liver lysates were quantified by ELISA assay (R&D Systems DuoSet kits) performed according to the manufacturer's recommendation. Briefly, the capture antibody was coated onto a 96-well half-area plate (Corning) in PBS overnight at room temperature. On the following day, the plates were washed three times with 200 μ L of Wash Buffer (0.05% Tween 20 in PBS) and blocked for one hour. After blocking and incubation, plates were washed again before adding samples of small intestinal tissue lysate as well as a standard curve. The plate was incubated for 2 hours at room temperature before being washed as described above. Detection Antibody provided in the kit was added at the suggested concentration and incubated for another 2 hours at room temperature. After incubation, plates were washed and Substrate Solution (1:1 mixture of Color Reagent A (H₂O₂) and Color Reagent B (Tetramethylbenzidine)) was added to each well and incubated at room temperature for 20 minutes avoiding direct light. After incubation, Stop Solution (2 N H₂SO₄) was added to each well. Plates were read an optical density of 450 with background subtraction at 570 nm using a Tecan plate reader.

Statistical Analysis

Statistical analyses were performed in GraphPad Prism (version 9.5.1) unless otherwise noted. V4 16s sequencing data was analyzed in R (version 4.2.3). Statistical

details including the number of animals or samples can be found in figure legends. Statistical significance was assessed by Mann-Whitney U test when comparing between two groups, or by Two-Way ANOVA with Šídák's multiple comparisons test when comparing >2 groups unless otherwise noted. P values are shown in figures or tables for samples with significant differences. Each data point represents an individual animal, and horizontal bars represent the mean.

Chapter 3: Maternal undernutrition exacerbates microbiota-driven growth stunting through pre and postnatal effects

Part of this chapter has been adapted from “Maternal undernutrition exacerbates microbiota-driven growth stunting through pre and postnatal effects”

Yadeliz A. Serrano Matos, Claire Williams, Jasmine Cano, Lindsey Bihuniak, Aria Kamal, Carrie A. Cowardin. 2025. *bioRxiv*. March 06.

Author contributions:

Conceptualization, Y.S.M and C.A.C.; Sample collection, Y.S.M, J.C., C.W., L. B., A.K. and C.A.C.; Investigation, Y.S.M, and C.A.C., Analysis; Y.S.M, and C.A.C., Visualization, Y.S.M, and C.A.C.; Resources, Y.S.M, C.W., and C.A.C; Funding, Y.S.M. and C.A.C, Supervision, C.A.C; Writing, Y.S.M, and C.A.C.

3.1 Introduction

Linear growth stunting (height-for-age Z score \leq two standard deviations below the WHO median) is a manifestation of undernutrition that affects 20% of children under five years of age in low and middle-income countries (LMICs)⁷. Relative to wasting (characterized by low weight-for-age), stunting has far-reaching consequences throughout the lifespan, including impaired cognitive development, increased rates of infection, and an elevated risk of metabolic disorders⁵. Stunting is an intergenerational and multifactorial syndrome¹⁹, with stunted mothers at higher risk of giving birth to underweight and pre-term newborns that experience stunting soon after birth^{10,105}. Longitudinal studies indicate that the onset of stunting often occurs within the first three months of life, with the reversal of stunting after this critical time period being less likely⁷. Current nutritional interventions have had little success in rescuing stunted growth²¹, indicating the importance of understanding additional factors beyond nutrition that lead to the development and persistence of stunting.

Environmental Enteric Dysfunction (EED) is pervasive in undernourished populations and may in part explain the poor effectiveness of current nutritional therapies¹⁰. EED is characterized by epithelial barrier dysfunction and malabsorption that is thought to be a consequence of microbiome disruption, pathogen carriage and accompanying intestinal inflammation¹⁴⁴. The microbiome plays a crucial role during undernutrition^{40,41,118,145,146}. However, the mechanisms by which microbial communities shape host growth are still being explored. Previous studies have demonstrated that undernourished Malawian children harbor microbiota that are chronologically immature compared to healthy controls⁴¹. Colonization of germ-free mice with these communities

lead to impaired growth, altered bone morphology, and metabolic abnormalities⁴¹. These results suggest compositional changes in the microbiome of undernourished children are linked to long-term growth deficits. Because a significant proportion of childhood stunting emerges *in utero*¹⁰⁵, an emergent hypothesis in the field suggests maternal microbes may also shape long-term growth and immunity during pregnancy and early life¹⁹. Maternal health is critical for healthy fetal development, and studies from high income countries suggest intestinal inflammation can lead to adverse birth outcomes. These findings have led to a renewed focus on maternal intestinal function during pregnancy in LMICs.

We previously demonstrated that intergenerational colonization with microbes from stunted infant donors leads to the development of stunting-like features in a gnotobiotic mouse model of undernutrition¹²². Our findings raised critical questions about when in life growth deficits arose and whether they could be rescued by exposure to healthy microbiota later on. To investigate these questions, we first explored the role of maternal undernutrition in offspring growth. We found that maternal exposure to a nutrient-deficient diet significantly impacted offspring survival in the context of a stunted donor (SD) but not a healthy donor (HD) microbiota. Maternal diet exposure also significantly impacted offspring linear and ponderal growth, intestinal physiology, and metabolism. Notably, maternal undernutrition significantly impacted the composition of the offspring microbiota, leading to increased abundance of *Enterococcus* and *Escherichia coli*. We next used two different cross-fostering approaches to determine the contribution of the maternal microbiota *in utero* and in the postnatal period. We observed that prenatal and postnatal exposures to SD microbiota both contribute to offspring development, with distinct effects on ponderal versus linear growth. This study sheds light

onto the role of maternal nutrition on offspring growth and microbiota development, revealing the importance of targeting diet and microbiota-directed interventions throughout early life.

3.2 Results

Maternal undernutrition exacerbates offspring growth stunting

To investigate the effects of maternal undernutrition on offspring growth, we modified our original intergenerational model of undernutrition discussed in Chapter 2, to include maternal diet and microbiota exposure in early life. In our original No Maternal Undernutrition (NMU) model (**Figure 3.1A**), 4-week-old germ-free sires were colonized with microbiota derived from a healthy or a severely stunted Malawian infant donor and fed a protein and micronutrient-deficient diet representative of what is consumed by this donor population^{41,102,122}. At 8 weeks of age, mice were switched to a nutrient-sufficient diet and 8-week-old germ-free females were introduced into the isolator and co-housed with sires as breeding pairs^{102,122}. Offspring from these breeding mice were weaned into the same undernourished diet as the sires at 3 weeks of age. Because the female mice in this arm of the experiment were not exposed to the M8 diet, these offspring represent the HD-NMU (Healthy Donor, No Maternal Undernutrition) and SD-NMU (Stunted Donor, No Maternal Undernutrition) groups. To more closely model human undernutrition, we also included a second arm of the experiment in which both sires and dams were colonized with donor microbiota and exposed to the M8 diet from 4 to 8 weeks of age (**Figure 3.1B**). At 8 weeks of age, these animals were swapped back to the nutrient-sufficient diet and co-housed as breeding pairs. Offspring of these breeding pairs were

weaned onto the M8 diet as described above. These animals represent the HD-MU (Healthy Donor, Maternal Undernutrition) and SD-MU (Stunted Donor, Maternal Undernutrition) groups. We hypothesized that direct colonization of dams and sires with donor microbiota and consumption of M8 diet for four weeks would exacerbate deficits in growth in both HD and SD groups.

Surprisingly, the introduction of maternal undernutrition in the MU model lead to a significant decrease in offspring survival in SD-MU compared to HD-NMU, SD-NMU and HD-MU pups (**Figure 3.1C**). This effect was reproducible across experiments (across four different iterations of the model – 8 dams/18 litters), with offspring mortality typically occurring within the first week of life. In addition to reducing offspring survival, maternal undernutrition also significantly exacerbated SD-MU growth stunting. At maturity, SD-MU offspring displayed shorter tail length compared to both HD groups as well as to SD-NMU offspring (**Figure 3.1D**). A similar trend was observed for overall weight at maturity (**Figure 3.1E**). These differences were not due to the number of pups per litter and were not sexually dimorphic¹⁰². These results suggest maternal undernutrition worsens growth deficits specifically in the presence of microbiota from a human donor with growth stunting, highlighting the important role of the early life microbiome in shaping long-term growth.

SD microbiota consistently alters small intestinal morphology

In early life, small intestinal function is vital for growth by enabling nutrient absorption and physical and immune protection during the establishment of intestinal microbial communities¹⁴⁷. Alteration in small intestinal tissue architecture is a hallmark

feature of EED which is thought to contribute to malabsorption and perpetuate growth¹⁴⁸. To investigate intestinal morphology, we performed histological scoring of H&E stained ileum tissue sections to assess established histological features of EED, including enterocyte injury and villous architecture^{122,125}. We observed an increase in Enterocyte Injury and Villus Architecture scores in SD-MU offspring compared to HD-MU offspring at maturity¹⁰². We also assessed quantitative measures of small intestinal physiology, including villus length, muscularis thickness, and villus/crypt ratio (**Figure 3.1F-G**). Results demonstrated a significant decrease in average villus length, villus/crypt ratio and muscularis thickness in the ileum of SD-MU compared to HD-MU offspring. No significant difference in crypt length was observed between the groups¹⁰², suggesting the decrease in villus/crypt ratio in 8-week-old SD-MU mice was not due to crypt hyperplasia and instead was caused by a reduction in the length of the villi. None of the differences in intestinal morphology were sexually dimorphic¹⁰².

Reductions in villus length have been associated with impaired gut function in stunted children and other mouse models of diet-dependent enteropathy^{74,149,150}. Taken together, these results suggest that the SD microbiota drives reduced intestinal absorptive surface area in SD-MU offspring at maturity, potentially contributing to impaired growth¹⁰.

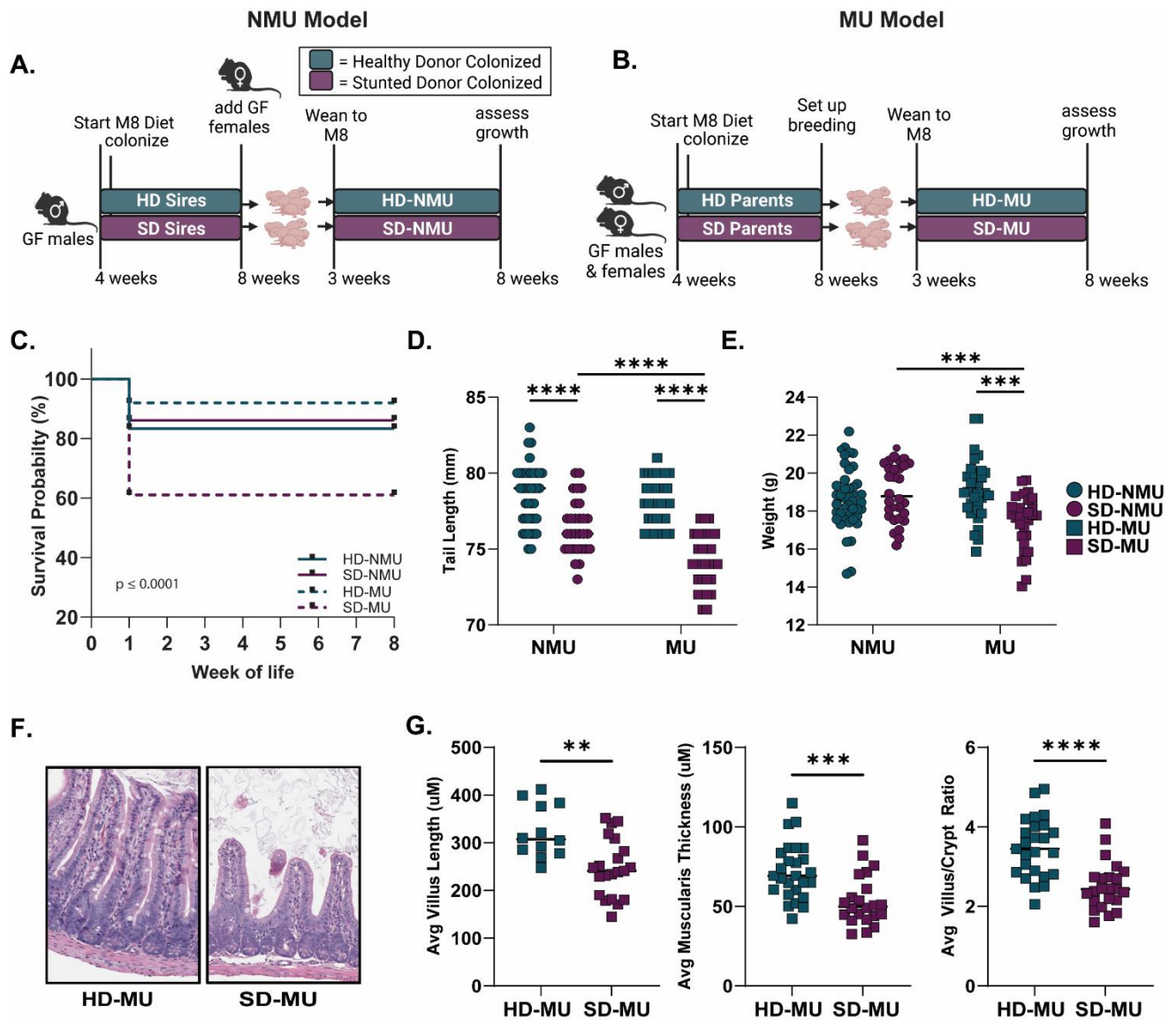


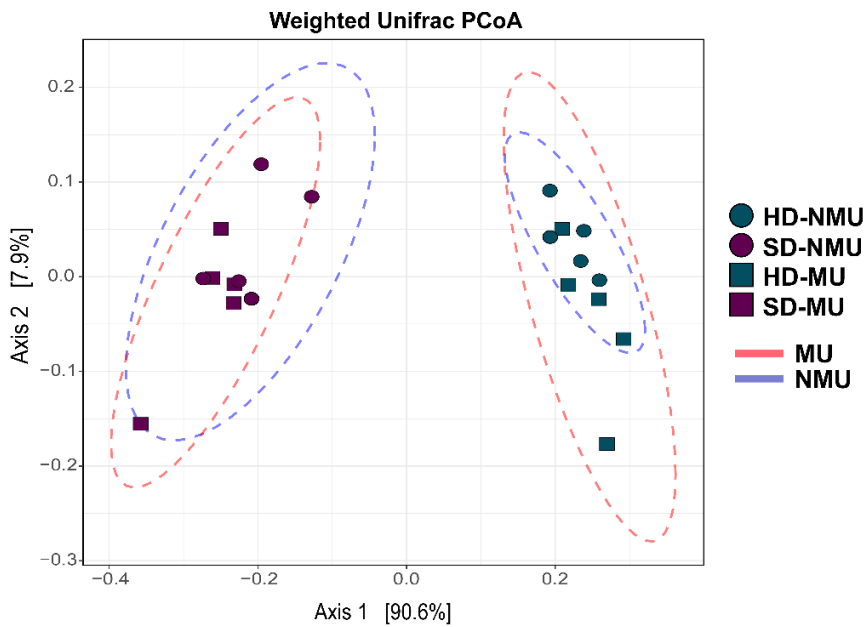
Figure 3.1. Maternal undernutrition exacerbates growth deficits in SD-MU mice. (A-B) Schematic of experimental design (created with Biorender.com). **(C)** Survival probability in both models. **(D)** Tail length at maturity. **(E)** Absolute body weight at maturity. **(F)** Representative histological images of H&E stained ileal tissue at 8 weeks of age. **(G)** Quantification of villus length, villus/crypt ratio and muscularis thickness in 8-week-old mice from NMU and MU models. Each data point represents an individual animal. * $p \leq 0.05$, ** $p \leq 0.01$, *** $p \leq 0.001$, **** $p \leq 0.0001$ by **(C)** Logrank (Mantel-Cox) test **(D-E)** Two-Way ANOVA with Holm-Šídák's multiple

comparisons test or **(G)** Mann-Whitney U test. **(C)** n=108-132 for NMU mice, n=136-149 for MU mice **(D)** n=29-40 for NMU mice, n=30-34 for MU mice **(G)** n = 12-21/group for Villus Length, n=22-25/group for Villus/Crypt Ratio and Muscularis Thickness.

Maternal undernutrition alters the abundance of specific taxa in the SD community

We next sought to investigate whether maternal undernutrition influenced the composition of the offspring microbiota at maturity. To address this question, we performed V3-V4 16s rRNA sequencing on the feces of offspring at 8 weeks of age. Principle Coordinate Analysis (PCoA) of Weighted UniFrac distances revealed that microbiota differences were largely driven by the donor microbiota received at birth (PERMANOVA, $R^2=.8742$, p-value ** ≤ 0.001), (**Figure 3.2A**, see Appendix A **Table 3.1**). However, there was a significant but modest difference in community composition due to maternal nutritional status within each donor context (p-value = 0.023, see Appendix A **Table 3.1**). Interestingly, this result was primarily driven by microbiota composition in SD pups rather than HD pups (**Figure 3.2B**, see Appendix A **Table 3.3-3.4**).

A.



B.

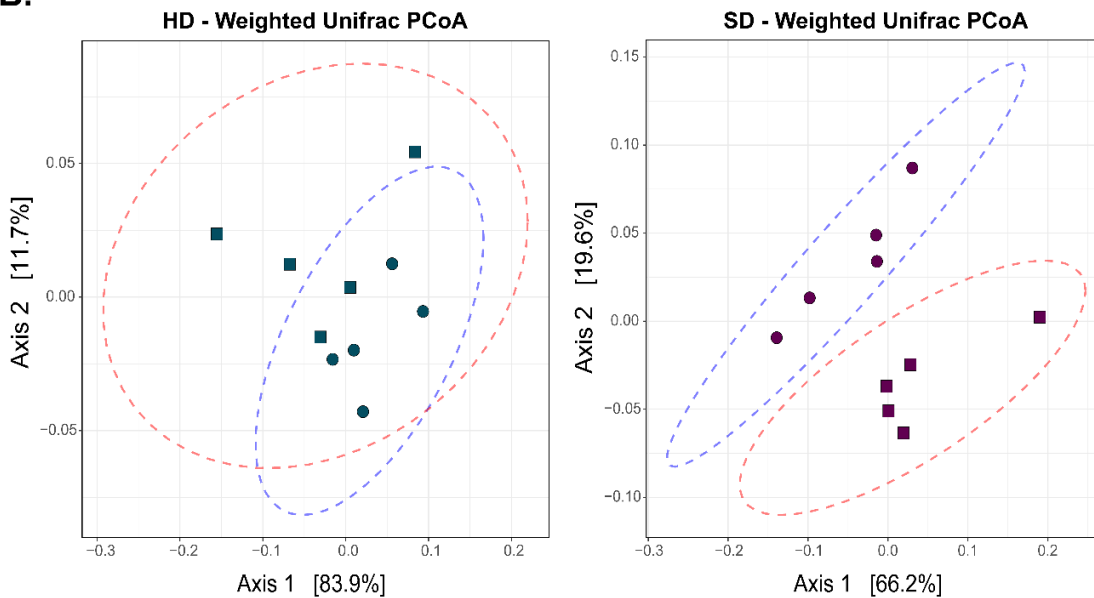


Figure 3.2. Maternal undernutrition alters the SD microbiota at maturity. Principal Component Analysis (PCoA) of Weighted Unifrac distances of the fecal microbiota measured by V3-V4 16s rRNA sequencing in **(A)** NMU and MU offspring of both donors **(B)** HD offspring and SD offspring individually. * $p \leq 0.05$, ** $p \leq 0.01$, *** $p \leq 0.001$, **** $p \leq 0.0001$ by **(A-B)** PERMANOVA and Pairwise Adonis. **(A-B)** $n=5/\text{group}$ [3 females and 2 males].

We next calculated alpha diversity by Shannon Diversity Index. Although the SD community had higher diversity overall, there was no significant difference in diversity between SD-NMU and SD-MU offspring (**Figure 3.3A**). However, when we quantified the number of ASVs present in each group, we observed that both SD and HD MU offspring had significantly more ASVs detected compared to offspring of non-malnourished dams (**Figure 3.3B**). We then explored differences in community composition in further detail (**Figure 3.3C**).

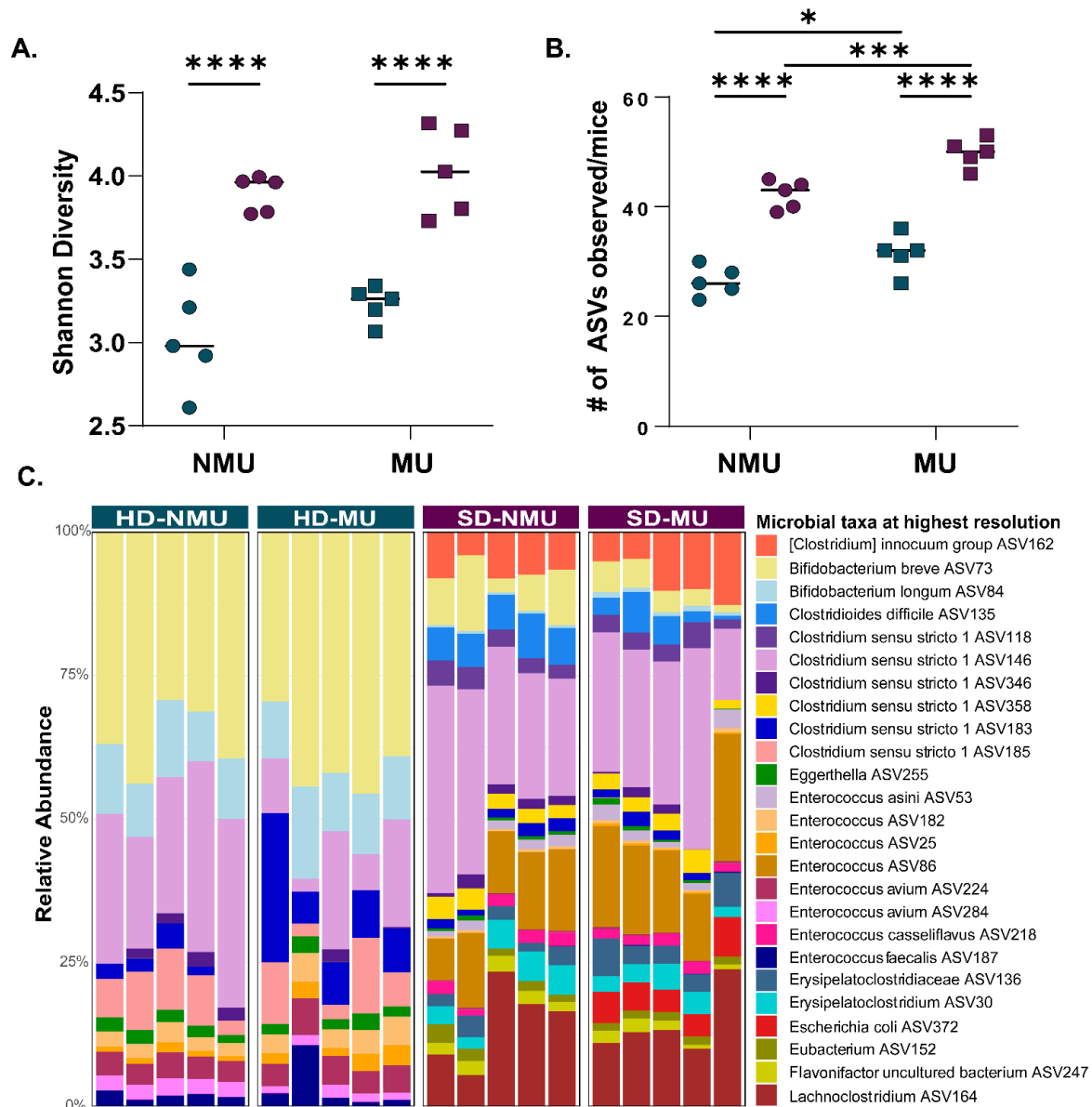


Figure 3.3. Maternal undernutrition increases α -diversity and the total number of microbes in the microbiota of offspring at maturity. (A) Shannon Diversity Index for NMU and MU mice. **(B)** Absolute number of observed ASVs in NMU and MU mice. **(C)** Stacked bar plot of the 25 most abundant taxa across NMU and MU mice. * $p \leq 0.05$, ** $p \leq 0.01$, *** $p \leq 0.001$, **** $p \leq 0.0001$ by **(A-B)** Two-Way ANOVA with Šídák's multiple comparisons test. **(A-C)** $n=5$ /group [3 females and 2 males].

SD-MU animals exhibit elevated levels of *Escherichia coli* at maturity

Major compositional differences between the SD and HD groups included lower relative abundance of *Bifidobacterium breve* in the SD community (**Figure 3.4A**), which did not change significantly based on maternal nutritional status (**Figure 3.4B**). However, maternal undernutrition did significantly increase the relative abundance of *Enterococcus* species as well as *Escherichia coli* while reducing the abundance of *Clostridium difficile* in SD-MU relative to SD-NMU offspring (**Figure 3.4C-D**). Thus, maternal undernutrition significantly impacted specific taxa within the SD community without altering the HD community profile. In particular, maternal undernutrition increased the abundance of two potential pathobionts within the SD microbiota. Pathogenic *Escherichia coli* are pervasive in undernourished populations and are capable of driving intestinal inflammation¹⁵¹ while *Enterococcus spp.* can become pathobionts in the immunocompromised host¹⁵². Although we cannot identify these ASVs as definitive pathogens based on these sequencing results, our findings highlight the importance of future investigation to determine what role *Enterococcus spp.* and *Escherichia coli* play in shaping early life growth outcomes in this model.

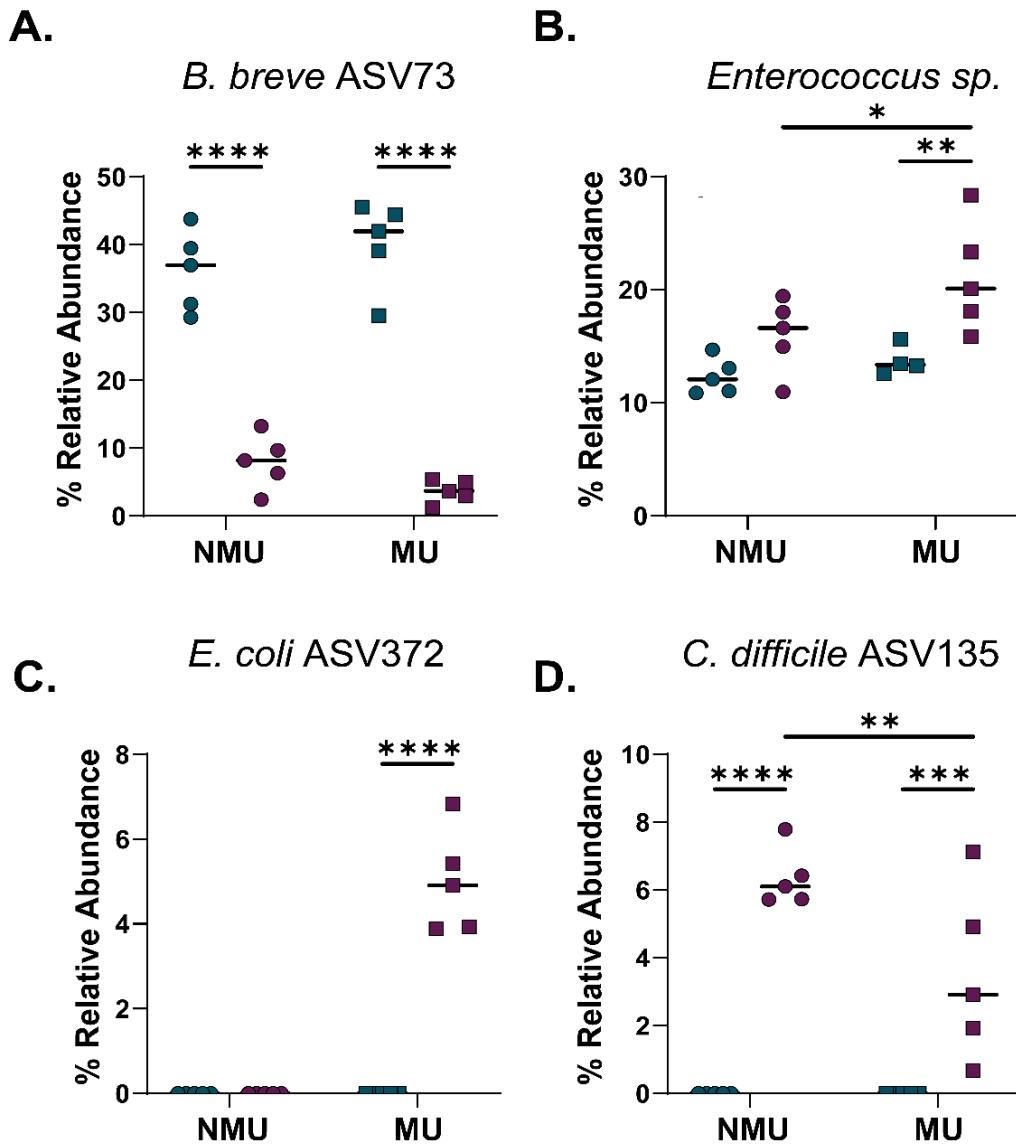


Figure 3.4. SD-MU animals exhibit an increased relative abundance of *Enterococcus* sp. and *Escherichia coli* at maturity. (A) % Relative abundance of *Bifidobacterium breve*, (B) *Enterococcus* spp., (C) *Escherichia coli*, and (D) *Clostridioides difficile* in NMU and MU animals. Each point represents one mouse. * $p \leq 0.05$, ** $p \leq 0.01$, * $p \leq 0.001$, **** $p \leq 0.0001$ by (A-D) Two-Way ANOVA with Šídák's multiple comparisons test (A-D) $n=5$ /group [3 females and 2 males].**

SD-MU offspring are born underweight and develop linear growth deficits after weaning

Because SD-MU offspring showed reduced survival soon after birth, we hypothesized that growth deficits would occur in the early postnatal period. To explore this possibility, we measured linear growth weekly starting in the first week of life. SD-MU offspring displayed significantly reduced tail length compared to HD-MU offspring starting at 4-weeks of age, one week after weaning onto the M8 diet (**Figure 3.5A**). In contrast, SD-MU pups had significantly decreased absolute body weight starting in the first week of life (**Figure 3.5B**). Rates of weight gain between SD-MU and HD-MU pups did not significantly differ over this time period (**Figure 3.5C**), suggesting that initial weight deficits in SD-MU pups were driving the observed reductions in weight at later time points. We next measured body weight in 1-day-old neonates, and again observed a reduction in body weight in SD-MU pups¹⁰². These results suggested that prenatal factors could be driving reduced ponderal growth in this group.

Early life undernutrition is strongly correlated with reduced Insulin-like Growth Factor 1 (IGF-1) in humans, and IGF-1 levels are predictive of later growth^{54,153}. This hormone is also influenced by intestinal microbes in other mouse models of undernutrition and growth stunting^{56,154}. Because we observed major growth deficits in SD-MU offspring, we next measured IGF-1 in the liver of these mice. SD-MU offspring exhibited a significant reduction in liver IGF-1 protein levels at 2, 4 and 8 weeks of life (**Figure 3.5D**). Because linear growth deficits in SD-MU pups began at 4 weeks, we hypothesized SD-MU pups would exhibit features of EED at this time point. To explore this, we assessed histological features of the small intestine. SD-MU mice had a significantly

higher histology score for both villus architecture and enterocyte injury compared to HD-MU mice at 4 weeks¹⁰². Quantification of villus length, villus/crypt ratio and muscularis thickness revealed a significant decrease for these three parameters in 4-week-old SD-MU relative to HD-MU mice (**Figure 3.5E-F**). These differences were not due to crypt hyperplasia and were not sexually dimorphic¹⁰². This suggests that as early as one-week post-weaning, SD-MU mice begin to develop intestinal dysfunction that may contribute to growth deficits over time.

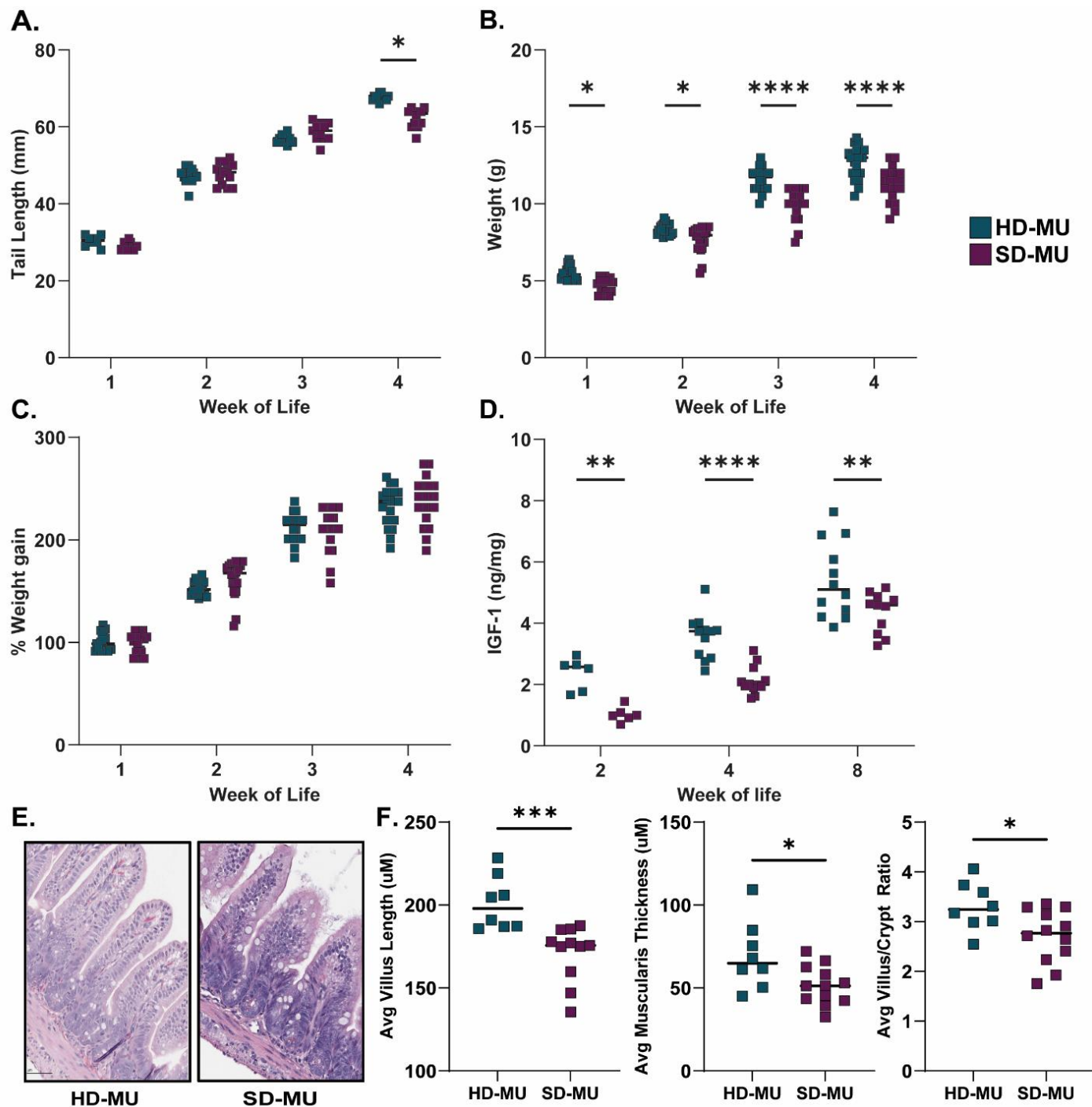


Figure 3.5. Microbiota composition in early life shapes physiological development. (A) Tail length and **(B)** absolute body weight in early life. **(C)** Percentage of weight gain over time. **(D)** Measurement of IGF-1 in liver tissue by ELISA in offspring from birth to maturity. **(E)** Representative histological images of H&E stained ileal tissue at 4 weeks of age. **(F)** Quantification of villus length, villus/crypt ratio and muscularis thickness in 4-week-old offspring

from the MU group. Each point represents an individual mouse. Data shown includes equal number of female and male healthy donor colonized mice and stunted donor colonized mice unless otherwise specified. **(D)** 2-week-old SD-MU n= 4M/2F. **(F)** HD-MU n=9 (7M/2F), SD-MU n=12(5M/7F). * $p \leq 0.05$, ** $p \leq 0.01$, *** $p \leq 0.001$, **** $p \leq 0.0001$ by **(A-D)** Two-Way ANOVA with Holm-Šídák's multiple comparisons test or **(F)** Mann-Whitney test.

The weaning phase shapes community composition and the abundance of specific taxa.

We next tracked microbiota establishment in early life to assess how these communities developed. We calculated weighted Unifrac distances (**Figure 3.6A**) for both HD-MU and SD-MU offspring, which showed that the age of the mice explained 92% of the differences within the HD group (see Appendix A **Table 3.5**). Pairwise comparisons of microbiota composition overtime showed significant differences between all times points (see Appendix A **Table 3.6**). Interestingly, differences in microbiota were explained the most by age (97%) when comparing HD-MU 2-week-old and 4-week-old mice (1 week before and after weaning), suggesting weaning and the introduction of the M8 diet strongly shapes the microbiota of HD-MU mice. In contrast, age explained a lower proportion of variance (64%) in SD-MU mice over time, although this result remained significant (**Figure 3.6B**, see Appendix A **Table 3.7-3.8**).

We next explored differences in early life community composition in further detail. Major compositional differences between the SD-MU and HD-MU groups over time included higher absolute number of ASVs and increased alpha diversity in SD-MU offspring in early life (**Figure 3.6C**)¹⁰². Interestingly, *Bifidobacterium breve* levels were comparable between 2- and 3-week-old HD-MU and SD-MU offspring. However, a

significant decrease in this ASV was observed in SD-MU mice after weaning and the introduction of the M8 diet, while levels remained stable in HD-MU mice (**Figure 3.6D**). Furthermore, we observed a decrease in the relative abundance of *Escherichia coli* in SD-MU offspring during weaning compared to pre-weaning and post-weaning time points (**Figure 3.6E**). These results highlight the importance of the weaning transition in shaping the gut microbiota in the MU model.

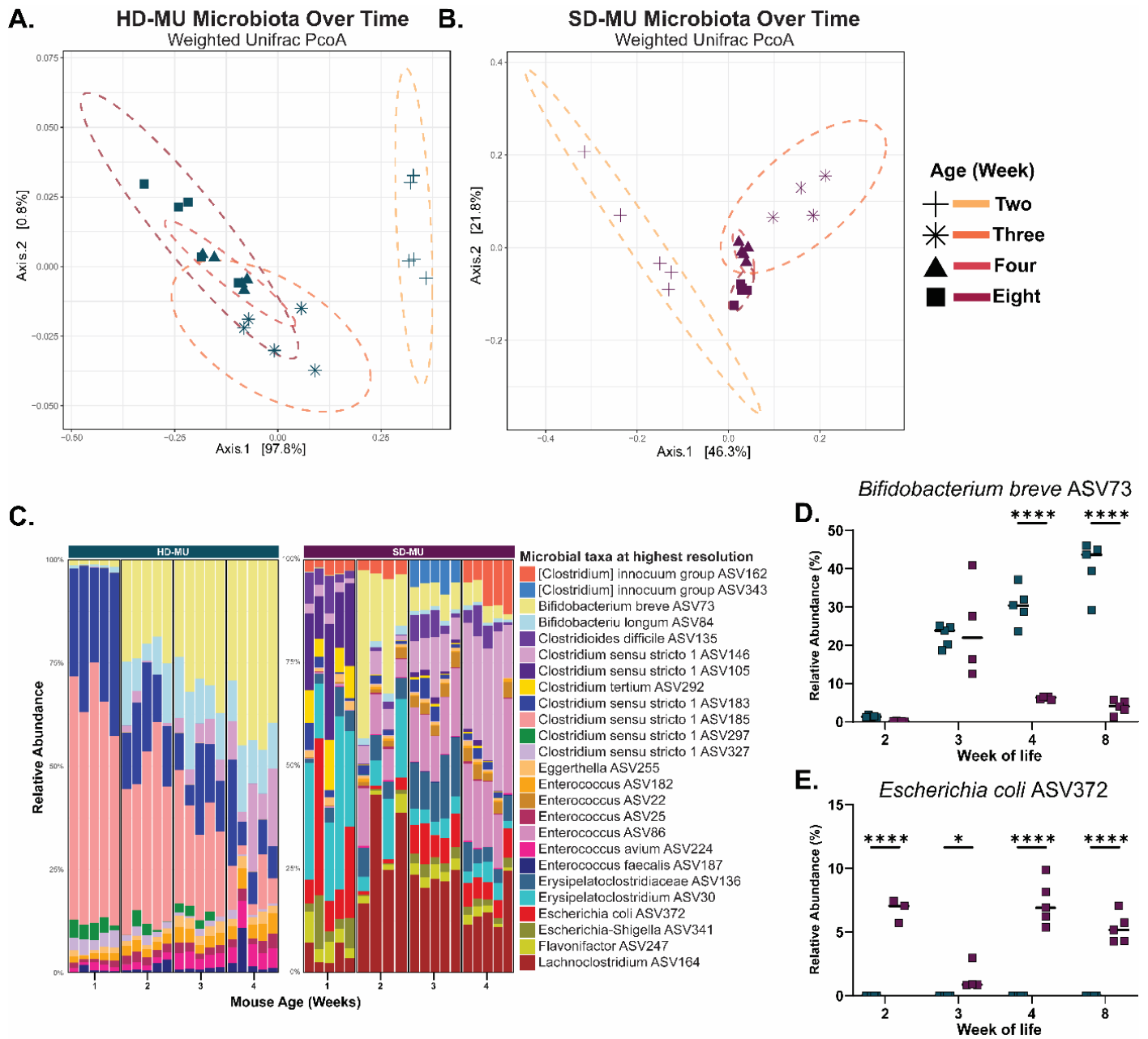


Figure 3.6. Development of the microbiota in early life. (A-B) Weighted Unifrac PCoA of the fecal microbiota measured by V3-V4 16s rRNA sequencing. **(C)** Stacked bar plot of the 25 most abundant taxa in HD-MU and SD-MU offspring in early life. **(D)** % Relative abundance of *Bifidobacterium breve* ASV73. **(E)** Relative abundance of *Escherichia coli* ASV372. Each individual point represents one mouse. * $p \leq 0.05$, ** $p \leq 0.01$, *** $p \leq 0.001$, **** $p \leq 0.0001$ **(A-B)**

PERMANOVA and Pairwise Adonis **(D-E)** Two-Way ANOVA with Holm-Šídák's multiple comparisons test. **(A-E)** n=5/group [3 females and 2 males].

Postnatal microbiota exposure shapes linear growth

Recent findings suggest undernutrition during pregnancy is associated with alterations in the maternal gut microbiota and changes in fetal development *in utero*¹⁵⁵. Because we observed reductions in weight in SD-MU offspring beginning in the first week of life, we next sought to investigate the relative contribution of prenatal versus postnatal microbial colonization. To do so, we made use of a cross-fostering system in which germ-free offspring born to undernourished germ-free parents were fostered immediately after birth by either an HD-MU or SD-MU dam (**Figure 3.7A**). After cross-fostering, pups were once again weaned onto the M8 diet at three weeks of age. At maturity, germ-free mice cross-fostered to HD dams (GF-HD pups) displayed similar tail length compared to HD pups reared by HD dams. Similarly, germ-free mice cross fostered to SD dams (GF-SD pups) exhibited similar tail length to SD pups reared by SD dams (**Figure 3.7B**). Furthermore, GF-SD pups exhibited similar body weight to SD-MU pups at maturity, while GF-HD pups gain similar body weight compared to HD-MU pups (**Figure 3.7C**), suggesting postnatal exposure to the maternal microbiome or other maternal factors were sufficient to drive growth differences in these groups. In contrast to SD-MU animals, deficits in ponderal growth in GF-SD pups were observed starting at 1 week post-weaning¹⁰².

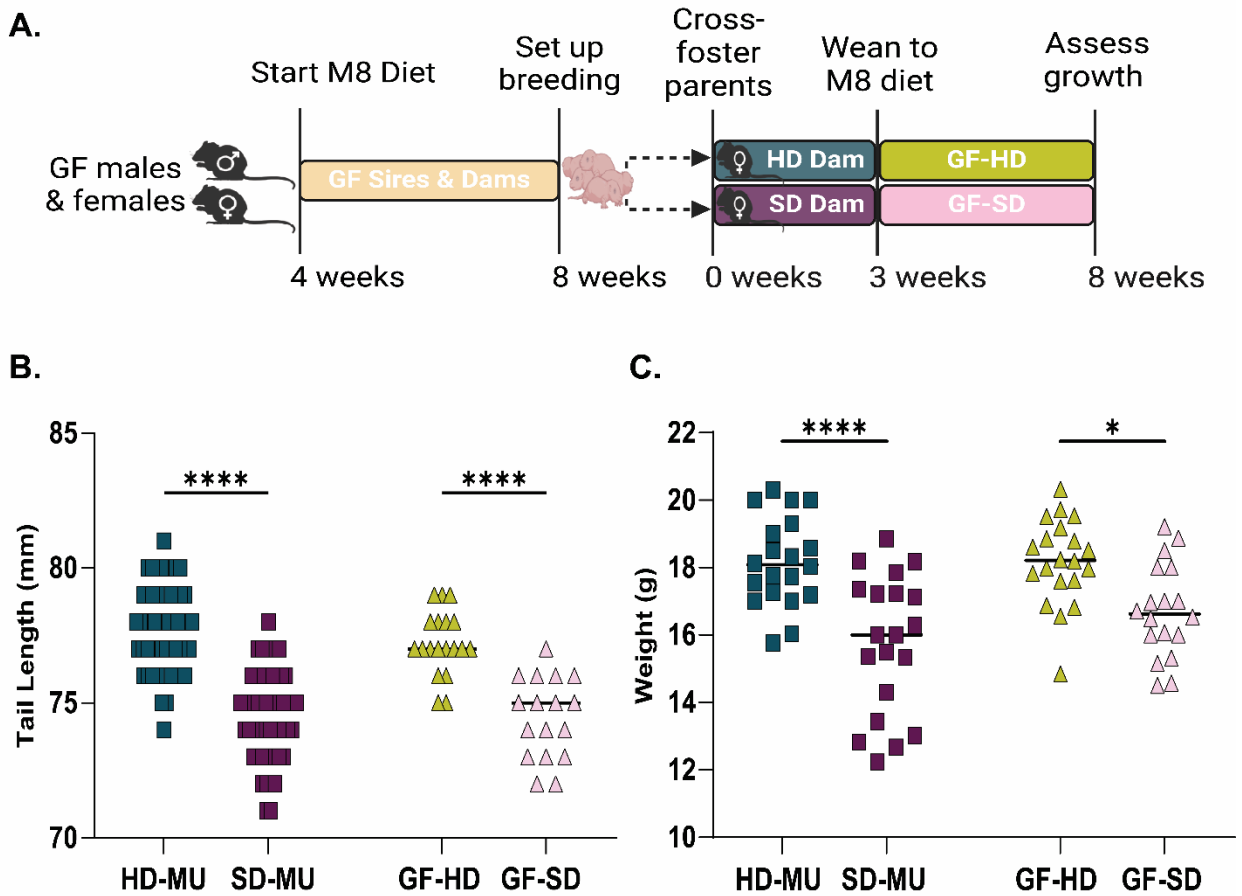


Figure 3.7. Postnatal exposure to SD microbiota is sufficient to drive long-term growth deficits. **(A)** Schematic of experimental design (created with Biorender.com). All measurements were performed at maturity (8 weeks). **(B)** Tail length. **(C)** Absolute body weight. Each point represents an individual animal. * $p \leq 0.05$, ** $p \leq 0.01$, *** $p \leq 0.001$, **** $p \leq 0.0001$ by **(B-C)** Two-Way ANOVA with Šídák's multiple comparisons test

Cross-fostered offspring show reduced abundance of *Bifidobacterium breve*

Due to the similarities in growth in GF-SD and SD-MU mice, we hypothesized that these animals would have a similar microbiome composition. Weighted UniFrac analysis of V3-V4 16S sequencing of the fecal microbiota at maturity demonstrated that cross-fostered GF pups clustered by donor with offspring born to colonized dams (**Figure 3.8A**), suggesting overall similar microbiome composition (**Figure 3.8B**). However, pairwise comparisons demonstrated significant differences between HD-MU, SD-MU, GF-HD, and GF-SD animals (see Appendix A **Table 3.9**). Interestingly, when comparing the colonization of *Bifidobacterium breve* in cross-foster groups, we observed that both GF-HD and GF-SD mice exhibited reduced relative abundance of this ASV at maturity compared to HD-MU and SD-MU offspring (**Figure 3.8C**). In contrast, *Escherichia coli* was present in GF-SD at a similar abundance to SD-MU mice (**Figure 3.8D**). These data could suggest that *Bifidobacterium breve* colonization may be more strongly shaped either by mode of acquisition (either at birth or in the postnatal period) or by prenatal maternal influences compared to *Escherichia coli*.

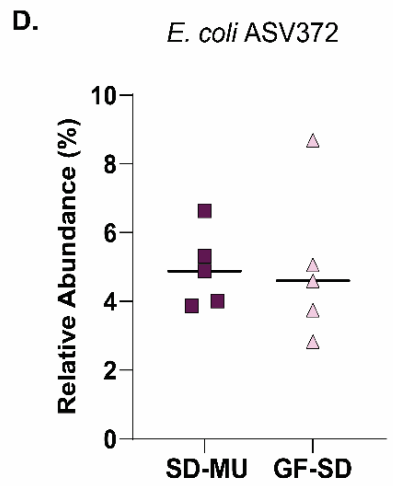
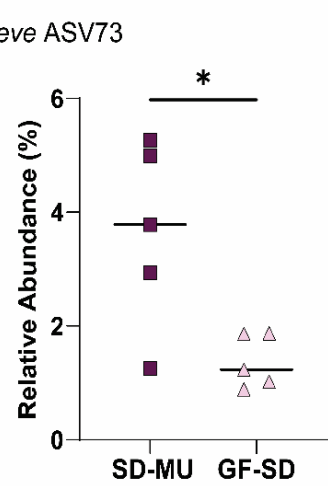
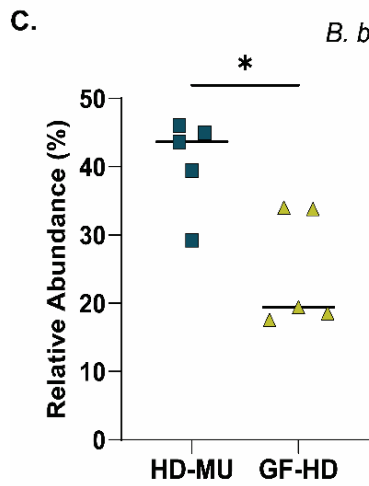
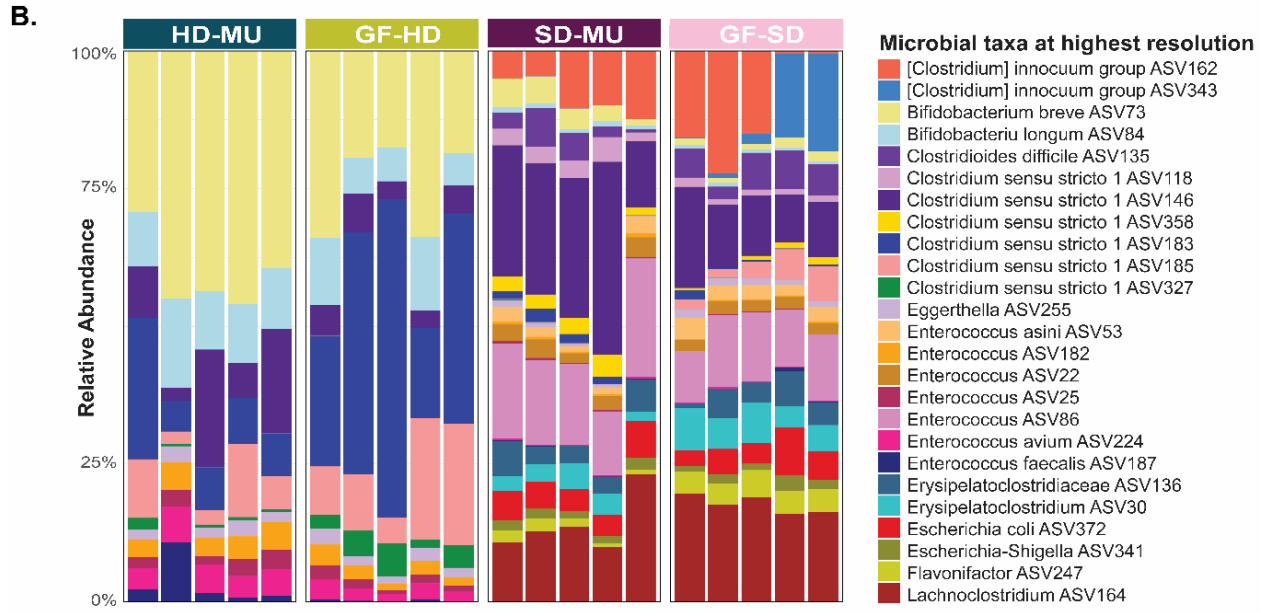
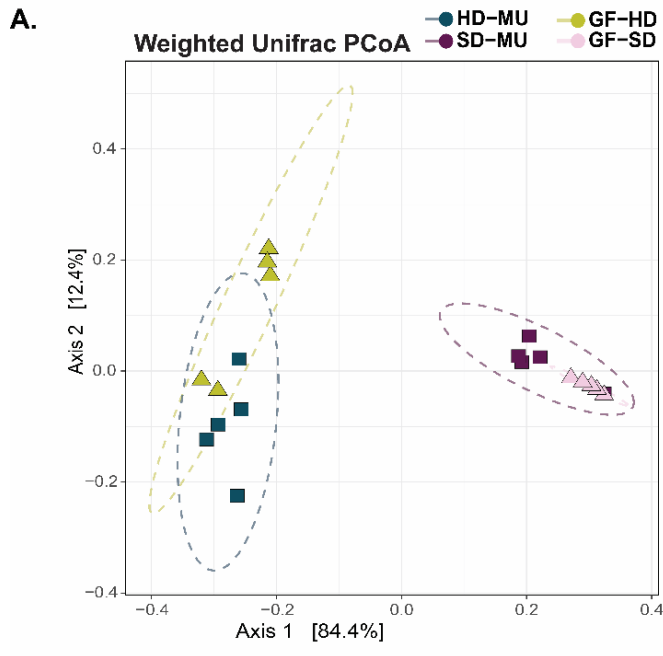


Figure 3.8. No exposure *in utero* to microbes leads to reduced levels *Bifidobacterium breve* at maturity. (A) Weighted Unifrac Principal Component Analysis (PCoA) of the fecal microbiome by V3-V4 16s rRNA sequencing. **(B)** 25 most abundant taxa across all groups. **(C)** Relative abundance of *Bifidobacterium breve* and **(D)** *Escherichia coli*. Each point represents an individual animal. * $p \leq 0.05$, ** $p \leq 0.01$, *** $p \leq 0.001$, **** $p \leq 0.0001$ by **(A)** PERMANOVA and **(C-D)** Mann-Whitney U test. **(A-D)** $n=5$ /group [3 females and 2 males].

Postnatal exposure is insufficient to shape some aspects of intestinal morphology

Low levels of IGF-1 are a strong predictor of reduced linear growth in stunted children and murine models of undernutrition^{54–56}. Therefore, we next measured IGF-1 levels in cross-fostered animals and observed a trend towards a reduction of this protein in the liver of GF-SD mice compared to GF-HD mice at maturity (**Figure 3.9A**). To explore this further, we assessed the role of the postnatal microbiome in intestinal morphology by histological scoring of H&E stained ileum sections from cross-fostered GF offspring. Scores for enterocyte injury and villus architecture were increased in GF-SD compared to GF-HD mice¹⁰². Quantitative measurements of villus length and muscularis thickness at maturity revealed no significant differences in SD-MU, GF-HD, and GF-SD groups (**Figure 3.9B-D**). Similarly, we also did not observe a significant difference in average villus/crypt ratio between GF-HD and GF-SD pups (**Figure 3.9E**). We next measured average crypt length to determine if the decrease in villus/crypt ratio is a result of crypt hyperplasia, but did not observe significant differences¹⁰². Likewise, we did not observe differences in histological parameters by sex¹⁰². The results from these cross-fostering experiments suggest that exposure to microbes in the SD community immediately after birth is sufficient to drive reductions in linear and ponderal growth that manifest after

weaning. In addition, germ-free cross-fostered mice show distinct intestinal morphology compared to SD-MU and HD-MU controls, suggesting prenatal exposure to the microbiota may contribute to these outcomes.

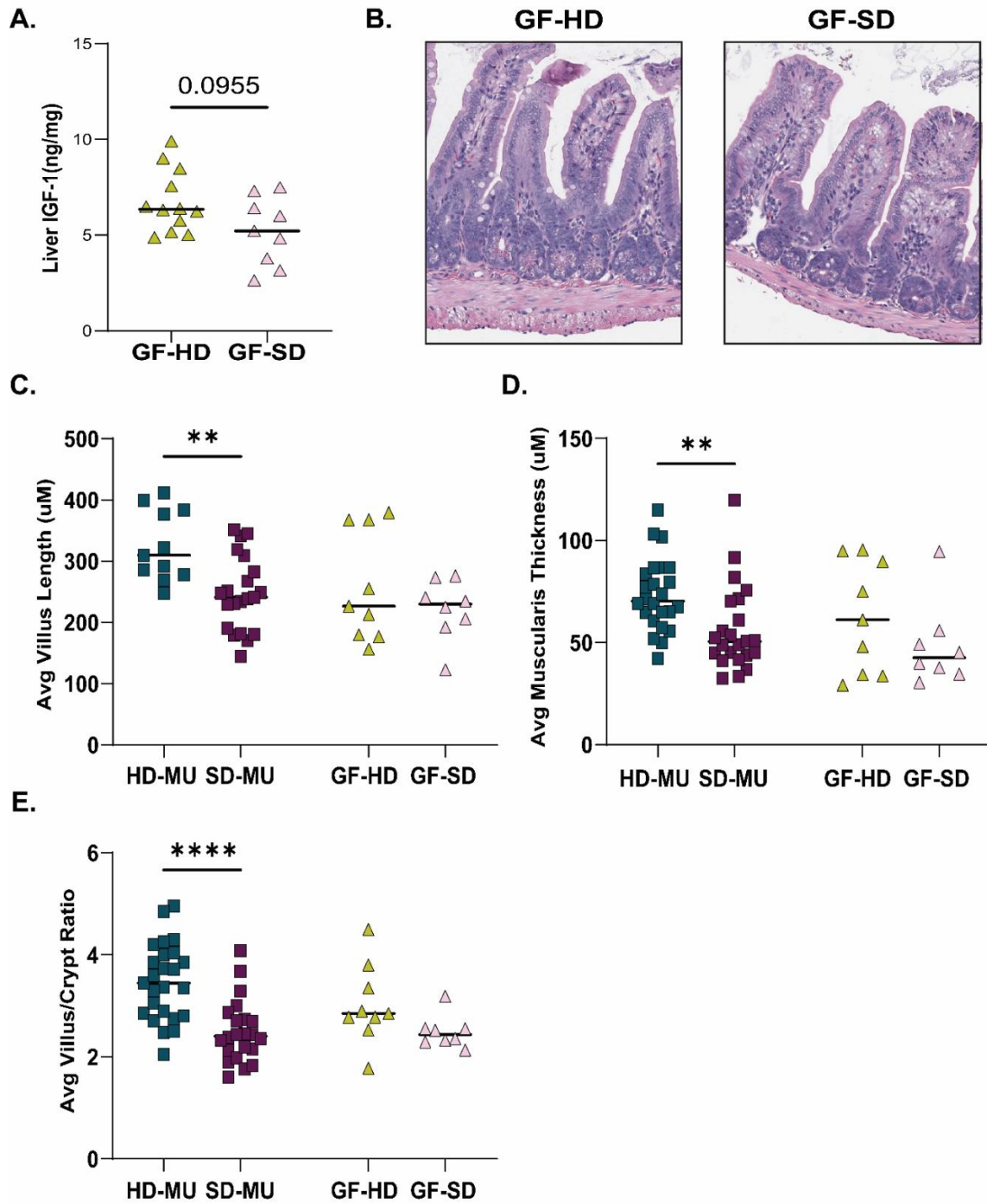


Figure 3.9. Postnatal exposure to SD microbiota is insufficient to shape intestinal morphology at maturity. (A) IGF-1 levels by ELISA in liver tissue of GF-HD and GF-SD. **(B)** Representative histological images of H&E stained ileal tissue at 8 weeks of age. **(C)** Quantification of villus length. **(D)** Quantification of muscularis thickness. **(E)** Quantification of villus/crypt ratio. Each point represents an individual animal. **(C-E)** GF-HD n=9, 4F/5M, GF-SD n=9 4F/4M. MU mice n = 12-21/group for Villus Length, n=22-25/group for Villus/Crypt Ratio and Muscularis Thickness. * $p \leq 0.05$, ** $p \leq 0.01$, *** $p \leq 0.001$, **** $p \leq 0.0001$ by **(C-E)** Two-Way ANOVA with Šídák's multiple comparisons test or **(A)** Mann-Whitney U test.

Long-term growth outcomes are shaped by prenatal and postnatal exposures

To further explore the relative contribution of prenatal versus postnatal microbiota exposure in this model of undernutrition, we next employed a second cross-foster approach in which litters born to HD and SD dams were cross-fostered to the opposite dam at birth (**Figure 3.10A**). Consistent with previous experiments, pups were weaned onto the M8 diet at 3 weeks of age. At 8 weeks of age, these animals were euthanized to assess growth and changes in intestinal morphology. Tail length measurements at maturity revealed that SD, SD-HD (SD pups reared by HD dams) and HD-SD (HD pups reared by SD dams) pups exhibited significantly shorter tails compared to HD pups; however, HD-SD pups had significantly longer tails than SD-HD pups (**Figure 3.10B**). Interestingly, HD-MU and HD-SD pups had significantly increased absolute body weight at maturity compared to SD-MU and SD-HD pups (**Figure 3.10C**) while IGF-1 protein levels in the liver were significantly reduced in SD, SD-HD and HD-SD groups relative to HD pups alone (**Figure 3.10D**). These results suggest any exposure to the SD microbiota

negatively impacted growth, but pups born to HD dams had slightly better growth outcomes than those born to SD dams.

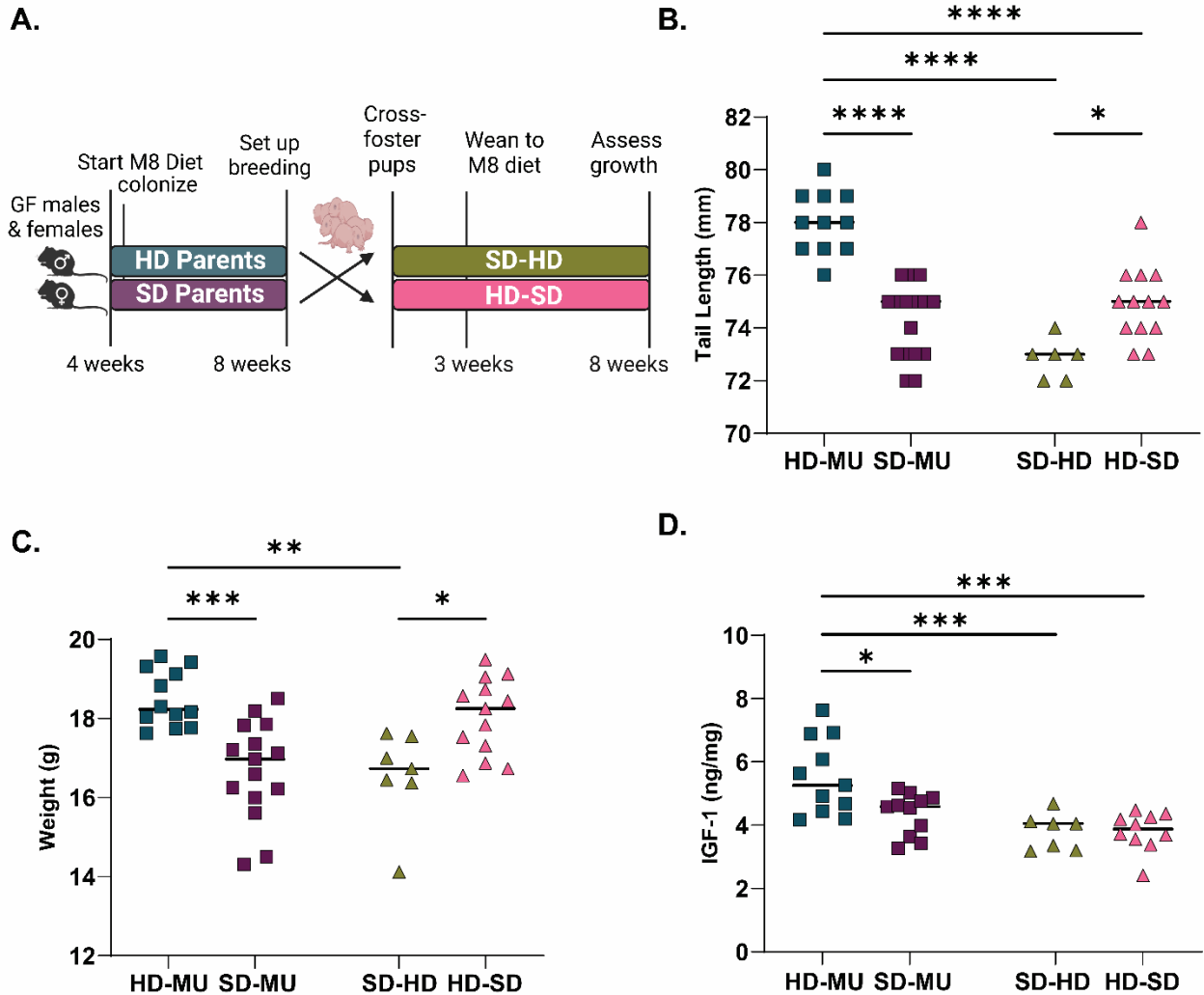


Figure 3.10. Postnatal exposure to SD microbiota negatively impacts linear but not ponderal growth. (A) Schematic of experimental design (created with Biorender.com). All measurements were performed at maturity (8 weeks of age). (B) Tail length. (C) Absolute body weight. (D) IGF-1 by ELISA in liver tissue. Each point represents an individual animal. * $p \leq 0.05$, ** $p \leq 0.01$, *** $p \leq 0.001$, **** $p \leq 0.0001$ by (B-D) Two-Way ANOVA with Šídák's multiple comparisons test.

Postnatal exposure to SD microbiota replaces HD microbiota at maturity.

We next investigated how the cross-fostering approach shaped the offspring microbiota. Analysis of Weighted UniFrac distances revealed HD-SD, SD-HD and SD-MU pups cluster closely together and form a distinct group compared to HD pups (**Figure 3.11A**), suggesting these animals have a more similar microbiome composition (**Figure 3.11B**). However, we did identify significant differences in composition between all groups at maturity (see Appendix A **Table 3.11**). Birth dam significantly influenced community composition ($R^2=0.25$, p -value=0.001, see Appendix A **Table 3.12**) as did the foster dam, with postnatal factors explaining slightly more of the differences at maturity ($R^2=0.34$, p -value=0.001). Interestingly, HD-SD and SD-HD pups had a significant increase in the number of ASVs in the community, similar to SD-MU mice¹⁰². Furthermore, cross-fostered mice also had an increase in alpha diversity similar to SD-MU offspring¹⁰².

We also observed a reduction in the relative abundance of *Bifidobacterium breve* in HD-SD and SD-HD mice at maturity relative to HD-MU offspring (**Figure 3.11C**), with a corresponding increase in *Escherichia coli* (**Figure 3.11D**). Interestingly, cross-fostered offspring showed a significant decrease in the relative abundance of *Enterococcus* spp., suggesting exposure to the HD microbiota can reduce the abundance of these taxa (**Figure 3.11E**). Overall, these results suggest that the SD community largely overtakes the HD community in pups born to HD dams but reared by SD dams. This exposure significantly impacts offspring growth, resulting in HD-SD pups that have reduced tail length and IGF-1 relative to HD pups alone.

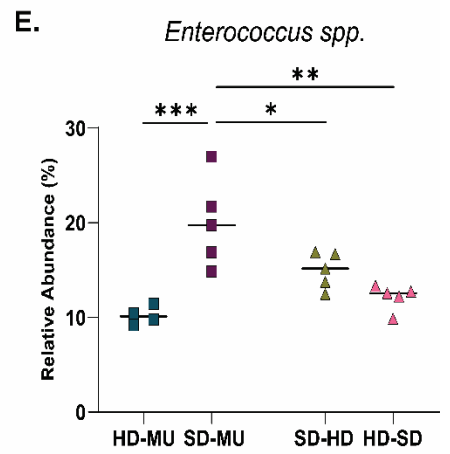
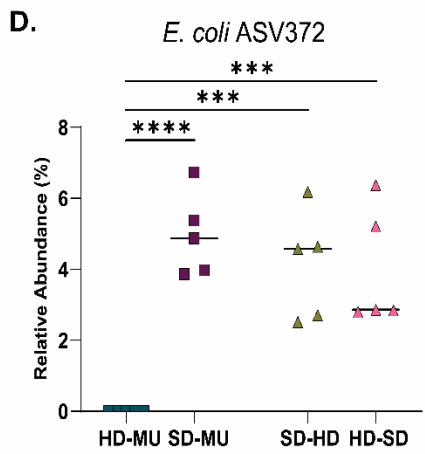
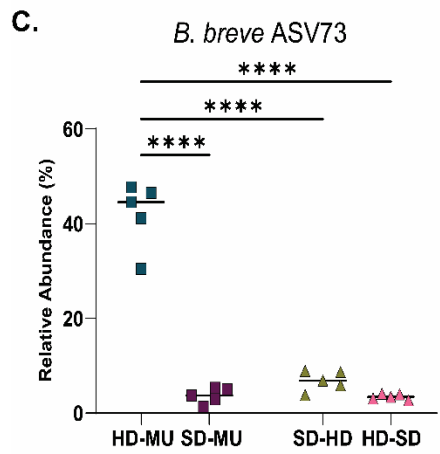
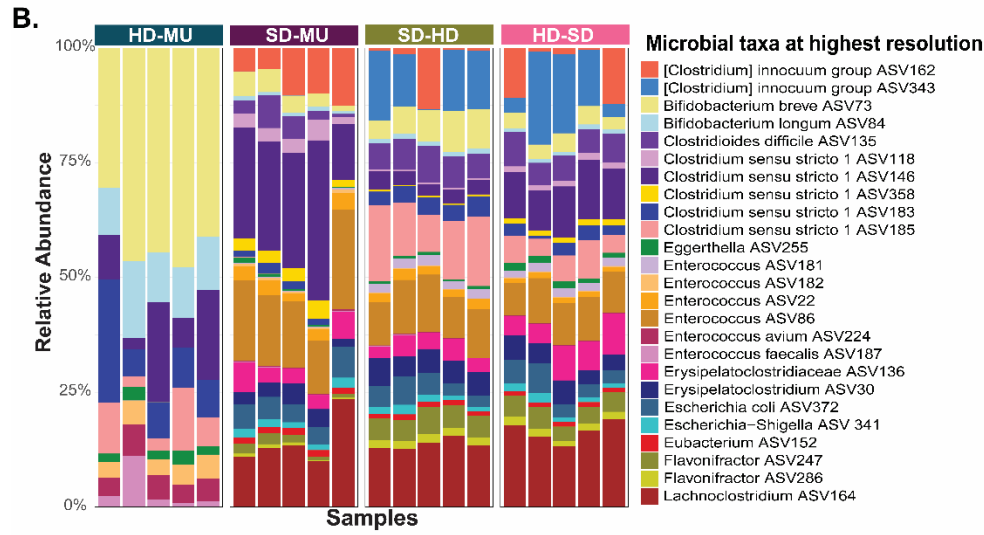
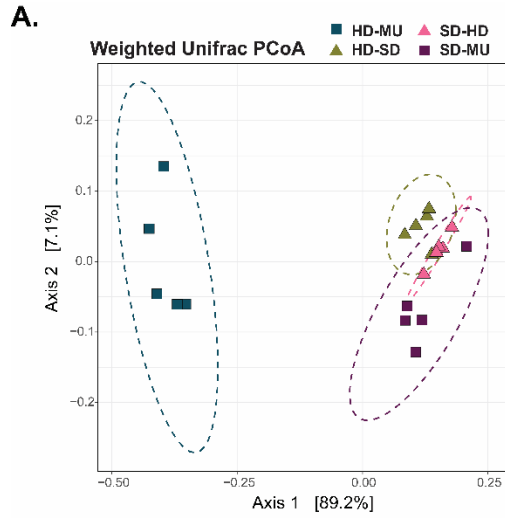


Figure 3.11. Postnatal exposure to SD microbiota displaces HD microbiota at maturity. (A) Weighted UniFrac Principal Component Analysis of the fecal microbiota, as measured by V3-V4 16S rRNA sequencing. **(B)** Stacked bar plot of the 25 most abundant taxa across groups. **(C)** Relative abundance of *Bifidobacterium breve* ASV43. **(D)** Relative abundance of *Escherichia coli* ASV372. **(E)** Relative abundance of *Enterococcus* spp. Each point represents an individual animal. All data presented was collected at maturity (8 weeks of age). * $p \leq 0.05$, ** $p \leq 0.01$, *** $p \leq 0.001$, **** $p \leq 0.0001$ by **(C-E)** Two-Way ANOVA with Šídák's multiple comparisons test or **(A)** PERMANOVA and Pairwise Adonis comparisons.

Pre and postnatal factors influence intestinal morphology at maturity

As a potential underlying mediator for changes in growth, we next investigated whether different windows of microbiota exposure influenced intestinal morphology in cross-fostered pups. Histological scoring did not reveal significant differences in enterocyte and villus architecture for cross-fostered mice, although HD-SD mice did show reduced crypt length relative to SD-HD animals¹⁰². Interestingly, HD, HD-SD and SD-HD pups exhibited similar villus length that was significantly greater than that of SD pups, and villus/crypt ratio followed a similar trend (**Figure 3.12A-C**). However, we observed a significant decrease in muscularis thickness for SD, SD-HD, and HD-SD pups compared to HD pups (**Figure 3.12D**). Thus, measurements of muscularis thickness in the small intestine appear to more closely correlate with growth outcomes in these animals. Overall, these results suggest microbiota exposure in early life influences specific aspects of intestinal morphology.

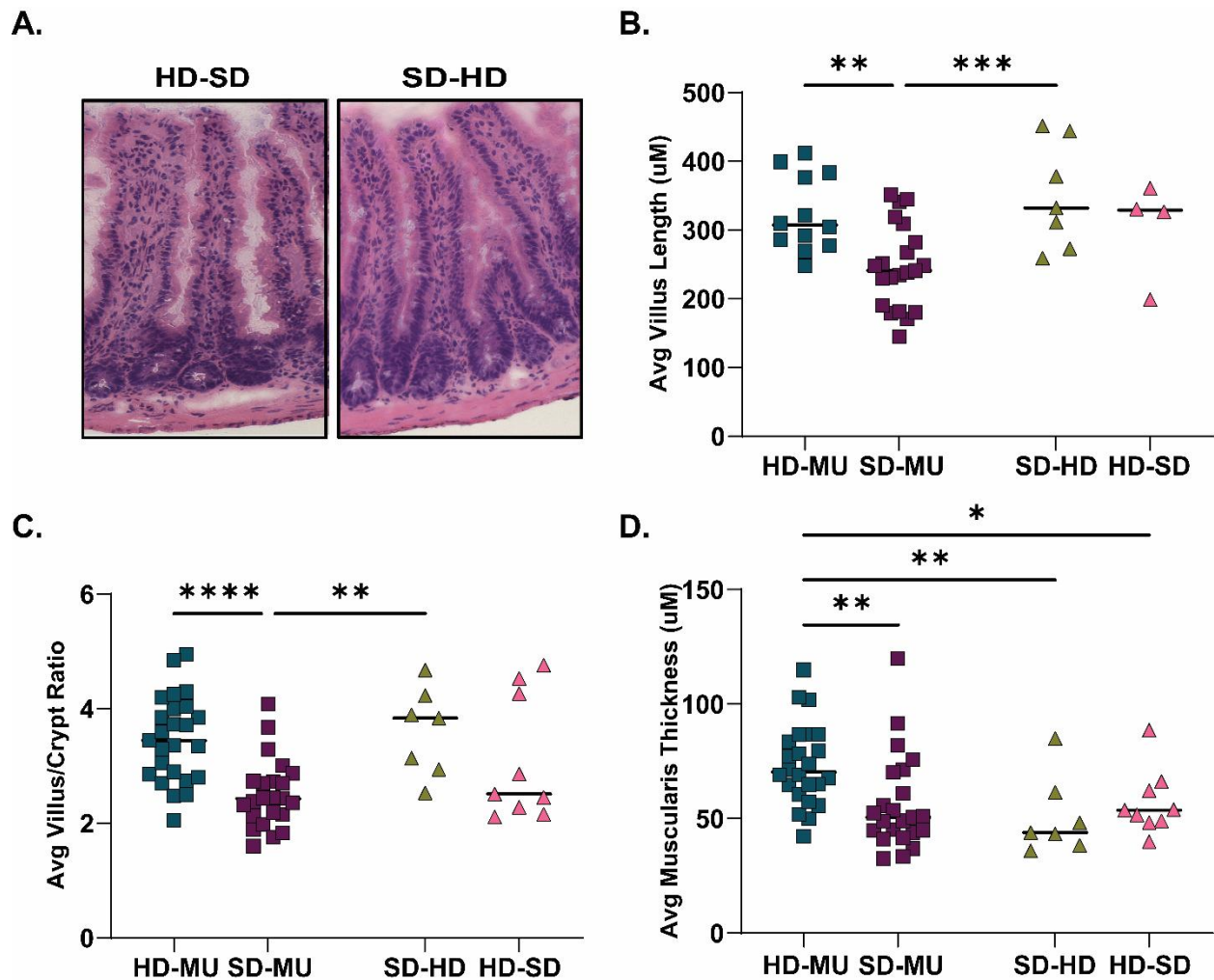


Figure 3.12. Postnatal exposure to SD microbiota negatively impacts muscularis thickness. (A) Representative histological images of H&E stained ileal tissue of HD-SD and SD-HD animals at maturity. **(B)** Quantification of villus length. **(C)** Quantification of villus/crypt ratio. **(D)** Quantification of muscularis thickness. Each point represents an individual animal. * $p \leq 0.05$, ** $p \leq 0.01$, *** $p \leq 0.001$, **** $p \leq 0.0001$ by **(B-D)** Two-Way ANOVA with Šídák's multiple comparisons test.

3.3 Discussion

Our group previously developed a model of intergenerational undernutrition in which paternal and post-weaning undernutrition led to stunting-like features in offspring colonized with microbiota from stunted human infant donors¹²². While our previous work stresses the importance of understanding intergenerational influences on early-life growth, it did not explore a major hypothesized cause of its persistence — maternal undernutrition. Maternal nutritional status plays a key role in fetal growth restriction, low birth weights and poor postnatal growth, all of which are predictors of persistent growth stunting^{156,157}. Furthermore, studies have shown that maternal undernutrition can lead to fetal epigenetic changes that influence metabolism, immune function and the microbiota in early life¹⁵⁸. Therefore, investigation of the role of maternal undernutrition is critical to understanding the intergenerational transmission of growth stunting.

Indeed, the dominant line of thinking regarding nutritional therapies has pivoted towards maternal treatment in recent years¹⁵⁹. However, major questions remain as to the precise timing and composition of these therapies. Because the impacts of undernutrition are both urgent and dire, the use of preclinical models to guide these approaches is critical. Here, we report that the introduction of maternal undernutrition exacerbated features of growth stunting and resulted in reduced linear and ponderal growth in offspring born to dams harboring microbiota from a stunted infant¹²². Interestingly, deficits in weight in SD pups were apparent from birth, while linear growth deficits developed post-weaning. These results mirror the development of stunting in children, who are frequently born underweight and go on to develop stunting within the first three months of life⁷. These observations demonstrate the utility of this model as a

tool for the mechanistic study of how the early life diet and microbiota shape long-term developmental outcomes.

Maternal high fat diet exposure has been previously shown to shape the offspring microbiome and alter cognitive development^{160,161}; however, the effects of maternal undernutrition on the offspring microbiome is less well understood. Our results demonstrate that maternal undernutrition shapes the abundance of specific microbial taxa at maturity, revealing persistent effects of maternal nutritional deficits. Taxa increased by maternal undernutrition included *Enterococcus* species as well as *Escherichia coli*. Undernourished children often exhibit increased burden of *Escherichia* spp., with the presence of virulence genes in this taxon negatively correlated to height and IGF-1^{55,162}. These findings highlight the importance of future studies to investigate microbial functions in further detail via more targeted and detailed analyses.

Recent work has also implicated the maternal microbiome in shaping offspring gastrointestinal development via expansion of intestinal stem cells, goblet cells, and enteroendocrine cells. This effect was not recapitulated in animals fostered by colonized dams but was instead dependent on the prenatal maternal microbiome¹⁶³. Our findings support this conclusion and add further nuance on the role of maternal diet. In our model, intestinal morphology was shaped to a greater extent by prenatal factors, particularly with respect to muscularis thickness. Further understanding of signals regulating these changes could help identify additional pathways that regulate small intestine development to reveal targeted therapies that improve child intestinal absorptive function in early life.

Lastly, our cross-fostering studies showed that postnatal exposure to the stunted donor microbiota in germ-free pups was sufficient to recapitulate growth deficits observed in animals born to colonized dams. Results from a second cross-foster model using pups born to colonized dams suggested that any exposure to the SD microbial community negatively impacted growth, but offspring born to dams with healthy donor microbiota showed better growth outcomes. Both groups of cross-fostered offspring harbored microbiota that largely resembled the SD community, suggesting the SD microbiota was able to largely displace HD microbes acquired at birth. These results have major implications for the use of nutritional therapies in undernourished children and suggest that both pre and postnatal interventions may be required to durably restore growth in these populations.

Limitations of this study

Due to the complexity and length of the experimental design employed, we were unable to investigate more than two microbiota donors. Future studies will be necessary to determine the generalizability of these results in additional human donor contexts. One potential mechanism to facilitate this goal involves the creation of a model community of microbes designed to capture common microbiota members present in many individuals within a specific population. Similarly, we did not investigate the role of the prenatal maternal microbiome through the delivery of offspring by Cesarean section, allowing sterile neonates to be fostered by SD, HD or GF dams. This approach would more clearly delineate the role of the microbiota at each time point. While technically challenging to

perform in gnotobiotic animals, this study would be extremely valuable and warrants further consideration.

3.4 Conclusions

Maternal and child undernutrition continue to be major global health challenges. Children who are born stunted frequently remain so despite available nutritional therapies. Because linear growth is strongly linked to later health outcomes, investigating the origins of linear growth deficits in early life is critical to improving the effectiveness of current therapies and to developing new treatment approaches. Our model of maternal undernutrition allows for the mechanistic dissection of different developmental outcomes linked to the gut microbiota that are also observed in stunted children. These results have major implications for the use of nutritional therapies in undernourished children and suggest that both pre and postnatal interventions may be required to durably restore growth in these populations. In addition, this model provides a useful preclinical approach to test nutritional and microbiota-directed interventions at distinct life stages to optimize therapeutic benefit in low-resource settings.

3.5 Methods

Donor microbiota and study protocol

Details of enrollment for the iLiNS-DYAD-M study were described in an earlier publication. Briefly, enrollment was open to consenting women over the age of 15 years with ultrasound confirmation of pregnancy of < 20 weeks gestation in the Mangochi District of southern Malawi. The randomized controlled clinical trial [clinicaltrials.gov

#NCT01239693] tested the effects of providing small quantities of Lipid-based Nutrient Supplements (SQ-LNS) to pregnant and lactating women through 6 months postpartum and to their children through 6-18 months of age¹²¹. During pregnancy and 6 months thereafter, women received one daily capsule of iron-folic acid supplement (IFA group), one capsule containing 18 micronutrients (MMN group), or one 20-g sachet of SQ-LNS [lipid-based nutrient supplements (LNS), containing 21 micronutrients, protein, carbohydrates, essential fatty acids, and 118 kcal]. Children in the IFA and MMN groups received no supplementation; children in the LNS group received SQ-LNSs from 6 to 18 months^{23,121}. Donors used in this study were selected from samples collected at the six-month time point (prior to supplementation) from a broader subset of donors based on their ability to colonize recipient gnotobiotic mice at an efficiency of >50% (more than half of taxa present in the original donor sample were identified in initial experiments). No significant differences in infant microbiota composition based on maternal supplementation at this time point were identified^{23,100}.

Gnotobiotic Mice

All gnotobiotic mouse experiments were performed using protocols approved by the University of Virginia Institutional Animal Care and Use Committee. All gnotobiotic animals used in this publication were germ-free C57BL/6NTac mice obtained from Taconic Biosciences. Upon arrival, germ-free status was verified by quantitative PCR. Mice were housed in plastic flexible film gnotobiotic isolators (Class Biologically Clean Ltd.) under a 12-hour light cycle. Animals received *ad libitum* access to food and water throughout the experiment, and were euthanized at the conclusion of the experiment

using AVMA approved procedures. For experiments featuring maternal undernutrition, male and female mice were obtained from Taconic Biosciences at 4 weeks of age and transitioned to the M8 diet. Three days later, they were colonized with donor microbiota and maintained on M8 diet until 8 weeks of age. Males and females were co-housed and switched to an autoclaved nutrient-sufficient breeder chow (LabDiet 5021 Autoclavable Mouse Breeder Diet, LabDiet Inc.). For experiments without maternal undernutrition, male mice were obtained from Taconic Biosciences at 4 weeks of age and transitioned to the M8 diet. Three days later, they were colonized with donor microbiota and maintained on M8 diet until 8 weeks of age. At this point, 8-week-old germ-free females (also from Taconic Biosciences) were introduced into the donor isolators. Males and females were co-housed and switched to the autoclaved nutrient-sufficient breeder chow listed above.

For cross-fostering experiments, male and female mice were obtained from Taconic Biosciences at 4 weeks of age and transitioned to the M8 diet. Three days later, germ-free mice were split into three groups, each in a unique gnotobiotic isolator (HD, SD and germ-free). HD and SD mice were colonized with donor microbiota, while germ-free mice remained uncolonized. All three groups were maintained thereafter on the M8 diet until 8 weeks of age. At this time, they were all switched to breeder diet. Estrous cycles were synchronized by swapping male and female bedding. For germ-free cross-fostering experiments, once litters were born to both germ-free and colonized dams, neonates were transferred to their cross-foster HD or SD dam within three days. Neonates born to HD or SD dams at this time point were euthanized to prevent overcrowding.

Breeding mice were refreshed after six months, and offspring used in these experiments were derived from breeders from five separate rounds of colonization (total

of 2-4 males and 6-8 females per colonization). Weight and tail length measurements were collected from birth to maturity. Tail length measurements in living mice were assessed using calipers sterilized to be used inside the isolators. The tail length measurements after euthanasia were performed using a standard laboratory ruler. All tail length measurements were done from the base of the tail to the tip along a straight line. For weight data collected in early life, animals were weighed weekly from 1 to 4 weeks of age inside the isolator. Weights taken inside the isolator were measured using a manual scale, while weights taken after euthanasia were measured on a digital scale outside the isolator. Neonatal weights were measured within 3 hours of birth for all mice inside the isolator using a manual scale. Fecal samples were collected at the indicated time points and immediately frozen. Samples were stored at -80°C until use. Data shown includes equal number of female and male healthy donor colonized mice and stunted donor colonized mice unless otherwise specified.

Colonization and Diets

To prepare infant fecal samples for colonization of germ-free mice, aliquots of each sample were removed from storage at -80°C, weighed and immediately transferred into anaerobic conditions (atmosphere of 75% N₂, 20% CO₂ and 5% H₂; vinyl anaerobic chambers from Coy Laboratory Products). Samples were subsequently resuspended in pre-reduced PBS containing 0.05% L-Cysteine Hydrochloride at a concentration of 10 mg/mL. Samples were vortexed for one minute and allowed to clarify by gravity for 5 minutes. The supernatant was removed to a fresh anaerobic tube and combined with an equal volume of sterile, pre-reduced PBS containing 0.05% L-Cysteine HCL and 30%

glycerol. Gavage mixtures were aliquoted into sterile 2 mL screw cap tubes (Axygen) and frozen at -80°C until use. To colonize recipient mice, pools of gavage mixtures were sterilized externally with ionized hydrogen peroxide (STERAMIST System, TOMI Inc.) and passed into each isolator after appropriate exposure time (20 minutes). Animals were colonized via a single oral gavage with a 200 µl volume of gavage mixture.

The low protein and micro-nutrient deficient Malawi-8 diet was prepared as previously described^{41,140} and obtained from Dyets, Inc. Briefly, ingredients (corn flour, mustard greens, onions, tomatoes, ground peanuts, red kidney beans, canned pumpkin and peeled bananas) were cooked and combined in an industrial mixer. Dry pellets of the M8 diet were extruded, vacuum-sealed and double bagged prior to sterilization by irradiation (Steris Co). The nutritional content of the cooked and irradiated diet was assessed by N.P. Analytical Laboratories as described in Blanton et al²⁴. LabDiet 5021 was sterilized by autoclaving at 129°C and 13.2 PSI for 15 minutes. Sterility of both diets was routinely assessed by culturing pellets in Brain Heart Infusion (BHI) broth (Millipore), Nutrient broth (Millipore), and Sabouraud-Dextrose (Millipore) broth for five days at 37 °C under aerobic conditions, and in BHI broth and Thioglycolate broth (Difco) supplemented with 0.05% L-Cysteine Hydrochloride (Sigma) under anaerobic conditions. After the five-day liquid culture, cultures of all diets were plated on BHI agar supplemented with sheep blood (Thermo Scientific). All diets were stored at -20 °C prior to use.

Histopathology and Anthropometry

At the time of euthanasia, a 1 cm section of the proximal ileum was dissected from each mouse and fixed in 10% neutral-buffered formalin overnight at room temperature

before being transferred to 70% Ethanol. Tissue processing and H&E staining were performed by the University of Virginia's Research Histology Core or at Histowiz Inc. Samples were paraffin embedded and sectioned before mounting. Slides were stained with hematoxylin & eosin prior to imaging at a 20x magnification using an EVOS M7000 microscope. To assess the histopathological features of the ileum, the stained tissues were scored in a blinded manner. Scores were assigned using a scoring system based off published findings in human intestinal biopsies ³⁵. Scoring parameters consisted of 2 qualitative features: villous architecture (0, majority of villi are >3 crypt lengths long; 1, majority of villi are <3 but >1 crypt length long, with abnormality; 2, majority of villi are absent or <1 crypt length long, with abnormality) and enterocyte injury (0, majority of enterocytes show tall columnar morphology; 1, < 50% of enterocytes show low columnar, cuboidal, or flat morphology; 2, > 50% of enterocytes show low columnar, cuboidal, or flat morphology). Cumulative scores were calculated as the sum of the averaged score for both parameters. ImageJ was used to obtain three quantitative parameters consisting of ileum villus height (μm), ileum muscularis thickness (μm) and ileum crypt length (μm). Two measurements were obtained for villus length and crypts, three measurements for muscularis thickness parameter and averaged.

Microbial Sequencing

Samples were shipped to SeqCenter for DNA extraction and sequencing. All standard DNA extractions at SeqCenter follow the ZymoBIOMICS™ DNA Miniprep Kit5. DNA was extracted from fecal samples following the guidelines in Appendix B of the ZymoBIOMICS™ DNA Miniprep Kit. Eluted DNA was then purified by running the effluent

through the prepared Zymo-Spin™ III-HRC Filter. Final DNA concentrations were determined via Qubit. After DNA extractions, library prep was performed using Zymo Research's Quick-16S kit with passed primers targeting the V3-V4 region of the 16S gene. The following sequencing primers were used: "CCTACGGGDGGCWCAG" (341F) and "GACTACNVGGGTMTCTAATCC" (806R). After cleanup and normalization, samples were sequenced using a P1 or P2 600-cycle NextSeq2000 Flowcell to generate 2x301 bp paired-end (PE) reads. Quality control and adapter trimming were conducted with bcl-convert1 (v4.2.4). Primer-dimer sequences, identified as PCR artifacts, were removed from the FASTQ files using the following criteria: read length greater than 150 bp, PolyN strings with fewer than 10 consecutive Ns, and PolyG strings with fewer than 150 consecutive Gs.

Sequencing Quality Control & Data Analysis

Sequences were then denoised using Qiime2's dada2 plugin³. Denoised sequences were assigned a microbial taxonomy by mapping to the Silva 138 99% ASVs full-length sequence database and the VSEARCH4 utility within Qiime2's feature-classifier plugin. Prevalence filtering threshold was set to remove any ASVs $\leq 1.21\%$ prevalence across all samples excluded from analysis. ASVs with a relative abundance across all samples $\leq 0.1\%$ were removed as spurious ASVs. Phylogenetic trees for distance matrices were constructed using the following R packages: msa¹⁶⁴ (version 1.38.0) and phagorn¹⁶⁵ (version 2.12.1). Percentage of relative abundance were calculated by subsetting samples according to analyses required.

Ordination plots showing weighted UniFrac distances (a measurement of β diversity based on phylogenetic relatedness) were produced using the phyloseq package¹⁴³ (version 1.50.0) in R. The stackbar plots shown in Fig. 2, Fig.4, Fig. 5 and Fig. 6 were created using the ggplot2¹⁶⁶ in R (version 3.5.1).

Protein Quantification

Liver tissue were collected at the time of euthanasia and flash frozen in liquid nitrogen. Liver samples were homogenized in Lysing Matrix F (MP Biomedicals, ref. 6540440) and 500uL of 1x HALT (Thermo Scientific, ref. 78429) in T-PER (Thermo Scientific, ref. 78510). Homogenates were centrifuged at 4 °C and 10,000 xg for 5 minutes. Protein concentration was determined by BCA assay (Thermo Scientific, ref. 23227) using the manufacturer's protocol. Lysates were normalized and stored at -80 °C until analysis. IGF-1 in liver lysates were quantified by ELISA assay (R&D Systems DuoSet kits) performed according to the manufacturer's recommendation. Briefly, the capture antibody was coated onto a 96-well half-area plate (Corning) in PBS overnight at room temperature. On the following day, the plates were washed three times with 200 uL of Wash Buffer (0.05% Tween 20 in PBS) and blocked for one hour. After blocking and incubation, plates were washed again before adding samples of small intestinal tissue lysate as well as a standard curve. The plate was incubated for 2 hours at room temperature before being washed as described above. Detection Antibody provided in the kit was added at the suggested concentration and incubated for another 2 hours at room temperature. After incubation, plates were washed and Substrate Solution (1:1 mixture of Color Reagent A (H₂O₂) and Color Reagent B (Tetramethylbenzidine)) was

added to each well and incubated at room temperature for 20 minutes avoiding direct light. After incubation, Stop Solution (2 N H₂SO₄) was added to each well. Plates were read an optical density of 450 with background subtraction at 570 nm using a Tecan plate reader.

Statistical Analysis

Statistical analyses were performed in GraphPad Prism (version 10.4.1) unless otherwise noted. V3-V4 16s sequencing data was analyzed in R (version 4.4.2). Statistical details including the number of animals or samples can be found in figure legends. Statistical significance was assessed by Mann-Whitney U test when comparing between two groups, or by Two-Way ANOVA with Šídák's multiple comparisons test when comparing >2 groups unless otherwise noted. PERMANOVA tests were performed using R package vegan (version 2.6-8) and pairwise comparisons from distance matrices were calculated using the pairwiseAdonis package¹⁶⁷ (version 0.4.1). P values are shown in figures or tables for samples with significant differences. Each data point represents an individual animal, and horizontal bars represent the mean.

Chapter 4: Immunoglobulin A selectively targets specific microbes in the SD microbiota.

Yadeliz A. Serrano, Jasmine Cano & Carrie A. Cowardin

Author contributions:

Conceptualization, Y.S.M and C.A.C.; Sample collection, Y.S.M, and J.C., Investigation, Y.S.M, and C.A.C., Analysis; Y.S.M, and C.A.C., Visualization, Y.S.M, and C.A.C.; Resources, Y.S.M, and C.A.C; Funding, Y.S.M. and C.A.C, Supervision, C.A.C; Writing, Y.S.M., Editing, C.A.C.

4.1 Introduction

Stunted children experience increased comorbidities in early life, including altered mucosal immunity^{4,168,169}. One example of this is their increased Immunoglobulin A (IgA) targeting of the fecal microbiome compared to non-stunted controls³⁹. This is further supported by elevated intestinal plasma cells in individuals with Environmental Enteric Dysfunction (EED), a syndrome often linked to stunted growth⁸². IgA is an antibody predominantly found at mucosal surfaces. In the small intestine, IgA plays a crucial role in maintaining gut homeostasis by regulating microbial composition and preventing pathogen colonization^{93,170}. Elevated IgA targeting of microbes may indicate an altered microbiome composition that is driving immune activation and gut inflammation. Additionally, studies have linked microbiota-reactive IgA antibodies as predictors of poor growth in children with EED¹⁷¹. Understanding the significance of this altered immune response can help identify microbial functions that drive immune recognition, providing insight into how microbes contribute to reduce linear growth in stunted children.

IgA has been shown to identify microbial taxa driving inflammation in Chron's and inflammatory bowel disease^{99,172,173}. Furthermore, studies have shown that colonization of 4-week-old germ-free mice with IgA-targeted microbes, isolated from undernourished children, causes diet-dependent enteropathy⁹⁶. However, this mouse model fails to address the intergenerational component of colonization as IgA-positive (IgA+) microbes were used to colonize germ free mice after weaning. Our previous work identified intergenerational colonization as a crucial approach to see growth deficits in offspring independent of nutritional status, since all the mice are in the same undernourished diet¹²².

In Chapter 2, we demonstrated offspring born with No Maternal Undernutrition (NMU), colonized with SD microbiota, SD-NMU animals, exhibit an increase in IgA-producing intestinal plasma¹²². This suggests SD-NMU mice recapitulate this feature of altered immunity observed in individuals with EED. In Chapter 3, we introduced the Maternal Undernutrition (MU) Model, which better recapitulates the cycle of stunting¹⁰² and demonstrated that maternal undernutrition worsens microbiome-driven stunting and increases early life mortality¹⁰². SD-MU mice also have an increase in the colonization of *Escherichia coli* and *Enterococcus* sp.¹⁰². This suggests specific microbes may contribute to worsened growth deficits observed in SD-MU animals. The goal of the experiments presented in this chapter was to establish a technique to identify microbes driving growth deficits in SD animals. Since IgA has discriminatory capabilities, we hypothesized this immune response can help identify drivers of stunted growth in our murine model of intergenerational undernutrition. A secondary goal described in this chapter was to evaluate how well fecal IgA targeting reflects IgA targeting in the small intestine.

We hypothesized MU animals will have similar IgA targeting of microbes in both their small intestine (SI) and fecal microbiome. We also hypothesized that SD-MU mice will have an increase in the number of microbes targeted by IgA compared to HD-MU animals. The findings from this study revealed SD-MU animals develop an altered IgA response in early life that is sustained until maturity. SD-MU mice developed an altered IgA response both in the small intestine and feces. Fluorescent Activated Cell Sorting (Bug-FACs) coupled with 16S V4-V3 sequencing revealed IgA targets specific microbes in the community. Bug-FACs is a technique used to sort and isolate specific bacterial populations based on fluorescence markers. In this chapter, we demonstrate that Bug-

FACs is a useful tool to identify immunogenic microbes in mouse models of intergenerational undernutrition.

4.2 Results

SD-MU animals develop altered fecal and small intestine luminal IgA response at maturity

To begin investigating IgA responses, we decided to employ our murine model of intergenerational undernutrition with Maternal Undernutrition (MU) due to its capacity to better recapitulate human stunting¹⁰². Briefly, both 4-week-old sires and dams were colonized with microbiota derived from a healthy or severely stunted Malawian infant donor¹²² and fed a low in protein and micronutrient-deficient diet (**Figure 4.1A**). At 8 weeks of age, these animals were swapped back to the nutrient-sufficient diet and co-housed as breeding pairs. Offspring of these breeding pairs were weaned onto the M8 diet from 3 weeks of age until maturity. These animals represent the HD-MU (Healthy Donor, Maternal Undernutrition) and SD-MU (Stunted Donor, Maternal Undernutrition) groups. Work from Chapter 3 demonstrates SD-MU have exacerbated growth deficits soon after weaning compared to HD-MU offspring¹⁰². We performed V4 16s rRNA sequencing of the fecal microbiota from HD-MU and SD-MU animals at maturity to determine whether changes due to maternal nutritional status were driving the exacerbation of growth deficits. Analysis revealed maternal undernutrition increased the colonization of *Escherichia coli* and *Enterococcus* sp.¹⁷⁴. These results may suggest that microbes in the SD microbiota drive reduced linear growth since maternal and post-weaning dietary exposures are identical in MU parents and offspring. Since SD-NMU mice

developed an altered Immunoglobulin A (IgA) response against their microbiota (**Figure 4.1B**), we decided to confirm the presence of this phenotype in SD-MU mice. We first performed flow cytometry in isolated immune cells from the small intestine of HD-MU and SD-MU animals at maturity and observed SD-MU mice have a significant increase in both the cell proportion and absolute cell number of IgA⁺ plasma cells in the lamina propria (**Figure 4.1C**).

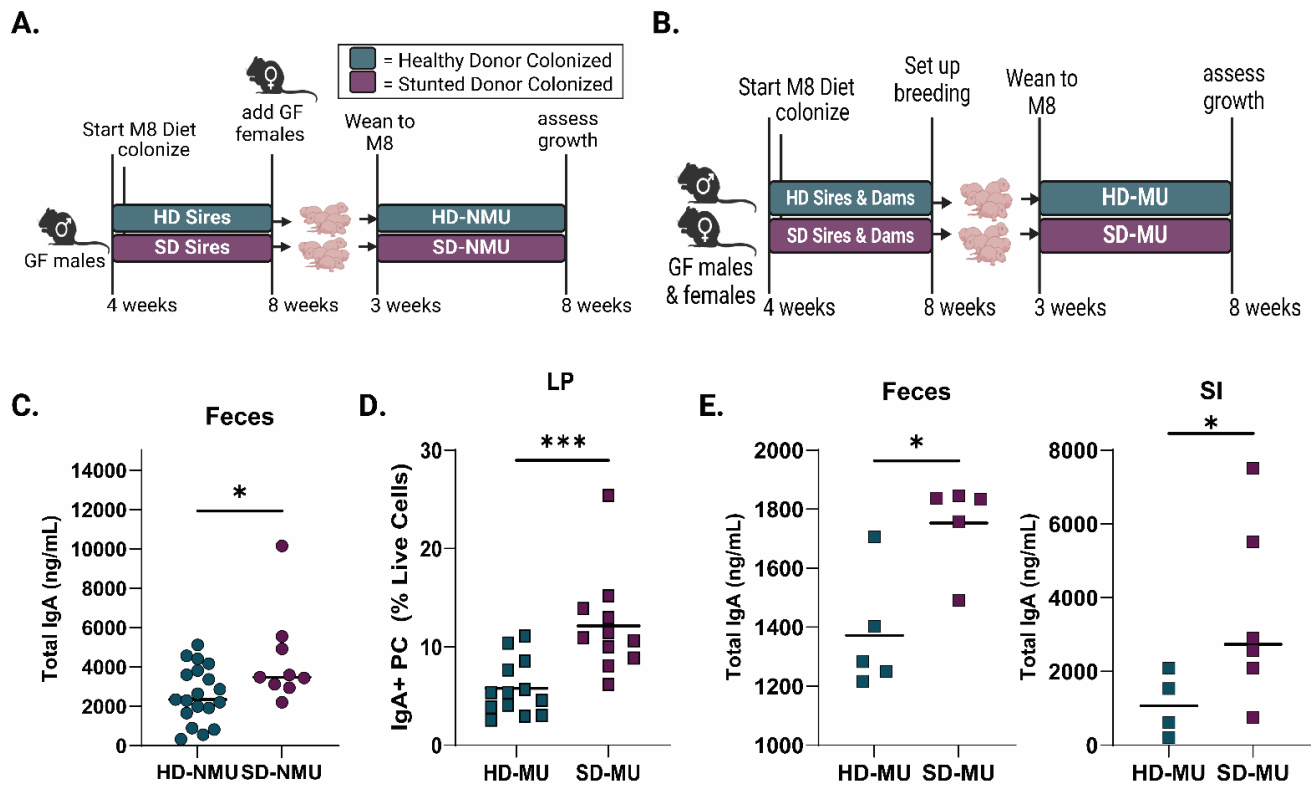


Figure 4.1. SD-MU mice develop an altered IgA response at maturity, similar to SD-NMU animals. (A) Schematics of NMU model and (B) MU model. (C) Quantification of total IgA protein levels in the feces of NMU animals at maturity. (D) Cell proportions of IgA⁺ Plasma Cells (PC) in the intestinal lamina propria (LP) of MU animals at maturity. (E) Quantification of total IgA protein levels in the feces and small intestine (SI) of MU animals at maturity. Each point represents one mouse. * $p \leq 0.05$ and * $p \leq 0.001$, by (C-E) Mann Whitney Test.**

Due to the increased number of IgA⁺ intestinal plasma cells in SD-MU animals at maturity, we next assessed whether this phenotype translated to IgA antibody production. We quantified total fecal and small intestine luminal IgA protein levels by enzyme-linked immunoassay (ELISA). Results revealed SD-MU mice have significantly increased levels of fecal and SI IgA compared HD-MU animals (**Figure 4.1E**). These results suggest exposure to SD microbiota in early life plays an important role in shaping immune responses, reiterating the need to identify when in early life long-term growth and immune outcomes are established and how host-microbiota interactions contribute to this process.

Because growth deficits were observed in SD-MU mice at 4 weeks of age¹⁰², we next measured IgA protein levels in early life (from pre-weaning to maturity). We observed that 4-week-old SD-MU have significantly increased levels of fecal IgA after the introduction of the M8 diet and these levels are sustained until maturity (**Figure 4.2A**). Because endogenous IgA production begins around weeks 3–4, we focused on characterizing the targeting of the IgA response at maturity, when this immune response is fully developed. Therefore, we next measured microbiota reactivity to IgA in 8-week-old MU animals by flow cytometry in the feces and SI luminal contents. Surprisingly, SD-MU animals did not have a higher targeting of the microbiota by IgA in both feces and SI contents compared to HD-MU mice (**Figure 4.2B-C**). These results contradict the findings from the Afribiota study, where stunted children were shown to have a significant increase in the proportion of IgA+ bacteria in their feces compared to non-stunted controls³⁹.

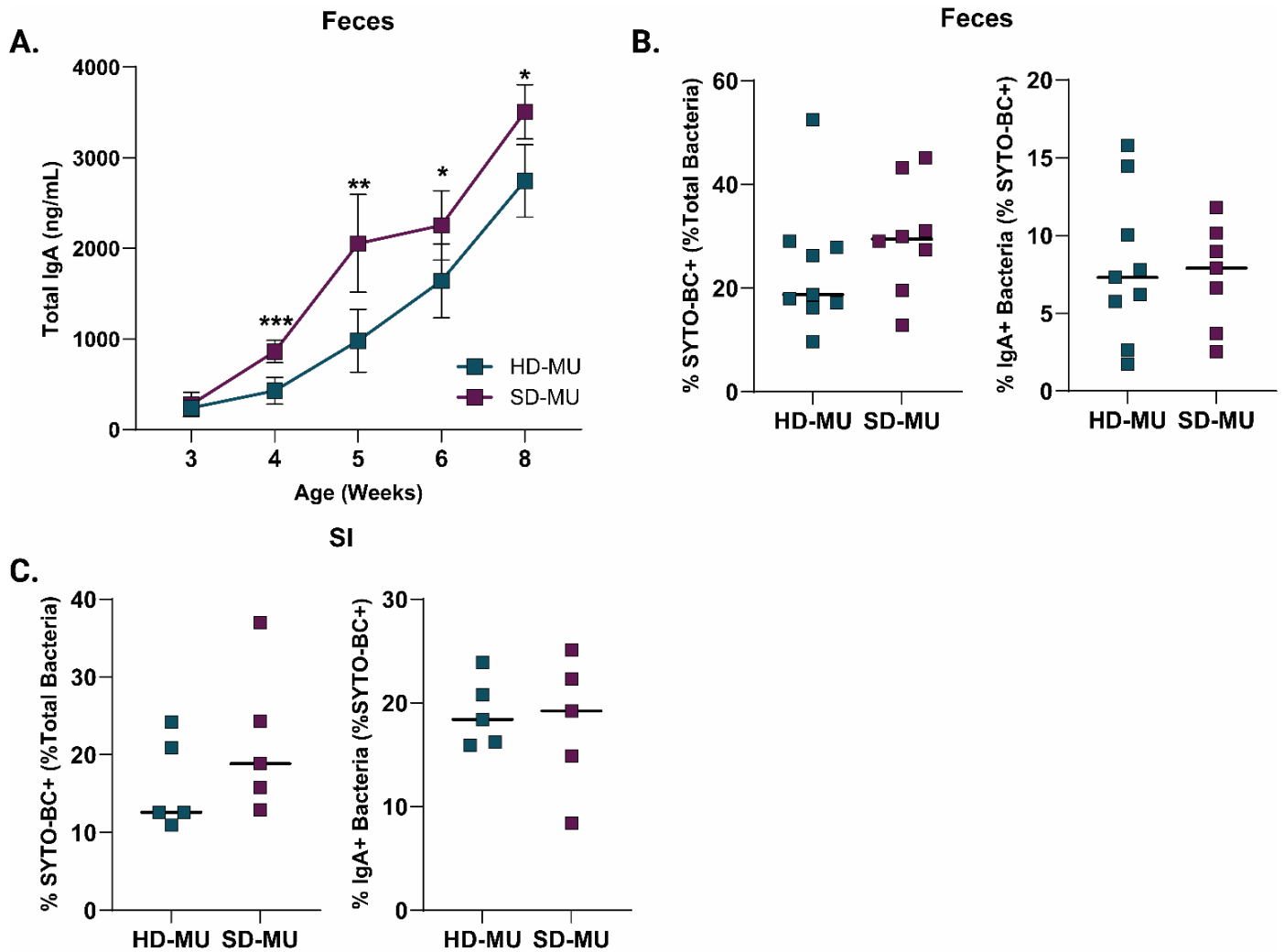


Figure 4.2. SD-MU animals have increased levels of total IgA soon after weaning. (A) Fecal IgA Time course from pre-weaning time to maturity (normalized 100 mg/mL). **(B)** Percentage of SYTO-BC+ from %Total Bacteria and proportion of IgA+ bacteria from SYTOB-C+ gate in the feces of MU animals at maturity. **(C)** Percentage of SYTO-BC+ from %Total Bacteria and proportion of IgA+ bacteria from SYTOB-C+ gate in the feces of MU animals at maturity. Each individual point represents one mouse. **(A)** Equal number of females and male in each group. **(B)** HD-MU group: n=9/group [4 females and 5 males]. SD-MU group: n=8/group [4 females and 4 males]. **(C)** n=5/group [3 females and 2 males]. **(A)** * $p \leq 0.05$, ** $p \leq 0.01$ and *** $p \leq 0.001$, by Mixed Effects Model with Sidak's-Holme correction. **(B-C)** Mann-U Whitney Test.

Sorting bacteria based of IgA targeting

Although we did not observe a significant difference in the proportions of microbes targeted by IgA, we aimed to identify whether specific microbes of interest were present within the IgA-targeted bacterial population (**Figure 4.2C**). In recent work, we demonstrated SD-MU mice have an increase in the relative abundance of *Escherichia coli* and *Enterococcus* sp.¹⁰² Recent studies have shown IgA targeting can be used as a tool to identify bacterial taxa that contribute to disease in undernutrition and inflammatory bowel disease^{96,99}. To uncover potential microbial effectors of stunted growth and differences in IgA targeting between feces and SI contents, we performed Bug-Fluorescent Activated Cell Sorting (Bug-FACS or IgA-Seq) (**Figure 4.3A**) in the mice described in **Table 4.1**. For comparisons between feces and SI targeting we collected samples from the same mice.

| Mouse Number | Donor Microbiota | Group | Age | Sex | Weight | Tail Length |
|--------------|------------------|-------|-----|-----|--------|-------------|
| 292 | 3176 | HD-MU | 8 | F | 19.02 | 80 |
| 295 | 3176 | HD-MU | 8 | M | 20.75 | 79 |
| 331 | 3176 | HD-MU | 8 | M | 20.02 | 79 |
| 331 | 3176 | HD-MU | 8 | F | 18.91 | 80 |
| 335 | 3176 | HD-MU | 8 | F | 17.62 | 77 |
| 308 | 4092 | SD-MU | 8 | F | 17.42 | 75 |
| 344 | 4092 | SD-MU | 8 | M | 17.63 | 72 |
| 346 | 4092 | SD-MU | 8 | F | 15.8 | 73 |
| 348 | 4092 | SD-MU | 8 | M | 17.5 | 74 |
| 427 | 4092 | SD-MU | 8 | F | 15.86 | 72 |

Table 4.1. Metadata of MU animals selected for fecal and small intestine Bug-FACs. We selected mice that had both fecal and small intestine contents available for comparisons within groups.

We isolated bacteria from the feces of MU animals, stained them with SYTO-BC and anti-IgA-APC, and sorted the bacteria based on SYTO-BC+/IgA-APC+ signals, distinguishing bacteria that were SYTO-BC+ and either bound by IgA (IgA+ fraction) or not (IgA- fraction). To control for non-specific binding of SYTO-BC, we utilized fecal/SI contents from germ-free mice as negative controls. To detect non-specific binding by IgA, we used fecal/SI luminal contents from *Rag*^{-/-} mice, which lack B and T cells, and therefore don't produce IgA. The gating strategy employed is outlined in **Figure 4.3B**. On average the purity of the IgA+ fractions from fecal sorts was 85.35%, and the IgA-Fraction, 91.68%. The average purity of the IgA+ and IgA- Fractions from SI content sorts was 89.27% and 88.17%, respectively.

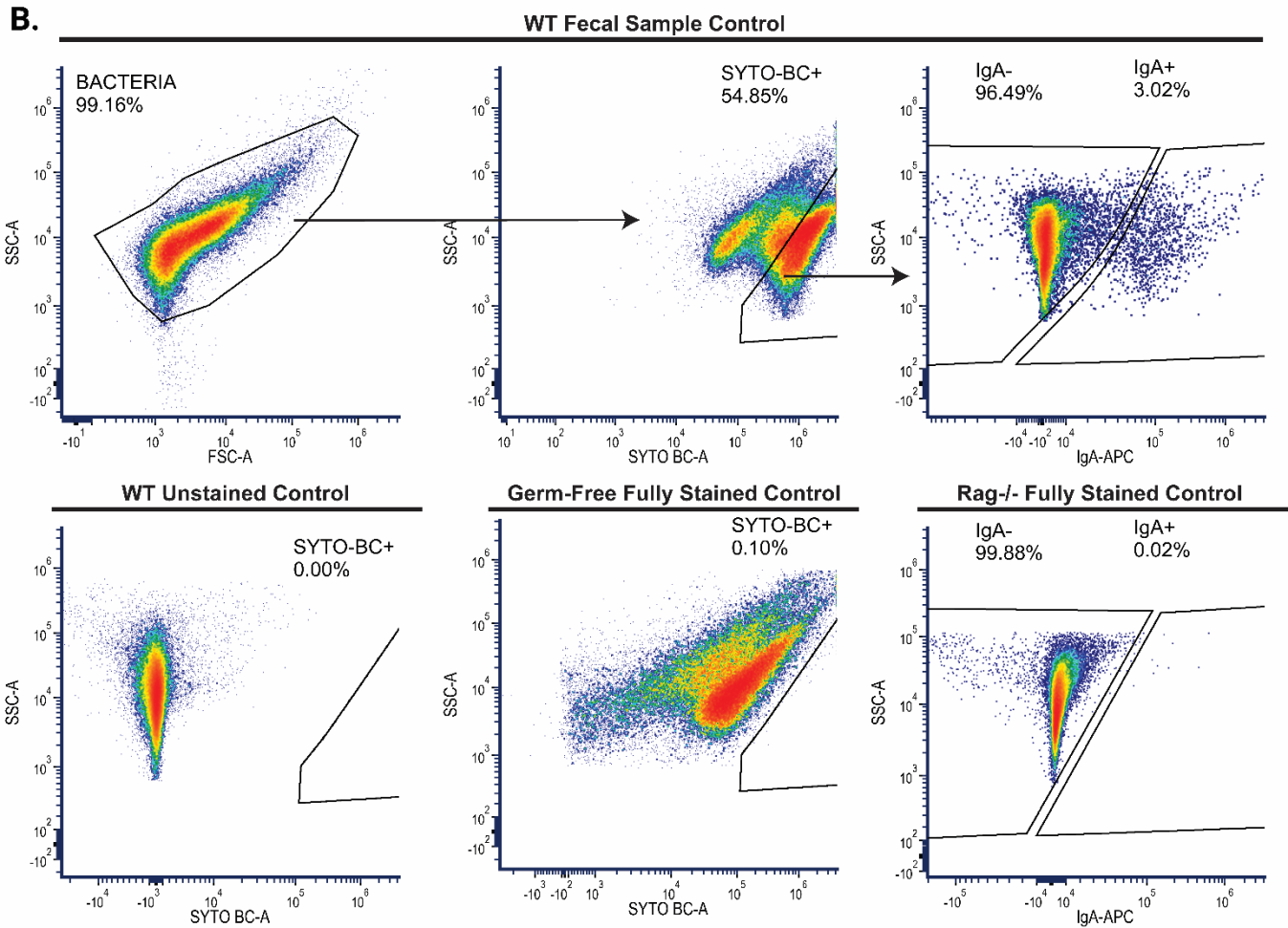
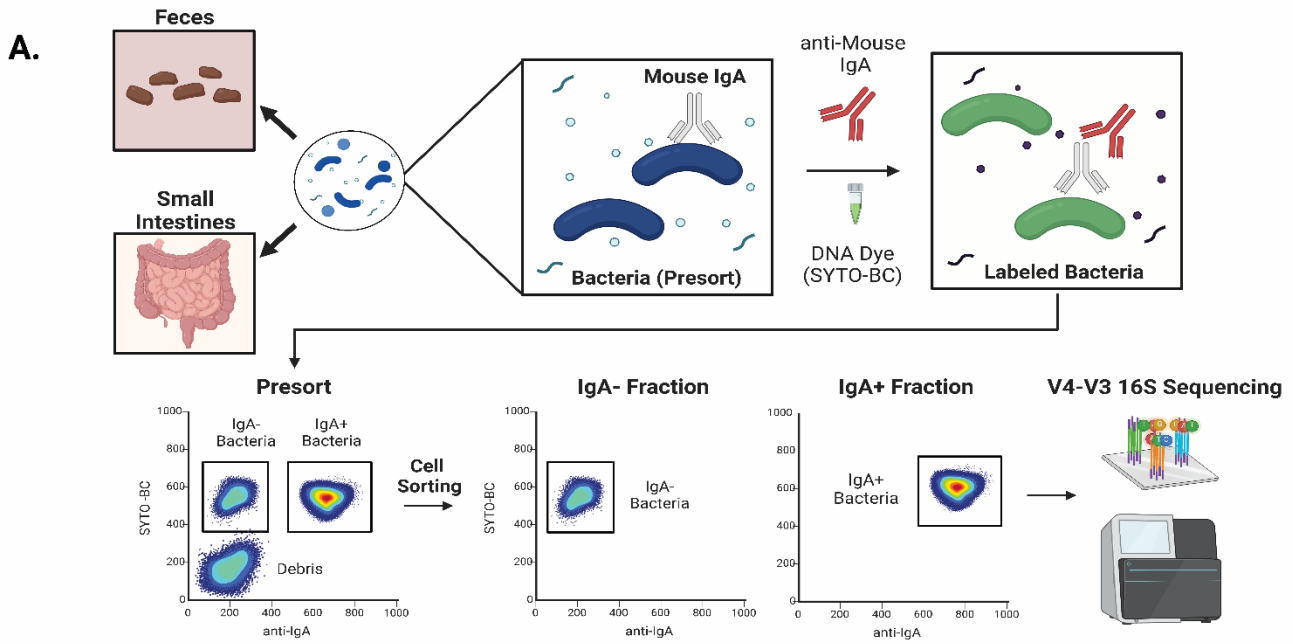


Figure 4.3. Bug-FACS protocol and gating strategy to sort IgA+ and IgA- microbes. (A) Schematic of Bug-FACS procedure where fecal samples or small intestine contents are collected from MU animals, stained and sorted using an Aurora CITEK cell sorter. **(B)** Representative gating strategy for sorting IgA+ and IgA- bacteria from feces. This same gating strategy was also applied to small intestine contents with controls sourced from this same area to ensure consistency.

Presort samples have similar composition regardless of source

To start analyzing the microbial composition in the presorted and sorted fractions and whether the location or source of bacteria impacts IgA targeting, we performed an unweighted Unifrac Principal Component Analysis (PCoA) to determine dissimilarity based on the presence and absence of microbes and their phylogenetic relationships. We found that the composition of presort samples from fecal and small intestine contents was not significantly different (**Table 4.1**) when comparing HD-MU and SD-MU respectively (**Figure 4.4A**). Fecal IgA+ and IgA- fractions from HD-MU had significantly different microbial compositions, while there were no differences in these fractions when sources from the small intestine. We did not observe any differences in composition between the IgA+ and IgA- fractions in SD-MU mice, regardless of the source. We next assessed alpha diversity in these fractions. We observed that IgA+ fraction sorted from the small intestine of HD-MU (paired animals) had a significant increase in alpha diversity compared to IgA+ fraction from feces (**Figure 4.4B**). We did not identify any significant differences in alpha diversity between fractions sorted from the feces and small intestine of SD-MU mice (**Figure 4.4C**).

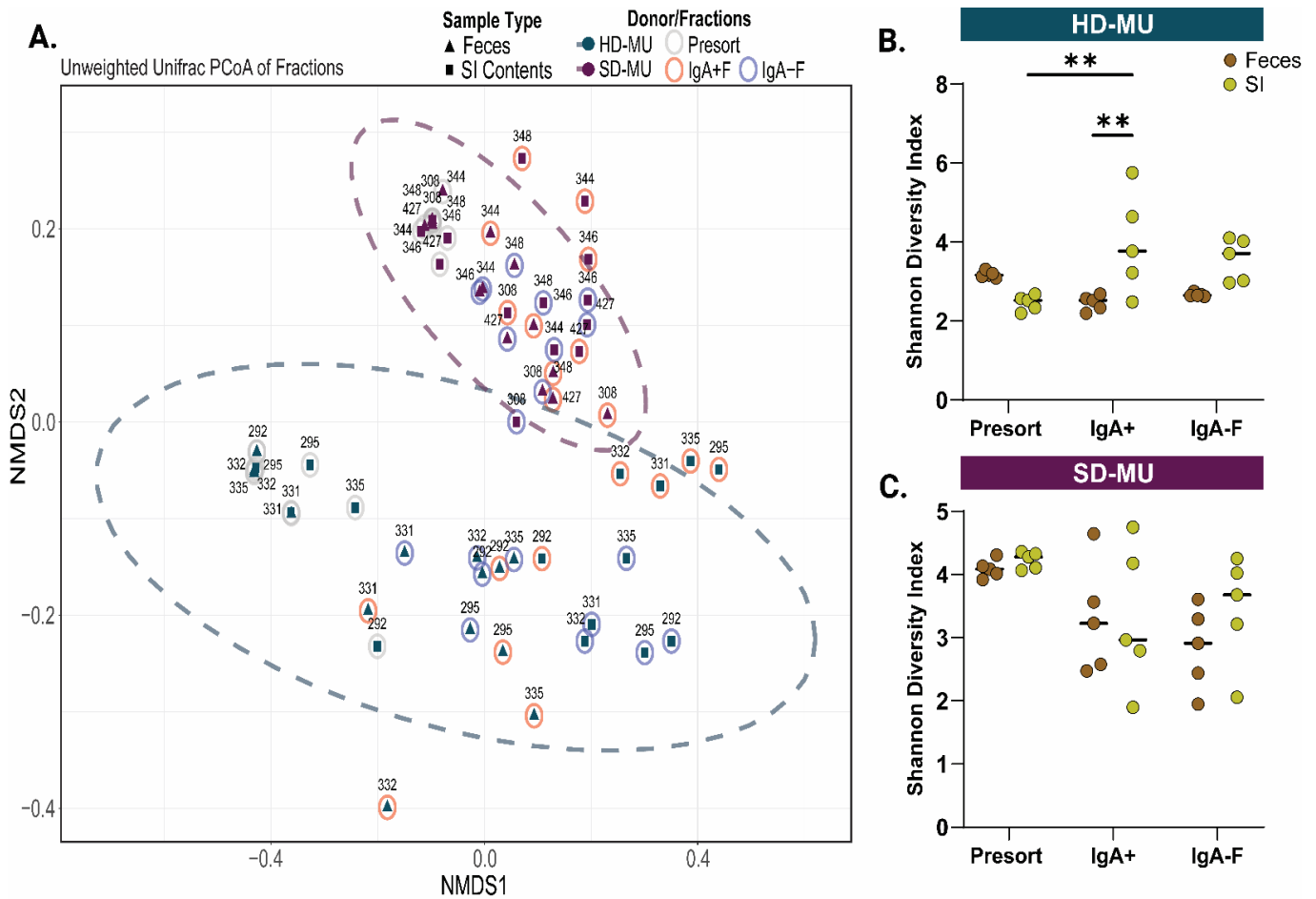


Figure 4.4. Enriched taxa in fractions are different between HD-MU and SD-MU mice. (A) Unweighted Unifrac NMDS analysis of presort and sorted fractions from feces and small intestine contents in MU animals. Numbers represent individual mice; metadata can be found in Table 3. **(B-C)** Shannon diversity across presorts and sorted fractions from feces and small intestine contents in MU animals. **(B-C)** Each point represents a mouse. **(A-C)** n=5/group [3 females and 2 males]. * $p \leq 0.05$, ** $p \leq 0.01$, *** $p \leq 0.001$, **** $p \leq 0.0001$ by **(B-C)** Two-Way ANOVA with Šídák's multiple comparisons test.

IgA Targeting patterns in SD-MU animals

To identify microbes with a higher likelihood of IgA binding in the feces and small intestine of SD-MU animals, we calculated the IgA Probability Ratio score for all taxa present in the sorted fractions. The IgA Probability Ratio score reflects the likelihood of a taxon being bound by IgA, with values near 1 indicating a high probability of IgA targeting, values around 0 suggesting a random likelihood, and values near -1 indicating the taxon is unlikely to be targeted by IgA¹⁷³. These calculations are done using the relative abundance fractions of all microbes present in the presort and sorted fractions. To identify microbes with the highest likelihood to be targeted by IgA, a Gaussian mixture model was applied to all IgA Probability Scores to establish thresholds for high, moderate and low likelihood of IgA binding (**see Appendix B Figure 4.2B**). This analysis was conducted for both fecal and small intestinal IgA to compare targeting patterns (**Figure 4.5A-B**). Both fecal and small intestine Bug-FACs revealed a high likelihood of *Enterococcus* sp. (ASV 352, ASV 361, ASV 348 and ASV131) being targeted by IgA in SD-MU animals (**Figure 4.5A**). Furthermore, two strains of *Escherichia* (ASV372 and ASV 341) had a medium likelihood of not being targeted by IgA (data not shown). IgA targeting in the small intestine was consistent with results from the feces, at genus levels. This suggest potentially fecal Bug-FACs is accurate and representative of immune recognition by IgA.

We also analyzed IgA targeting in the feces and small intestine contents of HD animals at maturity. However, comparing IgA targeting between HD and SD mice was not particularly productive due to their different baseline microbiotas. These differences make it difficult to determine whether variations in IgA binding reflect true differences in immune targeting or simply distinct microbial compositions. However, we plan to use the IgA⁺ and

IgA⁻ fractions from HD-MU animals as controls in future experiments where we will test the functional consequences of IgA targeted microbes isolated from SD-MU animals. For example, whether IgA⁺ microbes cause reduced linear growth in germ-free mice. Notably, we observed that *Escherichia coli* was found in the highly IgA-targeted zone in the feces of HD animals (**see Appendix B Figure 4.3B**). This suggests that IgA may be recognizing and containing *Escherichia coli*, since we do not detect this bacterium in the presorted fraction of these mice (data not shown).

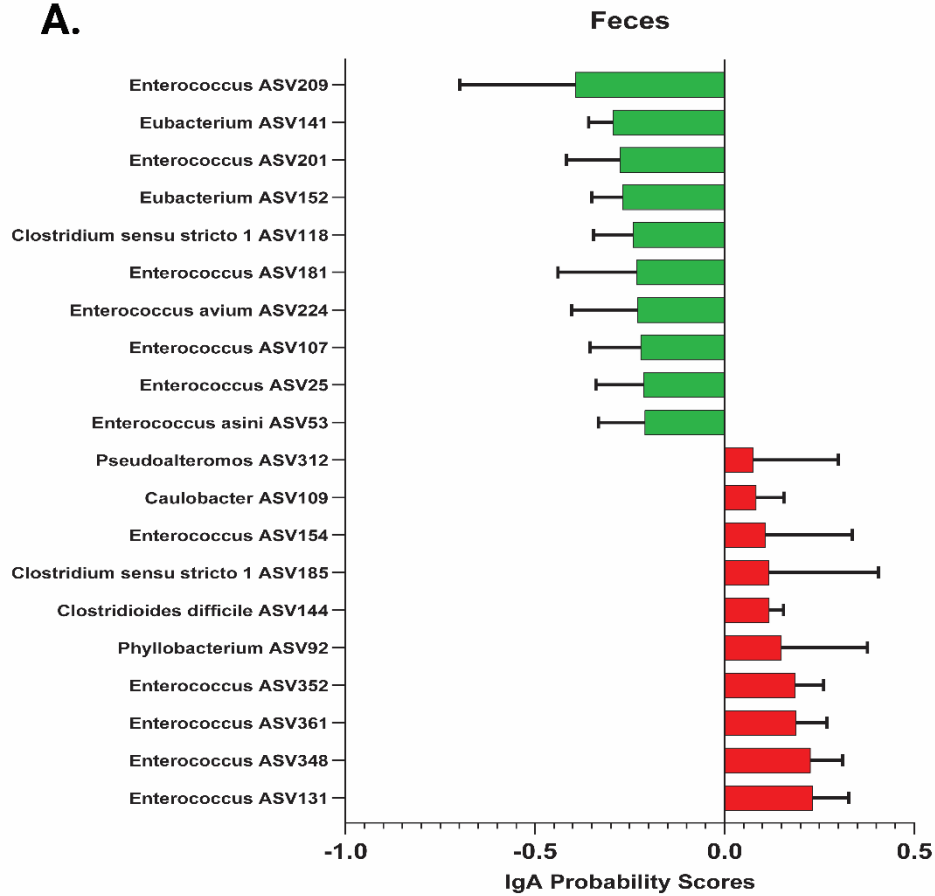
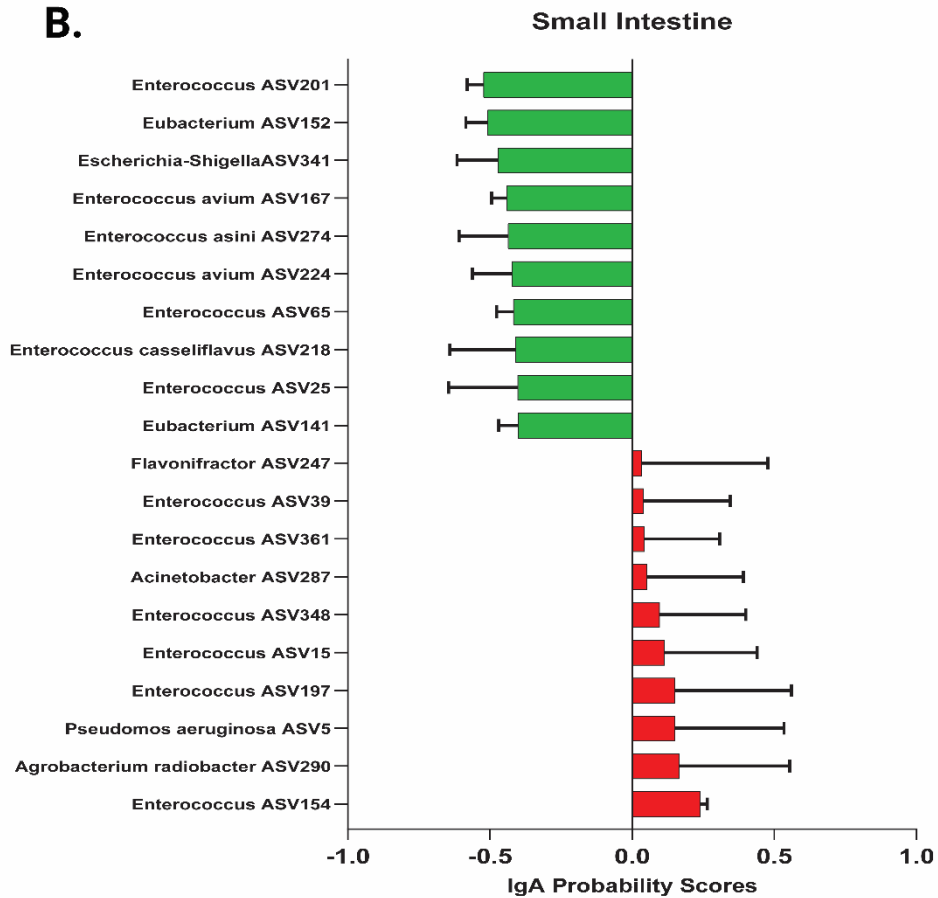
A.**B.**

Figure 4.5. SD-MU animals have an increased likelihood of having *Enterococcus* sp. targeted by IgA in both feces and small intestine. (A) IgA Probability Ratio Score for fecal and (B) intestinal microbes from SD-MU at 8 weeks of age. (A-B) Each bar represents the average IgA Probability Ratio Score calculated for a microbial taxon that had a score in at least three animals. This bar plot shows the top ten positive and negative scores, this can include intermediately likelihood of IgA targeting. The threshold for microbes highly likely to be targeted by IgA in the feces of SD-MU animals was ≥ 0.0072 , while the threshold for non-targeted microbes was ≤ -0.2907 . The threshold for microbes highly likely to be targeted by IgA in the small intestine of SD-MU animals was ≥ 0.1071 while the threshold for non-targeted microbes was ≤ -0.2061 . (A-B) n=5/group [3 females and 2 males].

4.3 Discussion

Here we demonstrated that offspring born to undernourished dams colonized with SD microbiota developed an altered IgA response soon after weaning. SD-MU mice exhibit elevated levels of intestinal plasma cells similar to children with EED and have elevated levels of fecal and intestinal IgA. Our model provides the opportunity for further characterizations of the functional consequences of having a dysregulated IgA response in the future. Surprisingly, while we reported an increase in total IgA and intestinal plasma cell increase in SD-MU mice, this didn't translate to a higher proportion of their microbiota being targeted by IgA. This may be because the IgA produced by the plasma cells might not be entirely against microbes, further investigation into microbiota reactivity against non-microbial products is necessary to understand this. It could also be that the IgA response is nonspecific or lacks high affinity against microbiota, this might lead to either

microbes not being targeted or losing targeting. This result could suggest that the IgA response is not protective.

Bug-FACs revealed interesting patterns in IgA targeting. We calculated the probability of finding a specific taxon bound by IgA in SD MU animals and observed a higher probability for specific *Enterococcus* sp. strains in the community to be in the IgA+ fraction, while a low probability for *Escherichia coli*. These results suggest the *Escherichia coli* strains might be evading immune recognition in the intestine, and suggest there is a need to investigate whether this *Escherichia coli* taxon is pathogenic. Among targeted *Enterococcus* sp., there was a bimodal distribution, suggesting it is important to determine what drives the increase in targeting of specific *Enterococcus* sp. Bug-FACS followed by shotgun metagenomics sequencing could shed light into this.

In the feces of HD-MU offspring, *Escherichia coli* was classified as having a high likelihood of IgA targeting. The absence of this taxa in the presort samples suggests potential clearing of this taxa (and low relative abundance, almost undetectable levels) in the gut of HD-MU mice due to IgA coating functions. This brings the question of potentially isolating IgA from the small intestine of HD-MU mice and gavaging SD-MU mice from 3 weeks of life and forward to test two things: 1) whether IgA isolated from HD-MU mice can remodel the SD-Microbiota at maturity and 2) can IgA supplementation in early life shape growth in SD-MU mice.

4.4 Conclusions

Our findings demonstrate that offspring born to undernourished dams colonized with SD microbiota develop an altered IgA response early in life, characterized by

increased intestinal plasma cells and elevated IgA levels. Despite this heightened immune response, the proportion of microbiota targeted by IgA did not significantly increase, suggesting that the IgA produced may not be entirely directed at microbes or may lack specificity. The IgA Probability Ratio analysis revealed distinct patterns of microbial targeting, with certain *Enterococcus* sp. strains showing a high likelihood of IgA binding, while *Escherichia coli* exhibited low probability, potentially indicating immune evasion. These observations raise important questions about the functional role of IgA in SD-MU mice, particularly whether the response is protective or dysregulated. Further investigation using Bug-FACS coupled with shotgun metagenomics could provide deeper insights into the factors influencing microbial targeting. Understanding these dynamics will be crucial in elucidating the broader implications of IgA dysregulation in early-life undernutrition.

Limitations of this study

Sample preparation for Bug-FACS is done in anaerobic conditions until sorting. While we sort into a buffer that helps preserve anaerobic bacteria, the duration of the sorts poses a significant problem with cell viability and potentially contributes to low cell yield limiting downstream analysis to V4-V3 16S sequencing. Therefore, there is a need to confirm IgA targeting outcomes via a secondary method such as ng-IgA-Seq, which allows for the magnetic bead separation of IgA+ and IgA- bacteria and for the entire protocol to be performed in anaerobic conditions. This technique has been recently demonstrated to increase cell yield after magnetic bead separation without sacrificing

purity, and allows for shotgun metagenomics downstream analysis, which will be beneficial to understanding what is driving IgA targeting in these microbial communities.

4.5 Methods

Donor microbiota and study protocol

Details of enrollment for the iLiNS-DYAD-M study were described in an earlier publication. Briefly, enrollment was open to consenting women over the age of 15 years with ultrasound confirmation of pregnancy of <20 weeks gestation in the Mangochi District of southern Malawi. The randomized controlled clinical trial [clinicaltrials.gov #NCT01239693] tested the effects of providing small quantities of Lipid-based Nutrient Supplements (SQ-LNS) to pregnant and lactating women through 6 months postpartum and to their children through 6-18 months of age¹²¹. During pregnancy and 6 months thereafter, women received one daily capsule of iron-folic acid supplement (IFA group), one capsule containing 18 micronutrients (MMN group), or one 20-g sachet of SQ-LNS [lipid-based nutrient supplements (LNS), containing 21 micronutrients, protein, carbohydrates, essential fatty acids, and 118 kcal]. Children in the IFA and MMN groups received no supplementation; children in the LNS group received SQ-LNSs from 6 to 18 months^{23,121}. Donors used in this study were selected from samples collected at the six-month time point (prior to supplementation) from a broader subset of donors based on their ability to colonize recipient gnotobiotic mice at an efficiency of >50% (more than half of taxa present in the original donor sample were identified in initial experiments). No significant differences in infant microbiota composition based on maternal supplementation at this time point were identified^{23,100}.

Gnotobiotic Mice

All gnotobiotic mouse experiments were performed using protocols approved by the University of Virginia Institutional Animal Care and Use Committee. All gnotobiotic animals used in this publication were germ-free C57BL/6NTac mice obtained from Taconic Biosciences. Upon arrival, germ-free status was verified by quantitative PCR. Mice were housed in plastic flexible film gnotobiotic isolators (Class Biologically Clean Ltd.) under a 12-hour light cycle. Animals received *ad libitum* access to food and water throughout the experiment, and were euthanized at the conclusion of the experiment using AVMA approved procedures. For experiments featuring maternal undernutrition, male and female mice were obtained from Taconic Biosciences at 4 weeks of age and transitioned to the M8 diet. Three days later, they were colonized with donor microbiota and maintained on M8 diet until 8 weeks of age. Males and females were co-housed and switched to an autoclaved nutrient-sufficient breeder chow (LabDiet 5021 Autoclavable Mouse Breeder Diet, LabDiet Inc. Breeding mice were refreshed after six months, and offspring used in these experiments were derived from breeders from two separate rounds of colonization (total of 2 males and 3 females per colonization). Weight and tail length measurements were collected from 1 week after weaning and at maturity. Tail length measurements in living mice were assessed using calipers sterilized to be used inside the isolators. The tail length measurements after euthanasia were performed using a standard laboratory ruler. All tail length measurements were done from the base of the tail to the tip along a straight line. Fecal samples for Bug-FACs and Protein quantification were collected at the indicated time points and immediately frozen. Samples were stored at -80°C until use. Anthropometry data shown includes an equal number of female and

male healthy donor colonized mice and stunted donor colonized mice unless otherwise specified.

Colonization and Diets

To prepare infant fecal samples for colonization of germ-free mice, aliquots of each sample were removed from storage at -80°C, weighed and immediately transferred into anaerobic conditions (atmosphere of 75% N₂, 20% CO₂ and 5% H₂; vinyl anaerobic chambers from Coy Laboratory Products). Samples were subsequently resuspended in pre-reduced PBS containing 0.05% L-Cysteine Hydrochloride at a concentration of 10 mg/mL. Samples were vortexed for one minute and allowed to clarify by gravity for 5 minutes. The supernatant was removed to a fresh anaerobic tube and combined with an equal volume of sterile, pre-reduced PBS containing 0.05% L-Cysteine HCL and 30% glycerol. Gavage mixtures were aliquoted into sterile 2 mL screw cap tubes (Axygen) and frozen at -80°C until use. To colonize recipient mice, pools of gavage mixtures were sterilized externally with ionized hydrogen peroxide (STERAMIST System, TOMI Inc.) and passed into each isolator after appropriate exposure time (20 minutes). Animals were colonized via a single oral gavage with a 200 µl volume of gavage mixture.

The low protein and micro-nutrient deficient Malawi-8 diet was prepared as previously described^{41,140} and obtained from Dyets, Inc. Briefly, ingredients (corn flour, mustard greens, onions, tomatoes, ground peanuts, red kidney beans, canned pumpkin and peeled bananas) were cooked and combined in an industrial mixer. Dry pellets of the M8 diet were extruded, vacuum-sealed and double bagged prior to sterilization by irradiation (Steris Co). The nutritional content of the cooked and irradiated diet was

assessed by N.P. Analytical Laboratories as described in Blanton et al ²⁴. LabDiet 5021 was sterilized by autoclaving at 129°C and 13.2 PSI for 15 minutes. Sterility of both diets was routinely assessed by culturing pellets in Brain Heart Infusion (BHI) broth (Millipore), Nutrient broth (Millipore), and Sabouraud-Dextrose (Millipore) broth for five days at 37 °C under aerobic conditions, and in BHI broth and Thioglycolate broth (Difco) supplemented with 0.05% L-Cysteine Hydrochloride (Sigma) under anaerobic conditions. After the five-day liquid culture, cultures of all diets were plated on BHI agar supplemented with sheep blood (Thermo Scientific). All diets were stored at -20 °C prior to use.

Bug-FACs

All preparations for Bug-FACs were done inside an anaerobic chamber to preserve the cell viability of facultative and strict anaerobes. Small intestine contents and fecal pellets that were flash frozen at -80 C immediately after collection, were resuspended in sterile 1X PBS supplemented with 0.05% cysteine (1X PBS+0.05%C) by vortexing. Resuspended samples were incubated in ice for 10 minutes, to separate bacteria from debris by gravity sedimentation. A 400 µL aliquot of supernatant was collected from each sample and filtered through a sterile 40 µm nylon filter into a new sterile tube. Bacteria that passed through the filter were pelleted by centrifugation at 10,000 rpm for three minutes. The supernatant, which did not contain bacteria, was discarded, and the pellet was washed with 1 mL of sterile 1X PBS+0.05%C before being centrifuged again. Pelleted bacteria were resuspended in 10% of filter-sterilized rat serum (blocking step) for ten minutes in wet ice. Another wash step was performed after the blocking step. At this point, all samples were resuspended in 500 µl sterile 10% FBS + 1X PBS

supplemented with 0.05% cysteine buffer (or Bug-FACs buffer). A 100 μ l of the resuspended samples were spun down and flash-freeze, as the presort or before sorting fraction for sequencing.

The remaining resuspended samples were centrifuged to form a pellet and stained with 1:50 anti-IgA-APC (BioLegends) in Bug-FACS buffer for 30 minutes on wet ice, protected from light. After incubation, two wash steps followed by centrifugation were performed to remove any residual staining. 500 μ l of 0.9% NaCl/0.1M HEPES buffer containing 1:800 diluted SYTO-BC (Invitrogen/Life Technologies) was added to each pellet. Samples were transported to UVA's Flow Core Facility in anaerobic containers with AnaeroPack-Anaero (MGC, Inc), disposable oxygen-absorbing and carbon dioxide-generating bags, to maintain anaerobic conditions outside Coy chamber. Samples were sorted using an Aurora CITEK spectral flow cytometer (BD Biosciences) in a laminar flow biocontainment hood. Standard thresholds to detect events in the Forward Scatter (FSC) and Side Scatter (SSC), were removed to allow maximum detection of small bacteria. The gating strategies are shown in the result section of Chapter 4. We sorted on average ~ 200,000 events (or microbes) for the IgA+ fractions and ~1,000,000 events for the IgA- fractions. Fractions were sorted into 200 μ l SYTO-BC buffer. IgA+ fractions on average were 500 μ l and IgA- fractions 3 mL. Fractions used for sequencing were immediately flash-freeze at 80 °C after spinning down for 3 minutes at 10,000 rpm.

To account for contamination 1X PBS buffer (or sheath) running through the system was filter-sterilized using a -- μ m nylon filter. In between sorted samples, a 10% bleach wash was performed. Before and after each sorting run, we collected sheath buffer running through the fluidics system of the sorter. This sheath was cultured in blood agar

BHI plates in both aerobic and anaerobic conditions, CFUs were counted after 48 h. 16S qPCR was also performed in some of the sheaths collected. Samples were selected for sequencing if both cultures and qPCR passed quality control.

Bug-FACs Sequencing

Bug-FACs samples were shipped to SeqCenter for DNA extraction and sequencing. All standard DNA extractions at SeqCenter follow the ZymoBIOMICS™ DNA Miniprep Kit5. DNA was extracted from fecal samples following the guidelines in Appendix B of the ZymoBIOMICS™ DNA Miniprep Kit. Eluted DNA was then purified by running the effluent through the prepared Zymo-Spin™ III-HRC Filter. Final DNA concentrations were determined via Qubit. After DNA extractions, library prep was performed using Zymo Research's Quick-16S kit with passed primers targeting the V3-V4 region of the 16S gene. The following sequencing primers were used: "CCTACGGGDGGCWGCAG" (341F) and "GACTACNVGGGTMTCTAATCC" (806R). After cleanup and normalization, samples were sequenced using a P1 or P2 600-cycle NextSeq2000 Flowcell to generate 2x301 bp paired-end (PE) reads. Quality control and adapter trimming were conducted with bcl-convert1 (v4.2.4). Primer-dimer sequences, identified as PCR artifacts, were removed from the FASTQ files using the following criteria: read length greater than 150 bp, PolyN strings with fewer than 10 consecutive Ns, and PolyG strings with fewer than 150 consecutive Gs.

Bug-FACs Quality Control & Data Analysis

Sequences were then denoised using Qiime2's dada2 plugin³. Denoised sequences were assigned a microbial taxonomy by mapping to the Silva 138 99% ASVs full-length sequence database and the VSEARCH⁴ utility within Qiime2's feature-classifier plugin. The prevalence filtering threshold was set to remove any ASVs that was present in 1 sample across sample type (fecal or small intestine luminal contents). ASVs with a relative abundance across sample type $\leq 0.1\%$ were removed as spurious ASVs. Probability ratio scores were calculated using IgAScore package (version 0.1.2). To determine thresholds for highly targeted taxa and not highly targeted, we did a Gaussian Mixture Model for Clustering. Phylogenetic trees for distance matrices were constructed using the following R packages: msa¹⁶⁴ (version 1.38.0) and phagorn¹⁶⁵ (version 2.12.1). Ordination plots showing weighted UniFrac distances (a measurement of β diversity based on phylogenetic relatedness) were produced using the phyloseq package¹⁴³ (version 1.50.0) in R.

Protein Quantification of IgA

Fecal and whole small intestine content samples were collected at the time of euthanasia and stored at $-80\text{ }^{\circ}\text{C}$ freezer. Fecal and small intestine luminal contents were homogenized in extraction buffer composed of 1x HALT (Thermo Scientific, ref. 78429) 5mM EDTA (Thermo Scientific, ref. 15575020), 1% Bovine Serum Albumin (BSA, Millipore Sigma, Inc, cat. A4737) in 1X PBS. All samples were normalized by weight to 100mg/mL. Resuspended samples were vortex horizontally for 10 minutes. Homogenates were centrifuged at $4\text{ }^{\circ}\text{C}$ and 2,000 RPM for 5 minutes. Supernatant

containing protein extract was stored at -80 °C until analysis. IgA in protein extracts isolated from feces and small intestine contents were quantified by ELISA assay (Thermofisher, Cat. #88-50450-88) performed according to the manufacturer's recommendation.

Briefly, the capture antibody was coated onto a 96-well half-area plate (Corning) in 1X PBS overnight at 4 °C. On the following day, the plates were washed three times with 200 uL of Wash Buffer (0.05% Tween 20 in PBS) and blocked for two hour at 4 °C. After blocking and incubation, plates were washed again before adding samples of protein extracts from feces and small intestine contents as well as a standard curve. The plate was incubated for 2 hours at room temperature before being washed as described above. Detection Antibody provided in the kit was added at the suggested concentration and incubated for another 1 hour at room temperature. After incubation, plates were washed and Substrate Solution (Tetramethylbenzidine or TMB)) was added to each well and incubated at room temperature for 15 minutes avoiding direct light. After incubation, Stop Solution (2 N H₂SO₄) was added to each well. Plates were reader an optical density of 450 with background subtraction at 570 nm using a Tecan plate reader.

Statistical Analysis

Statistical analyses were performed in GraphPad Prism (version 10.4.1) unless otherwise noted. V3-V4 16s sequencing data was analyzed in R (version 4.4.2). Statistical details including the number of animals or samples can be found in figure legends. Statistical significance was assessed by Mann-Whitney U test when comparing between two groups, or by Two-Way ANOVA with Šídák's multiple comparisons test when

comparing >2 groups unless otherwise noted. PERMANOVA tests were performed using R package vegan (version 2.6-8) and pairwise comparisons from distance matrices were calculated using the pairwiseAdonis package¹⁶⁷ (version 0.4.1). P values are shown in figures or tables for samples with significant differences. Each data point represents an individual animal, and horizontal bars represent the mean.

Chapter 5: General Discussion & Future Directions

Yadeliz A. Serrano Matos & Carrie Cowardin

Author contributions:

Writing, Y.S.M., Editing, C.A.C.

5.1 The microbiota shapes growth & immunity

In Chapter 2, we demonstrated that the intergenerational transmission of microbes from two stunted human infants causes stunting-like features in offspring. Stunted Donor (SD-IG) mice exhibited shorter tails and a trend towards a decrease in femur length. Tail length is a well-established surrogate for height in mouse models of undernutrition^{51,56,73,150}. Bone growth is also often used as a measurement of linear development^{51,56}. These physical changes were observed only when mice received their microbiota vertically from the dam and not when colonized directly post-weaning, indicating timing of colonization is important for the development of reduced linear growth. We did not observe changes in absolute body weight at maturity for intergenerationally colonized animals. Mice colonized post-weaning were significantly larger regardless of microbiota composition. Differences in weight between intergenerational and post-weaning colonized mice can be attributed to the duration of the undernutrition period in each model. Mice colonized intergenerationally were in the Malawi-8 (M8) diet, for five weeks, while mice colonized post-weaning were in the same diet for four weeks.

The lack of weight differences between intergenerationally colonized animals may suggest that a key factor is missing in this model. In the cycle of stunting mothers are commonly undernourished and our first model did not include this variable⁴². In the original model of intergenerational undernutrition, we introduced germ-free females for breeding at 8 weeks of age. Therefore, sires were the only animals exposed to the undernourished diet. The microbiota was therefore passed from sire to dam by co-housing. The fact that paternal perturbations contribute to changes in growth in offspring is surprising and warrants further study. Argaw-Denboba et al. (2021) demonstrated that

paternal microbiome perturbations alone can affect offspring fitness¹⁷⁵. Disrupting the microbiota of male mice with antibiotics resulted in increased instances of underweight offspring, severe growth restriction, and premature mortality¹⁷⁵. Another important question that stems from this work is whether parental undernutrition is sufficient alone to cause growth deficits in SD animals because offspring were weaned onto the same undernourished diet the parents consumed. Omitting offspring diet exposure would allow us to identify distinct effects of poor diet *in utero* versus during the postnatal period.

These questions were partially answered in Chapter 2. The introduction of maternal undernutrition into our MU model caused reduced ponderal growth from birth to maturity in offspring colonized intergenerationally with Stunted Donor microbiota (SD-MU). This reduction in ponderal weight at birth could be caused by limited nutrient availability during gestation due to the mothers being on the M8 diet. This finding also warrants further exploration in these models. The first approach that could help understand what is happening during gestation is to measure fetal development. These could be assessed by determining whether these animals have intrauterine growth restriction (IUGR) during gestation. As a potential mediator of reduced fetal growth, studies have shown that corticosterone regulates nutrient allocation to fetal growth in mice during stress¹⁷⁶. Undernutrition, particularly low protein diets, can induce stress responses in mice¹⁷⁶. The M8 diet is low in protein; therefore measuring the gene expression or protein levels of this steroid hormone during gestation could shed light onto potentially altered nutrient allocation to fetal development in our mouse models.

Beyond the differences in ponderal growth between groups, we also observed a significant increase in early-life mortality in SD animals born to undernourished mothers.

Interestingly, a decrease in survival probability was not detected in our first model of intergenerational undernutrition, highlighting the need for further investigation. Understanding fetal health in this context is crucial, as it could help pinpoint when and how developmental disruptions occur and determine if this timepoint will be beneficial for therapeutic interventions in this model. One approach is to assess fetal viability at different gestational stages to determine whether offspring fate is established *in utero* or if postnatal factors contribute to the increased mortality rates. This could help differentiate between potential causes such as placental insufficiency, impaired fetal growth, or postnatal metabolic and immune challenges. Conducting these assessments will provide critical insights into the mechanisms underlying early-life mortality in our model.

In the small intestine, a site vital for growth in early life, the immune responses observed in SD offspring colonized intergenerationally were not present in mice colonized post-weaning, indicating the impact of early-life microbial exposure in immune development. Remarkably, the small intestine immune profiles in SD offspring resembled those reported in stunted and EED-affected children, including an increased number of intestinal epithelial cells, a reduction in CD4⁺ T cells, an increase in CD8⁺ T cells, and a lower abundance of macrophages. Additionally, SD offspring exhibited intestinal morphological changes characteristic of EED, such as villus blunting.

In Chapter 4, we demonstrated that SD offspring showed significantly higher IgA protein levels in both the small intestine and feces compared to HD offspring. Furthermore, we characterized this immune response in SD offspring and observed similar highly IgA-targeted microbes in both the feces and small intestine at the genus level, indicating a shared microbiota-driven host response across these compartments.

This suggests an altered IgA response in SD offspring, potentially mirroring the immune profiles observed in stunted children. These similarities between SD offspring and stunted children emphasize the relevance of this model in understanding the mechanisms underlying this immune response.

Overall, our studies demonstrate that parental diet and microbiota play a crucial role in shaping growth outcomes, immunity and the microbiome of the offspring. We found that exposure to an undernourished diet and altered microbiota has cumulative effects throughout the lifespan, underscoring the need for early and sustained interventions in stunted pregnant mothers and their offspring. Additionally, our work demonstrates that microbiota from human stunted infants can be utilized to model environmental enteric dysfunction (EED) in germ-free mice, enabling us to investigate the role of specific immune cells and pathways previously observed in stunted children. Finally, we demonstrate that the microbiome drives differential IgA targeting, highlighting that key microbes elicit strong immune recognition and may have a negative impact on gut physiology. Together, these findings provide valuable insights into the interplay between diet, microbiota, and immunity during early life development.

5.2 What about the maternal microbiome?

Notably, undernourished dams led to reduced ponderal growth and lower survival probability in SD offspring but did not have the same effect on HD offspring. This disparity suggests that the HD microbiota may play a protective or mediating role in HD offspring outcomes, potentially influencing resilience to maternal undernutrition. Sequencing the maternal microbiome through pregnancy in both HD and SD dams will help determine if

there are changes in the microbial communities that could be correlated to a reduction in ponderal growth and an increase in early life mortality in offspring. In humans, it has been reported that *Bifidobacterium* sp. levels increase during pregnancy. Furthermore, *Bifidobacterium breve* have been associated with positive fetal development in germ-free mice^{177,178}. Across our mouse models, we consistently observe a reduction in the relative abundance of *Bifidobacterium breve* in SD offspring, regardless of maternal nutritional status.

Research should focus on preventing stunting rather than treating it, as studies show stunting is largely irreversible if onset happens within the first three months of life⁷. Preventing stunting could be far more effective than attempting to reverse its long-term consequences, as early-life growth deficits are often irreversible and associated with lasting impacts on cognition, immunity, and metabolic health⁵. To explore whether maternal supplementation with *Bifidobacterium breve* can prevent stunting in SD-MU offspring, we propose an experiment in which female mice receive supplementation at two key time points in our mouse model: before conception and during gestation (**Figure 5.1**). This approach is encouraged by studies in Bangladesh showing that *Bifidobacterium infantis* supplementation in stunted children promotes weight gain but not linear growth, raising the question of whether earlier intervention—through the mother—could provide even greater benefits. SD offspring from supplemented and non-supplemented dams will be monitored for growth and microbiome composition (from birth to maturity). If supplementation proves to be beneficial, fetal metabolomics could be performed at different times points during gestation and supplementation (and controls), to understand how this probiotic impacts fetal development in our mouse model. If effective, this strategy

could offer a preventative approach to stunting by promoting an optimal maternal microbiome in stunted mothers that fosters healthier early-life development. If no benefits are observed from supplementation, characterizing fetal development in our mouse model of intergenerational undernutrition will still be important and innovative, as there is limited research available about fetal development in mouse models of undernutrition that consider intergenerational transmission of microbes.

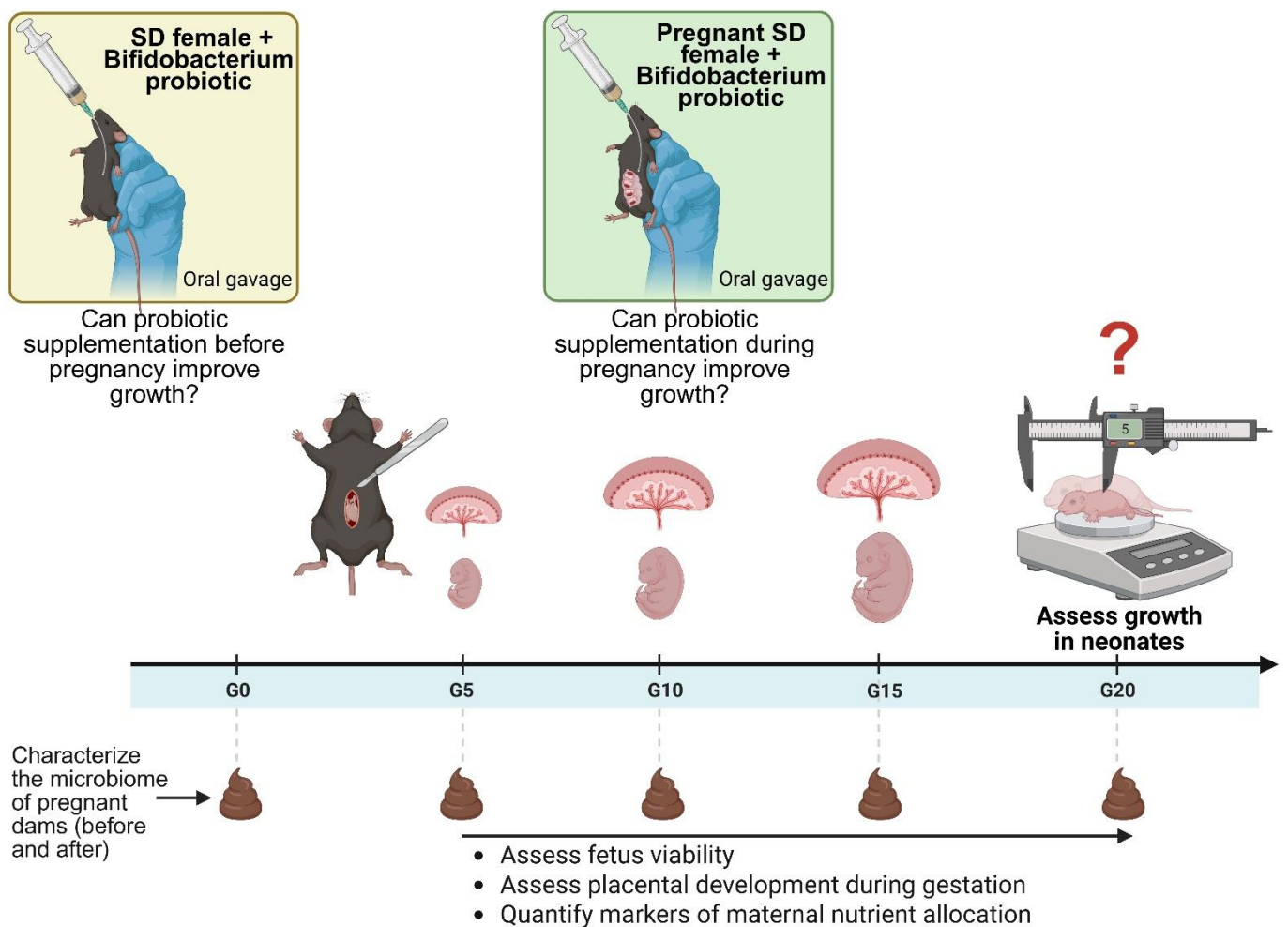


Figure 5.1. Understanding *Bifidobacterium* sp. roles in growth. This experimental design explores the potential of *Bifidobacterium* sp. supplementation during pregnancy and before to

change growth outcomes in SD offspring. Mothers are divided into three groups: the first group receives a vehicle control (not shown), the second group receives *Bifidobacterium* supplementation before pregnancy, and the third group receives *Bifidobacterium* supplementation in the middle of the pregnancy. Fetal growth and viability will be assessed at different time points by measuring the placenta and fetal body weight. Fecal samples will be collected weekly to analyze microbiota composition and measure inflammatory markers in SD dams before, during, and after pregnancy. At the end of the experiment, mothers and neonates (and growth assessed) will be euthanized for tissue collection, including small intestine and liver samples, to assess gut histology, immune cell populations (via flow cytometry), and systemic inflammation (via ELISA), if necessary. The results will determine whether *Bifidobacterium* supplementation improves growth in SD offspring.

5.3 Do immune responses regulate growth in our model?

In Chapter 2, we did flow cytometry in the small intestine epithelium and lamina propria of HD and SD animals colonized intergenerationally. Findings from this experiment revealed similar immune responses reported in stunted children were observed in SD offspring. These immune responses were not observed in mice colonized post-weaning. SD offspring exhibit an increase in leukocytes in the epithelium signaling immune cell infiltration, similar to what is observed in children with environmental enteric dysfunction (EED). SD offspring also displayed a decrease in CD4+ T cells and an increase in CD8+ T cells in this same compartment, suggesting a shift toward a more cytotoxic and inflammatory immune response. CD4+ T cells are generally associated with helper functions and regulation, while CD8+ T cells are involved in direct killing of infected or damaged cells¹⁷⁹. This shift could indicate a dysregulated immune response in the gut,

potentially contributing to inflammation and epithelial damage, which is linked to impaired intestinal functioning in undernutrition.

A decrease in the CD4+ T cells in SD offspring from our first intergenerational model of undernutrition may indicate impaired antigen-specific responses, potentially affecting immune memory and vaccine efficacy. Stunted children often exhibit poor responses to rotavirus vaccines, making it important to determine whether our model can be used to study the underlying mechanisms of this phenomenon. To evaluate this, we could assess whether these CD4+ T cells exhibit reduced proliferation or cytokine production upon antigen stimulation. Additionally, our model could be used to evaluate vaccine efficiency by administering a rotavirus vaccine and measuring antibody responses, T cell activation, and viral clearance. This could provide insights into how early-life undernutrition affects long-term immune function and vaccine responsiveness.

SD offspring from our main mouse model exhibit an increase in granzyme A producing natural intraepithelial lymphocytes (Natural IELs) in the intestinal epithelium. These cytotoxic immune cells surveil and protect the epithelial barrier integrity against infections¹²⁸. Granzyme A is a serine protease released by cytotoxic cells that induces apoptosis in infected or damaged cells¹⁸⁰. While intracellular staining confirmed elevated levels of granzyme A-producing natural IELs in SD offspring compared to HD offspring, it does not indicate active secretion. Therefore, there is a need to understand the functional consequences of elevated Natural IELs in SD offspring. Thus, determining whether granzyme A is released into the gut environment of SD animals is essential for understanding the role of these immune cells in this model. To address this, we could

quantify granzyme A in gut luminal contents by Enzyme-Linked Immunosorbent Assay (ELISA) or western blot.

We could also quantify more localized secretion of this protease by separating the intestinal lamina propria and epithelium and determining granzyme A levels in these respective compartments either by gene expression or at the protein level. Next, assessing epithelial integrity could help clarify whether granzyme A contributes to barrier dysfunction in SD offspring. If we identify active secretion of granzyme A, we can then look into whether this response is protective or not, by assessing epithelial cell damage via Terminal deoxynucleotidyl transferase dUTP nick end labeling (TUNNEL) assay. Furthermore, we can also determine the direct influence of granzyme A secretion on epithelial cell damage by blocking granzyme A production in Natural IELs. If blocking of granzyme A causes changes in intestinal morphology, then it should be investigated if these changes associate with better growth outcomes in SD offspring.

In Chapters 2 and 3, both murine models of intergenerational undernutrition consistently exhibited characteristics of environmental enteric dysfunction (EED) in the small intestine, including villus blunting. However, we did not observe all key hallmarks of EED, such as significant disruption of the epithelial barrier. Despite this, our findings highlight aspects of intestinal dysfunction relevant to EED pathology. Further characterization of the small intestine beyond immune responses is necessary to strengthen our model as one of EED. Immune responses in the lamina propria and epithelium provide valuable insights into the underlying processes at play. In the lamina propria compartment, we observed less pronounced immune differences compared to the epithelium, which is a critical finding in understanding immune dysregulation in SD

offspring. A more pronounced shift in immune cell populations within the epithelial barrier may be driven by its direct interaction with the gut microbiota. However, it is important to assess whether microbiota stimuli remain within normal levels in SD offspring or if there is excessive stimulation by the microbiota, potentially due to a reduction in the mucus layer as has been suggested in human undernutrition.

In individuals with environmental enteric dysfunction (EED), a syndrome closely linked to stunting, a reduction in goblet and paneth cell numbers is commonly observed¹³. This decrease is believed to contribute to impaired intestinal function and nutrient malabsorption. One approach to determine mucus layer integrity would be to measure goblet cells, which produce mucin in the small intestine to protect the epithelium barrier. Mucus production could be quantified through histological staining and mucin gene expression. We could also assess paneth cells, which secrete antimicrobial peptides; both these cells are key components of barrier integrity and intestinal immune homeostasis⁵⁸. Paneth cell function could be evaluated by measuring antimicrobial peptide levels such as lysozyme and α -defensins in the intestinal lumen. Investigating these features would not only clarify the mechanisms underlying more pronounced immune shifts in the epithelium of SD offspring but also enhance the relevance of our model in studying EED-associated gut dysfunction.

SD offspring also exhibited increased levels of CCL5 (C-C motif ligand 5), also known as RANTES, a chemokine involved in immune response, inflammation, and tissue repair^{122,181}. CCL5 levels can be induced by the microbiota and have been shown to exacerbate inflammation in DSS colitis mouse models¹³¹. Interestingly, CCL5 gene expression is elevated in duodenal biopsies from children with EED compared to healthy

US controls and celiac patients⁶⁸. This raises the question of whether CCL5 plays a protective role or contributes to growth deficits in our model (**Figure 5.2**). To test this, we could use Maraviroc, a CCR5 antagonist that blocks the interaction between CCL5 and its receptor¹⁸². Assessing the effects of CCL5 inhibition on intestinal inflammation and growth could help identify novel biomarkers or therapeutic targets for mitigating growth impairments in humans.

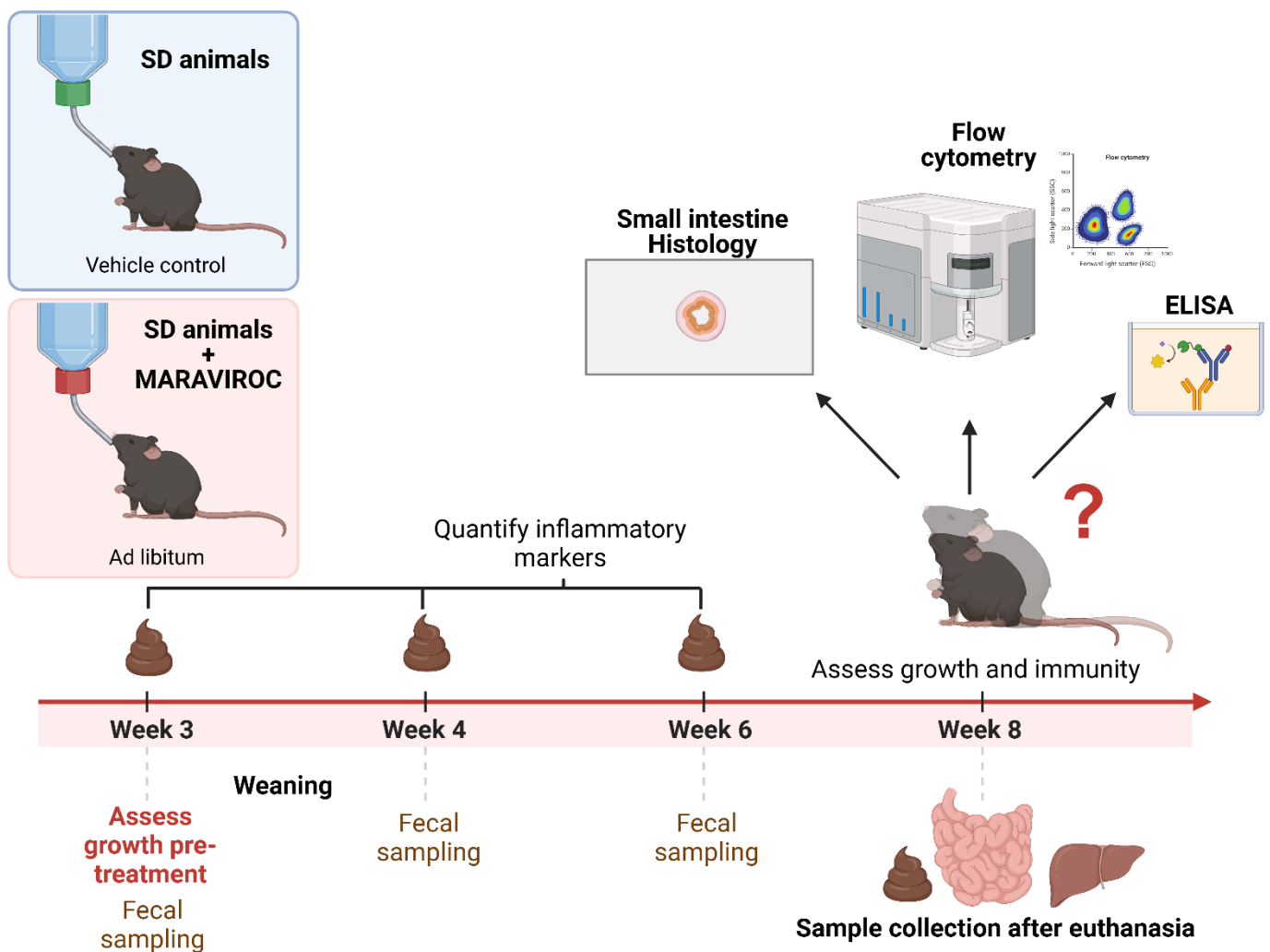


Figure 5.2. Understanding the Role of CCL5 in Undernutrition and Stunting. This experimental design investigates the effects of Maraviroc treatment on growth and immunity in

SD offspring. Two groups of animals are studied: SD mice weaned into regular water with no Maraviroc and SD animals weaned into water with a specific dose of Maraviroc. Ponderal and linear growth will be assessed starting at three weeks, and fecal samples will be collected at the indicated time points to measure protein levels for known markers of inflammation. At Week 8 (maturity), animals are euthanized for sample collection, including tissues from the small intestine and liver. Immune responses in the small intestine will be assessed through histology and flow cytometry. This experiment aims to determine how Maraviroc, a CCR5 antagonist, the receptor for CCL5, influences intestinal inflammation, immune function, and overall growth outcomes in SD offspring.

5.4 Which microbes are driving reduced linear growth?

In Chapter 3, we demonstrate SD offspring born to undernourished dams have exacerbated growth deficits¹⁰². In contrast, mice colonized with the same SD microbiota but born to non-undernourished dams showed reduced linear growth but not early life mortality. While HD and SD offspring have distinct microbial communities, there were few differences in microbiota composition between SD-NMU mice and SD-MU animals. Among the differences between SD-NMU and SD-MU animals, we observed an increase in the relative abundance of *Escherichia coli* and *Enterococcus* sp. in the latter. This suggests two things; first, it is necessary to identify the microbial functions driving reduced linear growth and that V3-V4 16S sequencing is insufficient to achieve this. Therefore, metagenomics and microbial RNA-seq may help identify microbial functions and active gene expression, offering a comprehensive view of the microbiome's role in host growth and immunity.

Another way to start understanding how the microbiome shapes host growth and immunity was investigated in Chapter 4. Immunoglobulin A (IgA) is known for having discriminatory functions between good and bad bugs, in undernutrition and inflammatory bowel diseases^{96,173}. Therefore, we characterized IgA responses hypothesizing immune recognition by the host can provide information about microbial drivers of stunting. Both SD-NMU and SD-MU developed an altered IgA response, including elevated levels of total IgA in the small intestine and feces and increased proportion of IgA-producing intestinal plasma cells. These results suggest the SD microbiota induces the activation of an immune response that culminates in IgA production. However, this did not translate to an increase in the overall IgA targeting of the microbiota in SD animals. This was surprising, since the Afribiota study and Kau et al have demonstrated stunted and undernourished children have a significantly higher number of their fecal microbiota targeted by IgA³⁹. However, IgA's ability to target immunogenic bacteria that cause disease does not depend on the proportion of bacteria targeted⁹⁶. We decided to do Bug-FACs to identify microbes eliciting strong IgA responses, and discovered SD-MU animals have different IgA targeting patterns in their fecal microbiota compared to HD-MU animals.

Future studies are necessary for this project. We hypothesize that highly IgA-targeted microbes in SD offspring are sufficient to cause reduced linear growth compared to HD pups. Testing this hypothesis will allow us to simplify the SD microbiota to a defined community, enabling the mechanistical studies of how specific microbes effect linear growth and immune function in our murine models of intergenerational undernutrition. To identify microbial effectors of stunted growth we can use sorted fractions from the feces

of SD mice. We can orally gavage germ-free mice with the IgA+ fraction and the IgA- fraction respectively and determine if the offspring of these animals develop reduced linear growth (**Figure 5.3**). If transfer of IgA+ microbes into germ-free mice through Bug-FACs results in inefficient colonization, we could switch to next-generation IgA-Seq (ng-IgA-Seq) instead for the isolation of IgA+ bacteria. ng-IgA-Seq allows for a higher yield of bacteria after sorting without compromising purity making possible other downstream analyses besides V3-V4 16S sequencing or experimental assay requiring a certain concentration of inoculum¹⁸³. This technique can be fully implemented under anaerobic conditions, unlike Bug-FACs. A key limitation of our current system is the potential loss of anaerobic bacteria during sorting in the flow cytometer, which may result in an inaccurate representation of IgA targeting.

Another alternative to ng-IgA-Seq is to do Bug-FACs followed by the same technique described by Palm et al (**Figure 5.3**)⁹⁹. In this study, the authors were successful in studying the functional impact of IgA+ bacteria in inflammatory bowel disease by creating bacterial culture collections (BCC) from the sorted fractions. The creation of BCCs will enable more precise control over the microbes introduced into the germ-free breeders, allowing us to selectively colonize them with microorganisms that exhibit the highest levels of IgA targeting.

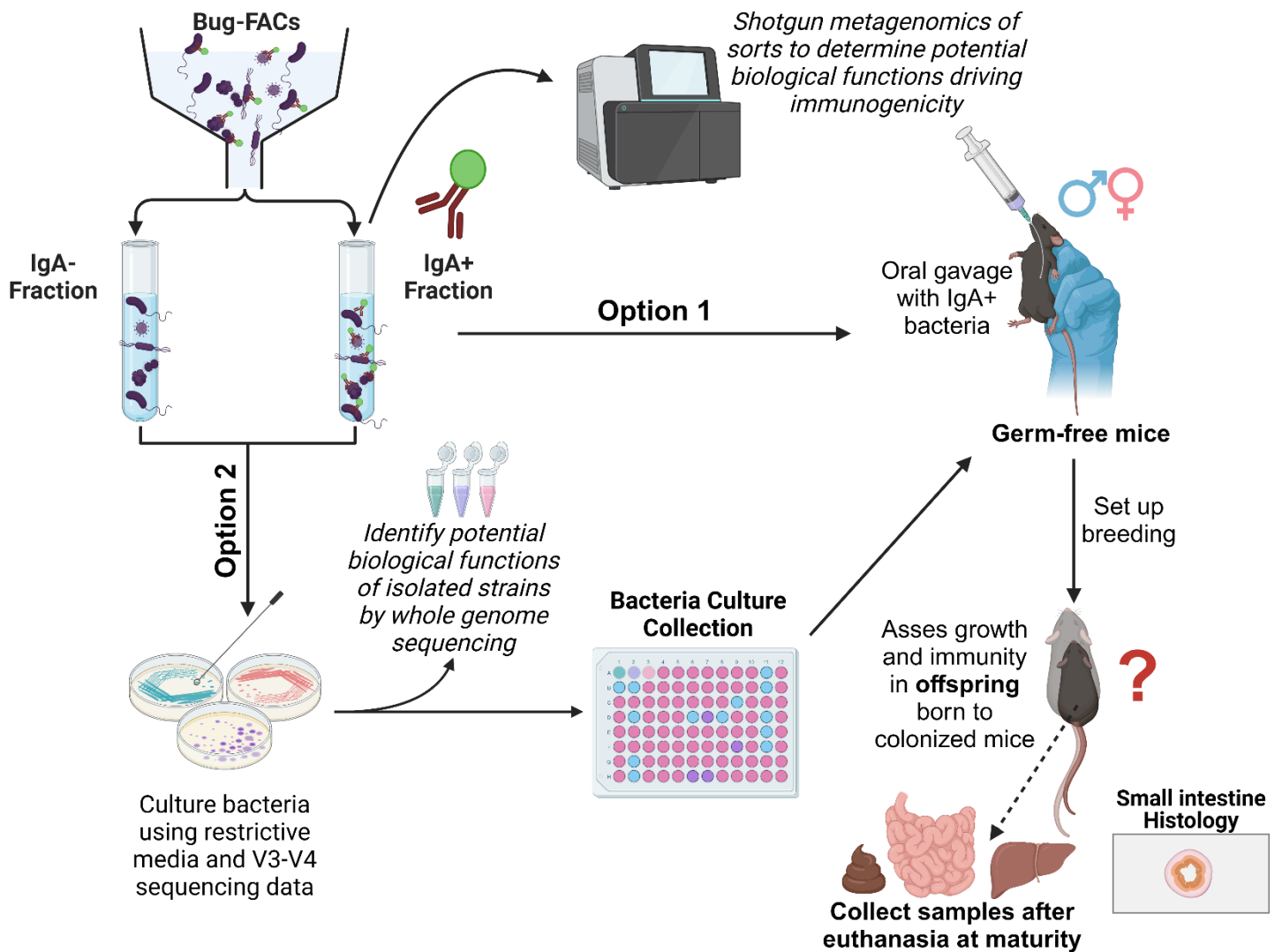


Figure 5.3. Evaluating the impact of immunogenic bacteria on reduced linear growth. This diagram illustrates how we can utilize IgA to identify bacterial drivers of stunted growth in our models of intergenerational undernutrition. We have two options; the first is the simplest: if purity is high in the fractions and sorted microbes are representative of what is targeted by IgA, we could directly administer the sorted fractions to germ-free mice, then breed and assess growth and immunity in the offspring. To understand the biological functions driving immunogenicity, we can perform shotgun metagenomics directly to the sorted fractions in this first approach. The second option includes sorting and culturing IgA+ and IgA- bacteria in selective media based on V4 16S sequencing data obtained in Chapter Four. We can create Bacterial Culture Collections and select

from these highly targeted microbes to administer via gavage to germ-free mice. We could perform whole genome sequencing on each individual isolate to determine what is potentially driving IgA targeting.

We have already addressed the necessity of simplifying the whole donor community into a more manageable subset of microbes that can be more effectively manipulated. If this can't be achieved via Bug-FACs, we can still address the variability by pooling the human infant donors microbiota we have available, with the goal of potentially minimizing variability between microbiotas. Since all individual human donor microbiotas presented in this study vary significantly in composition, combining multiple microbial communities allows us to reduce stochastic differences and focus on common, functionally relevant microbial taxa driving growth deficits in our models. This approach also makes our model more reproducible and biologically relevant. Ultimately, this strategy strengthens our ability to dissect the mechanisms linking microbiota composition to undernutrition and immune function.

5.5 Pre- and post- natal factors influences in growth

In Chapter 3, we investigated when in early life mice develop reduced linear growth. This is crucial because it allows us to identify specific developmental windows during which the microbiota may be playing a crucial role in setting long-term growth outcomes. This question is important to address since current nutritional interventions are not usually successful in rescuing stunted children. Our cross-fostering studies showed that postnatal exposure to the stunted donor microbiota in germ-free pups was sufficient to recapitulate growth deficits observed in animals born to colonized dams. Results from

a second cross-foster model where we switch colonized pups to SD and HD colonized dams showed that exposure to the SD microbial community negatively affected growth in an additive manner. Both groups of this second cross-fostered model had microbiota that predominantly resembled the SD community, suggesting that the SD microbiota largely displaced the HD microbes acquired at birth.

Interestingly, cross-fostering data also revealed intestinal morphology was shaped to a greater extent by prenatal factors, particularly with regards to muscularis thickness. Further understanding of signals regulating intestinal morphology changes could help identify additional pathways that regulate small intestine development to reveal targeted therapies that improve child intestinal absorptive function in early life. A caveat of cross-fostering is that neonates still are exposed to postnatal factors from their birth parents since cross-fostering happens within the first three days of life. This limitation might result in discrepancies between the early-life microbiota development and long-term growth outcomes. Therefore, further investigation into this is required. We could do cesarean sections and then cross-foster the neonates to a dam that gave birth recently in order to prevent pup colonization with birth dam microbiota. Other future directions include characterizing immune responses in cross-fostered mice to determine the influence of pre- and post-natal factors in immune development by flow cytometry of the small intestine lamina propria and epithelium.

5.6 Implications of this dissertation work

The findings in this thesis highlight the critical role of the gut microbiota in mediating the effects of early-life undernutrition and its long-term consequences on growth and immune development. We developed multiple novel gnotobiotic murine models of intergenerational undernutrition and utilized them to demonstrate that intergenerational colonization with the microbiota from a stunted infant donor resulted in reduced linear growth and altered immune responses in offspring. We also showed that maternal undernutrition exacerbates microbiome-driven stunting and early life mortality. Our murine models of intergenerational undernutrition provide a tool for understanding the mechanisms underlying stunting and EED, both complex conditions influenced by nutritional deficiencies and microbiota composition.

The cross-fostering experiments employed in these studies have significant implications for nutritional therapies in undernourished children, suggesting that both prenatal and postnatal interventions may be necessary to effectively restore growth in these populations. Overall, the implications of this research extend beyond basic science, offering potential avenues to enhance therapeutic interventions by pinpointing critical windows for improving maternal and child health (**Figure 5.4**). By identifying potential key microbial and immune responses contributing to stunting, this work lays the foundation for developing microbiota and host health-based interventions, such as probiotics aimed at improving growth outcomes in at-risk populations.

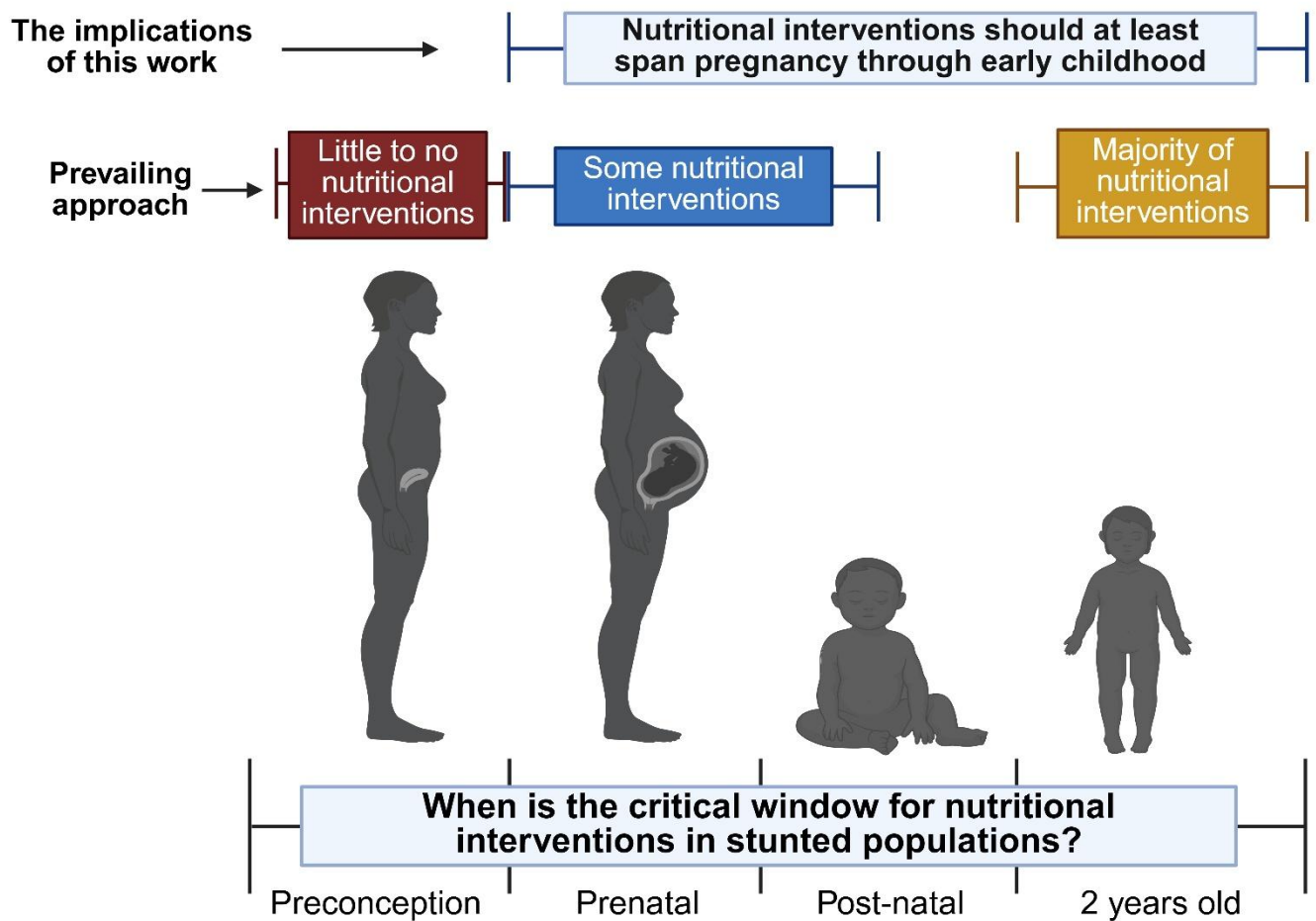


Figure 5.4. When is the critical window for nutritional interventions in stunted populations?

This diagram illustrates the prevailing approach and proposed implications (of this dissertation work) regarding the timing of current nutritional interventions for stunted populations. The silhouettes represent key developmental stages: preconception (stunted woman), prenatal (pregnant woman with fetus), postnatal or immediately after birth (infant), and early childhood (toddler). Findings from this work suggest that nutritional interventions should not be limited to the post-natal period or prenatal period but instead should start early during pregnancy and continue (cumulative nutritional interventions) into early childhood to optimize growth and health outcomes. Furthermore, considering pre-conception nutritional interventions for stunted women could help prevent stunting, rather than treating it in their future children.

References

1. McDonald, C. M. *et al.* The effect of multiple anthropometric deficits on child mortality: meta-analysis of individual data in 10 prospective studies from developing countries. *Am. J. Clin. Nutr.* **97**, 896–901 (2013).
2. Maleta, K. Undernutrition. *Malawi Med. J.* **18**, 189–205 (2006).
3. Briend, A. The complex relationship between wasting and stunting. *The American journal of clinical nutrition* vol. 110 271–272 (2019).
4. DeBoer, M. D. *et al.* Early childhood growth failure and the developmental origins of adult disease: do enteric infections and malnutrition increase risk for the metabolic syndrome? *Nutr. Rev.* **70**, 642–653 (2012).
5. De Sanctis, V. *et al.* Early and Long-term Consequences of Nutritional Stunting: From Childhood to Adulthood. *Acta Biomed.* **92**, e2021168 (2021).
6. Khadija, U. *et al.* Nutritional health status: association of stunted and wasted children and their mothers. *BMC Pediatr.* **22**, 255 (2022).
7. Benjamin-Chung, J. *et al.* Early-childhood linear growth faltering in low- and middle-income countries. *Nature* **621**, 550–557 (2023).
8. Black, R. E. *et al.* Maternal and child undernutrition: global and regional exposures and health consequences. *Lancet* **371**, 243–260 (2008).
9. Black, R. E. *et al.* Maternal and child undernutrition and overweight in low-income and middle-income countries. *Lancet* **382**, 427–451 (2013).
10. Cowardin, C. A. *et al.* Environmental enteric dysfunction: gut and microbiota adaptation in pregnancy and infancy. *Nat. Rev. Gastroenterol. Hepatol.* (2022) doi:10.1038/s41575-022-00714-7.

11. Katona, P. & Katona-Apte, J. The interaction between nutrition and infection. *Clin. Infect. Dis.* **46**, 1582–1588 (2008).
12. Chen, R. Y. *et al.* Linking the duodenal microbiota to stunting in a cohort of undernourished Bangladeshi children with enteropathy. *N. Engl. J. Med.* **383**, 321–333 (2020).
13. Ehsan, L. *et al.* Duodenal quantitative mucosal morphometry in children with environmental enteric dysfunction: a cross-sectional multicountry analysis. *Am. J. Clin. Nutr.* **120 Suppl 1**, S41–S50 (2024).
14. Bourke, C. D., Berkley, J. A. & Prendergast, A. J. Immune Dysfunction as a Cause and Consequence of Malnutrition. *Trends Immunol.* **37**, 386–398 (2016-6).
15. Loli, S. & Carcamo, C. P. Rotavirus vaccination and stunting: Secondary Data Analysis from the Peruvian Demographic and Health Survey. *Vaccine* **38**, 8010–8015 (2020).
16. Alves, J. G., Siqueira, L. C., Melo, L. M. & Figueiroa, J. N. Smaller pelvic size in pregnant adolescents contributes to lower birth weight. *Int. J. Adolesc. Med. Health* **25**, 139–142 (2013).
17. Krebs, N. F. *et al.* Birth length is the strongest predictor of linear growth status and stunting in the first 2 years of life after a preconception maternal nutrition intervention: the children of the Women First trial. *Am. J. Clin. Nutr.* **116**, 86–96 (2022).
18. Khatun, W., Rasheed, S., Alam, A., Huda, T. M. & Dibley, M. J. Assessing the intergenerational linkage between short maternal stature and under-five stunting and wasting in Bangladesh. *Nutrients* **11**, 1818 (2019).

19. Robertson, R. C., Manges, A. R., Finlay, B. B. & Prendergast, A. J. The Human Microbiome and Child Growth - First 1000 Days and Beyond. *Trends Microbiol.* **27**, 131–147 (2019).
20. Georgiadis, A. & Penny, M. E. Child undernutrition: opportunities beyond the first 1000 days. *Lancet Public Health* **2**, e399 (2017).
21. Elisaria, E., Mrema, J., Bogale, T., Segafredo, G. & Festo, C. Effectiveness of integrated nutrition interventions on childhood stunting: a quasi-experimental evaluation design. *BMC Nutr* **7**, 17 (2021).
22. Arsenault, J. E. & Brown, K. H. Effects of protein or amino-acid supplementation on the physical growth of young children in low-income countries. *Nutr. Rev.* **75**, 699–717 (2017).
23. Ashorn, P. *et al.* Supplementation of maternal diets during pregnancy and for 6 months postpartum and infant diets thereafter with small-quantity lipid-based nutrient supplements does not promote child growth by 18 months of age in rural Malawi: A randomized controlled trial. *J. Nutr.* **145**, 1345–1353 (2015).
24. Bhutta, Z. A. *et al.* What works? Interventions for maternal and child undernutrition and survival. *Lancet* **371**, 417–440 (2008).
25. Goudet, S. M., Bogin, B. A., Madise, N. J. & Griffiths, P. L. Nutritional interventions for preventing stunting in children (birth to 59 months) living in urban slums in low- and middle-income countries (LMIC). *Cochrane Database Syst. Rev.* **6**, CD011695 (2019).
26. Amon, P. & Sanderson, I. What is the microbiome? *Arch. Dis. Child. Educ. Pract. Ed.* **102**, 257–260 (2017).

27. Hou, K. *et al.* Microbiota in health and diseases. *Signal Transduct. Target. Ther.* **7**, 135 (2022).
28. Rowland, I. *et al.* Gut microbiota functions: metabolism of nutrients and other food components. *Eur. J. Nutr.* **57**, 1–24 (2018).
29. Cox, T. O., Lundgren, P., Nath, K. & Thaiss, C. A. Metabolic control by the microbiome. *Genome Med.* **14**, 80 (2022).
30. Buffie, C. G. & Pamer, E. G. Microbiota-mediated colonization resistance against intestinal pathogens. *Nat. Rev. Immunol.* **13**, 790–801 (2013).
31. Gieryńska, M., Szulc-Dąbrowska, L., Struzik, J., Mielcarska, M. B. & Gregorczyk-Zboroch, K. P. Integrity of the intestinal barrier: The involvement of epithelial cells and Microbiota-A mutual relationship. *Animals (Basel)* **12**, 145 (2022).
32. Kaur, H., Ali, S. A. & Yan, F. Interactions between the gut microbiota-derived functional factors and intestinal epithelial cells - implication in the microbiota-host mutualism. *Front. Immunol.* **13**, 1006081 (2022).
33. Belkaid, Y. & Hand, T. W. Role of the microbiota in immunity and inflammation. *Cell* **157**, 121–141 (2014).
34. Al Nabhani, Z. *et al.* A Weaning Reaction to Microbiota Is Required for Resistance to Immunopathologies in the Adult. *Immunity* **50**, 1276-1288.e5 (2019).
35. Honda, K. & Littman, D. R. The microbiome in infectious disease and inflammation. *Annu. Rev. Immunol.* **30**, 759–795 (2012).
36. Round, J. L. & Mazmanian, S. K. The gut microbiota shapes intestinal immune responses during health and disease. *Nat. Rev. Immunol.* **9**, 313–323 (2009).

37. Hill, D. A. & Artis, D. Intestinal bacteria and the regulation of immune cell homeostasis. *Annu. Rev. Immunol.* **28**, 623–667 (2010).
38. Surono, I. S., Widiyanti, D., Kusumo, P. D. & Venema, K. Gut microbiota profile of Indonesian stunted children and children with normal nutritional status. *PLoS One* **16**, e0245399 (2021).
39. Huus, K. E. *et al.* Immunoglobulin recognition of fecal bacteria in stunted and non-stunted children: findings from the AfriBiota study. *Microbiome* **8**, 113 (2020).
40. Aziz, I. *et al.* A prospective study on linking diarrheagenic *E. coli* with stunted childhood growth in relation to gut microbiome. *Sci. Rep.* **13**, 6802 (2023).
41. Blanton, L. V. *et al.* Gut bacteria that prevent growth impairments transmitted by microbiota from malnourished children. *Science* **351**, (2016).
42. Hardjo, J. & Selene, N. B. Stunting and gut Microbiota: A literature review. *Pediatr. Gastroenterol. Hepatol. Nutr.* **27**, 137–145 (2024).
43. Fahim, S. M., Das, S., Gazi, M. A., Mahfuz, M. & Ahmed, T. Association of intestinal pathogens with faecal markers of environmental enteric dysfunction among slum-dwelling children in the first 2 years of life in Bangladesh. *Trop. Med. Int. Health* **23**, 1242–1250 (2018).
44. Surono, I. S. *et al.* Gut microbiota differences in stunted and normal-length children aged 36-45 months in East Nusa Tenggara, Indonesia. *PLoS One* **19**, e0299349 (2024).
45. Silva, Y. P., Bernardi, A. & Frozza, R. L. The role of short-chain fatty acids from gut Microbiota in gut-brain communication. *Front. Endocrinol. (Lausanne)* **11**, 25 (2020).

46. Ahn-Jarvis, J. *et al.* Modelling the gut microbiota of children with malnutrition:*in vitro* models reveal differences in fermentability of widely consumed carbohydrates. *bioRxiv* 2024.05.08.593150 (2024) doi:10.1101/2024.05.08.593150.
47. Lewis, K. *et al.* Enhanced translocation of bacteria across metabolically stressed epithelia is reduced by butyrate. *Inflamm. Bowel Dis.* **16**, 1138–1148 (2010).
48. Peng, L., Li, Z.-R., Green, R. S., Holzman, I. R. & Lin, J. Butyrate enhances the intestinal barrier by facilitating tight junction assembly via activation of AMP-activated protein kinase in Caco-2 cell monolayers. *J. Nutr.* **139**, 1619–1625 (2009).
49. Gaudier, E., Rival, M., Buisine, M.-P., Robineau, I. & Hoebler, C. Butyrate enemas upregulate Muc genes expression but decrease adherent mucus thickness in mice colon. *Physiol. Res.* **58**, 111–119 (2009).
50. Sjögren, K., Jansson, J.-O., Isaksson, O. G. P. & Ohlsson, C. A model for tissue-specific inducible insulin-like growth factor-I (IGF-I) inactivation to determine the physiological role of liver-derived IGF-I. *Endocrine* **19**, 249–256 (2002).
51. Schwarzer, M. *et al.* Lactobacillus plantarum strain maintains growth of infant mice during chronic undernutrition. *Science* **351**, 854–857 (2016).
52. Ohlsson, C. *et al.* The role of liver-derived insulin-like growth factor-I. *Endocr. Rev.* **30**, 494–535 (2009).
53. Locatelli, V. & Bianchi, V. E. Effect of GH/IGF-1 on bone metabolism and osteoporosis. *Int. J. Endocrinol.* **2014**, 235060 (2014).
54. Nuryandari, S., Widjaja, N. A. & Husada, D. TNF- α and IGF-1 levels in stunting children with chronic infection. *Acta Biomed. Ateneo Parmense* **95**, e2024182 (2024).

55. Rinanda, T., Riani, C., Artarini, A. & Sasongko, L. Correlation between gut microbiota composition, enteric infections and linear growth impairment: a case-control study in childhood stunting in Pidie, Aceh, Indonesia. *Gut Pathog.* **15**, 54 (2023).
56. Schwarzer, M. *et al.* Microbe-mediated intestinal NOD2 stimulation improves linear growth of undernourished infant mice. *Science* **379**, 826–833 (2023).
57. Arrieta, M.-C., Stiemsma, L. T., Amenyogbe, N., Brown, E. M. & Finlay, B. The intestinal microbiome in early life: health and disease. *Front. Immunol.* **5**, 427 (2014).
58. Blaker, P. A. & Irving, P. Physiology and function of the small intestine. in *Advanced Nutrition and Dietetics in Gastroenterology* 21–27 (John Wiley & Sons, Ltd., Oxford, 2014).
59. Regassa, R., Belachew, T., Duguma, M. & Tamiru, D. Factors associated with stunting in under-five children with environmental enteropathy in slum areas of Jimma town, Ethiopia. *Front. Nutr.* **11**, 1335961 (2024).
60. Tickell, K. D. & Walson, J. L. Nutritional Enteric failure: Neglected tropical diseases and childhood stunting. *PLoS Negl. Trop. Dis.* **10**, e0004523 (2016).
61. Gizaw, Z., Yalew, A. W., Bitew, B. D., Lee, J. & Bisesi, M. Stunting among children aged 24-59 months and associations with sanitation, enteric infections, and environmental enteric dysfunction in rural northwest Ethiopia. *Sci. Rep.* **12**, 19293 (2022).
62. Crane, R. J., Jones, K. D. J. & Berkley, J. A. Environmental Enteric Dysfunction: An Overview. *Food Nutr. Bull.* **36**, S76–S87 (2015).
63. Lunn, P. G., Northrop-Clewes, C. A. & Downes, R. M. Intestinal permeability, mucosal injury, and growth faltering in Gambian infants. *Lancet* **338**, 907–910 (1991).

64. Campbell, D. I., Elia, M. & Lunn, P. G. Growth faltering in rural Gambian infants is associated with impaired small intestinal barrier function, leading to endotoxemia and systemic inflammation. *J. Nutr.* **133**, 1332–1338 (2003).
65. Denno, D. M., Tarr, P. I. & Nataro, J. P. Environmental Enteric dysfunction: A case definition for intervention trials. *Am. J. Trop. Med. Hyg.* **97**, 1643–1646 (2017).
66. Iqbal, N. T. *et al.* Study of Environmental Enteropathy and Malnutrition (SEEM) in Pakistan: protocols for biopsy based biomarker discovery and validation. *BMC Pediatr.* **19**, 247 (2019).
67. VanBuskirk, K. *et al.* Multiplexed immunohistochemical evaluation of small bowel inflammatory and epithelial parameters in environmental enteric dysfunction. *Am. J. Clin. Nutr.* **120 Suppl 1**, S31–S40 (2024).
68. Haberman, Y. *et al.* Mucosal genomics implicate lymphocyte activation and lipid metabolism in refractory environmental Enteric dysfunction. *Gastroenterology* **160**, 2055-2071.e0 (2021).
69. Chandwe, K., Amadi, B., Chipunza, M., Zyambo, M. & Kelly, P. Safety and ethics in endoscopic studies in children: Evidence from the BEECH study in Zambia. *J. Trop. Pediatr.* **67**, fmaa074 (2021).
70. Mahfuz, M. *et al.* Bangladesh Environmental Enteric Dysfunction (BEED) study: protocol for a community-based intervention study to validate non-invasive biomarkers of environmental enteric dysfunction. *BMJ Open* **7**, e017768 (2017).
71. Mahfuz, M. *et al.* Biomarker relationships with small bowel histopathology among malnourished children with environmental enteric dysfunction in a multicountry cohort study. *Am. J. Clin. Nutr.* **120 Suppl 1**, S73–S83 (2024).

72. Arndt, M. B. *et al.* Fecal markers of environmental enteropathy and subsequent growth in Bangladeshi children. *Am. J. Trop. Med. Hyg.* **95**, 694–701 (2016).
73. Bhattacharjee, A. *et al.* Environmental enteric dysfunction induces regulatory T cells that inhibit local CD4+ T cell responses and impair oral vaccine efficacy. *Immunity* **54**, 1745-1757.e7 (2021).
74. Malique, A. *et al.* NAD+ precursors and bile acid sequestration treat preclinical refractory environmental enteric dysfunction. *Sci. Transl. Med.* **16**, eabq4145 (2024).
75. Morales, F., Montserrat-de la Paz, S., Leon, M. J. & Rivero-Pino, F. Effects of malnutrition on the immune system and infection and the role of nutritional strategies regarding improvements in children's health status: A literature review. *Nutrients* **16**, 1 (2023).
76. Cunningham-Rundles, S., McNeeley, D. F. & Moon, A. Mechanisms of nutrient modulation of the immune response. *J. Allergy Clin. Immunol.* **115**, 1119–28; quiz 1129 (2005).
77. Olofin, I. *et al.* Associations of suboptimal growth with all-cause and cause-specific mortality in children under five years: a pooled analysis of ten prospective studies. *PLoS One* **8**, e64636 (2013).
78. Remien, K. & Jan, A. Anatomy, head and neck, thymus. in *StatPearls* (StatPearls Publishing, Treasure Island (FL), 2025).
79. Dominguez-Salas, P. *et al.* Maternal nutrition at conception modulates DNA methylation of human metastable epialleles. *Nat. Commun.* **5**, 3746 (2014).

80. Cooper, W. N. *et al.* DNA methylation profiling at imprinted loci after periconceptual micronutrient supplementation in humans: results of a pilot randomized controlled trial. *FASEB J.* **26**, 1782–1790 (2012).
81. Mutasa, K. *et al.* Stunting status and exposure to infection and inflammation in early life shape antibacterial immune cell function among Zimbabwean children. *Front. Immunol.* **13**, 899296 (2022).
82. Kummerlowe, C. *et al.* Single-cell profiling of environmental enteropathy reveals signatures of epithelial remodeling and immune activation. *Sci. Transl. Med.* **14**, eabi8633 (2022).
83. van Wijk, F. & Cheroutre, H. Mucosal T cells in gut homeostasis and inflammation. *Expert Rev. Clin. Immunol.* **6**, 559–566 (2010).
84. Ramanan, D. *et al.* Regulatory T cells in the face of the intestinal microbiota. *Nat. Rev. Immunol.* **23**, 749–762 (2023).
85. Khagayi, S. *et al.* Effectiveness of monovalent Rotavirus vaccine against hospitalization with acute Rotavirus gastroenteritis in Kenyan children. *Clin. Infect. Dis.* **70**, 2298–2305 (2020).
86. Carvalho, M. F. & Gill, D. Rotavirus vaccine efficacy: current status and areas for improvement. *Hum. Vaccin. Immunother.* **15**, 1237–1250 (2019).
87. Marie, C., Ali, A., Chandwe, K., Petri, W. A. & Kelly, P. Pathophysiology of environmental enteric dysfunction and its impact on oral vaccine efficacy. *Mucosal Immunol.* **11**, 1290–1298 (9/2018).
88. Herrera, D., Vásquez, C., Corthésy, B., Franco, M. A. & Angel, J. Rotavirus specific plasma secretory immunoglobulin in children with acute gastroenteritis and children

- vaccinated with an attenuated human rotavirus vaccine. *Hum. Vaccin. Immunother.* **9**, 2409–2417 (2013).
89. Steffen, U. *et al.* IgA subclasses have different effector functions associated with distinct glycosylation profiles. *Nat. Commun.* **11**, 120 (2020).
90. Johansen, F.-E. & Kaetzel, C. S. Regulation of the polymeric immunoglobulin receptor and IgA transport: new advances in environmental factors that stimulate pIgR expression and its role in mucosal immunity. *Mucosal Immunol.* **4**, 598–602 (2011).
91. Leong, K. W. & Ding, J. L. The unexplored roles of human serum IgA. *DNA Cell Biol.* **33**, 823–829 (2014).
92. Cerutti, A., Chen, K. & Chorny, A. Immunoglobulin Responses at the Mucosal Interface. *Annu. Rev. Immunol.* **29**, 273–293 (2011).
93. Pabst, O. & Slack, E. IgA and the intestinal microbiota: the importance of being specific. *Mucosal Immunol.* **13**, 12–21 (01/2020).
94. Bunker, J. J. *et al.* Innate and Adaptive Humoral Responses Coat Distinct Commensal Bacteria with Immunoglobulin A. *Immunity* **43**, 541–553 (2015).
95. Tezuka, H. & Ohteki, T. Regulation of IgA Production by Intestinal Dendritic Cells and Related Cells. *Front. Immunol.* **10**, 1891 (2019).
96. Kau, A. L. *et al.* Functional characterization of IgA-targeted bacterial taxa from undernourished Malawian children that produce diet-dependent enteropathy. *Sci. Transl. Med.* **7**, 276ra24-276ra24 (2015).

97. Suryadinata, R. V., Wijono, H., Putra Sanwersko, F. V., Susanto, Y. E. & Lorensia, A. The comparison of carbohydrate, fiber, and immunoglobulin-A levels in feces against stunting children in Tuban Regency. *Healthc. Low Resour. Settings* **12**, (2024).
98. Hansen, I. S., Baeten, D. L. P. & den Dunnen, J. The inflammatory function of human IgA. *Cell. Mol. Life Sci.* **76**, 1041–1055 (3/2019).
99. Palm, N. W. *et al.* Immunoglobulin A Coating Identifies Colitogenic Bacteria in Inflammatory Bowel Disease. *El Sevier* (2014).
100. Hughes, R. L. *et al.* Infant gut microbiota characteristics generally do not modify effects of lipid-based nutrient supplementation on growth or inflammation: secondary analysis of a randomized controlled trial in Malawi. *Sci. Rep.* **10**, 14861 (2020).
101. Kamng'ona, A. W. *et al.* Provision of lipid-based nutrient supplements to mothers during pregnancy and 6 months postpartum and to their infants from 6 to 18 months promotes infant gut Microbiota diversity at 18 months of age but not Microbiota maturation in a rural Malawian setting: Secondary outcomes of a randomized trial. *J. Nutr.* **150**, 918–928 (2020).
102. Serrano Matos, Y. *et al.* Maternal undernutrition exacerbates microbiota-driven growth stunting through pre and postnatal effects. *bioRxiv* 2025.03.06.641866 (2025) doi:10.1101/2025.03.06.641866.
103. Levels and trends in child malnutrition: UNICEF/WHO/The World Bank Group joint child malnutrition estimates: key findings of the 2021 edition. <https://www.who.int/publications/i/item/9789240025257> (2021).
104. Martorell, R. Improved nutrition in the first 1000 days and adult human capital and health. *Am. J. Hum. Biol.* **29**, (2017).

105. Prendergast, A. J. & Humphrey, J. H. The stunting syndrome in developing countries. *Paediatr. Int. Child Health* **34**, 250–265 (2014-4).
106. de Onis, M. & Blössner, M. The World Health Organization Global Database on Child Growth and Malnutrition: methodology and applications. *Int. J. Epidemiol.* **32**, 518–526 (2003).
107. de Onis, M. & Branca, F. Childhood stunting: a global perspective. *Matern. Child Nutr.* **12 Suppl 1**, 12–26 (2016).
108. Prentice, A. M. *et al.* Critical windows for nutritional interventions against stunting. *The American Journal of Clinical Nutrition* **97**, 911–918 (2013).
109. Donowitz, J. R. *et al.* Role of maternal health and infant inflammation in nutritional and neurodevelopmental outcomes of two-year-old Bangladeshi children. *PLoS Negl. Trop. Dis.* **12**, e0006363 (2018).
110. Gonete, A. T., Kassahun, B., Mekonnen, E. G. & Takele, W. W. Stunting at birth and associated factors among newborns delivered at the University of Gondar Comprehensive Specialized Referral Hospital. *PLoS One* **16**, e0245528 (2021).
111. Lauer, J. M. *et al.* Biomarkers of maternal environmental enteric dysfunction are associated with shorter gestation and reduced length in newborn infants in Uganda. *Am. J. Clin. Nutr.* **108**, 889–896 (2018).
112. Prado, E. L. *et al.* Path analyses of risk factors for linear growth faltering in four prospective cohorts of young children in Ghana, Malawi and Burkina Faso. *BMJ Glob. Health* **4**, e001155 (2019).
113. WHO Multicentre Growth Reference Study Group. WHO Child Growth Standards based on length/height, weight and age. *Acta Paediatr. Suppl.* **450**, 76–85 (2006).

114. Kosek, M. N. & MAL-ED Network Investigators. Causal pathways from enteropathogens to environmental enteropathy: Findings from the MAL-ED birth cohort study. *EBioMedicine* **18**, 109–117 (2017).
115. Tickell, K. D., Atlas, H. E. & Walson, J. L. Environmental enteric dysfunction: a review of potential mechanisms, consequences and management strategies. *BMC Med.* **17**, 181 (2019).
116. Campbell, D. I. *et al.* Chronic T cell-mediated enteropathy in rural west African children: relationship with nutritional status and small bowel function. *Pediatr. Res.* **54**, 306–311 (2003).
117. Pickering, A. J. *et al.* The WASH Benefits and SHINE trials: interpretation of WASH intervention effects on linear growth and diarrhoea. *Lancet Glob. Health* **7**, e1139–e1146 (2019).
118. Subramanian, S. *et al.* Persistent gut Microbiota immaturity in malnourished Bangladeshi children. *Nature* **510**, 417–421 (2014).
119. Di Luccia, B. *et al.* Combined prebiotic and microbial intervention improves oral cholera vaccination responses in a mouse model of childhood undernutrition. *Cell Host Microbe* **27**, 899-908.e5 (2020).
120. Knoop, K. A. *et al.* Microbial antigen encounter during a preweaning interval is critical for tolerance to gut bacteria. *Sci. Immunol.* **2**, (2017).
121. Ashorn, P. *et al.* The impact of lipid-based nutrient supplement provision to pregnant women on newborn size in rural Malawi: a randomized controlled trial. *Am. J. Clin. Nutr.* **101**, 387–397 (2015).

122. Serrano Matos, Y. A. *et al.* Colonization during a key developmental window reveals microbiota-dependent shifts in growth and immunity during undernutrition. *Microbiome* **12**, 71 (2024).
123. Gehrig, J. L. *et al.* Effects of microbiota-directed foods in gnotobiotic animals and undernourished children. *Science* **365**, eaau4732 (2019).
124. Syed, S., Ali, A. & Duggan, C. Environmental Enteric dysfunction in children. *J. Pediatr. Gastroenterol. Nutr.* **63**, 6–14 (2016).
125. Liu, T.-C. *et al.* A novel histological index for evaluation of environmental enteric dysfunction identifies geographic-specific features of enteropathy among children with suboptimal growth. *PLoS Negl. Trop. Dis.* **14**, e0007975 (2020).
126. Hossain, M. S. *et al.* Environmental enteric dysfunction and small intestinal histomorphology of stunted children in Bangladesh. *PLoS Negl. Trop. Dis.* **17**, e0010472 (2023).
127. Beagley, K. W. & Husband, A. J. Intraepithelial lymphocytes: origins, distribution, and function. *Crit. Rev. Immunol.* **18**, 237–254 (1998).
128. Cheroutre, H., Lambolez, F. & Mucida, D. The light and dark sides of intestinal intraepithelial lymphocytes. *Nat. Rev. Immunol.* **11**, 445–456 (2011).
129. Hoytema van Konijnenburg, D. P. *et al.* Intestinal epithelial and intraepithelial T cell crosstalk mediates a dynamic response to infection. *Cell* **171**, 783–794.e13 (2017).
130. Jiang, W. *et al.* Recognition of gut microbiota by NOD2 is essential for the homeostasis of intestinal intraepithelial lymphocytes. *J. Exp. Med.* **210**, 2791–2791 (2013).

131. Elinav, E. *et al.* NLRP6 inflammasome regulates colonic microbial ecology and risk for colitis. *Cell* **145**, 745–757 (2011).
132. Cowardin, C. A. *et al.* Inflammasome activation contributes to interleukin-23 production in response to *Clostridium difficile*. *MBio* **6**, (2015).
133. Martorell, R. & Zongrone, A. Intergenerational influences on child growth and undernutrition. *Paediatr. Perinat. Epidemiol.* **26 Suppl 1**, 302–314 (2012).
134. Khatun, W., Alam, A., Rasheed, S., Huda, T. M. & Dibley, M. J. Exploring the intergenerational effects of undernutrition: association of maternal height with neonatal, infant and under-five mortality in Bangladesh. *BMJ Glob. Health* **3**, e000881 (2018).
135. Bogaert, D. *et al.* Mother-to-infant microbiota transmission and infant microbiota development across multiple body sites. *Cell Host Microbe* **31**, 447-460.e6 (2023).
136. Chen, R. Y. *et al.* A Microbiota-directed food intervention for undernourished children. *N. Engl. J. Med.* **384**, 1517–1528 (2021).
137. Yatsunenkov, T. *et al.* Human gut microbiome viewed across age and geography. *Nature* **486**, 222–227 (2012).
138. Faith, J. J., Ahern, P. P., Ridaura, V. K., Cheng, J. & Gordon, J. I. Identifying gut microbe-host phenotype relationships using combinatorial communities in gnotobiotic mice. *Sci. Transl. Med.* **6**, 220ra11 (2014).
139. Brown, E. M. *et al.* Diet and specific microbial exposure trigger features of environmental enteropathy in a novel murine model. *Nat. Commun.* **6**, 7806 (2015).

140. Cowardin, C. A. *et al.* Mechanisms by which sialylated milk oligosaccharides impact bone biology in a gnotobiotic mouse model of infant undernutrition. *Proc. Natl. Acad. Sci. U. S. A.* **116**, 11988–11996 (2019).
141. Caporaso, J. G. *et al.* Global patterns of 16S rRNA diversity at a depth of millions of sequences per sample. *Proc. Natl. Acad. Sci. U. S. A.* **108 Suppl 1**, 4516–4522 (2011).
142. Callahan, B. J., Sankaran, K., Fukuyama, J. A., McMurdie, P. J. & Holmes, S. P. Bioconductor workflow for microbiome data analysis: from raw reads to community analyses. *F1000Res.* **5**, 1492 (2016).
143. McMurdie, P. J. & Holmes, S. phyloseq: an R package for reproducible interactive analysis and graphics of microbiome census data. *PLoS One* **8**, e61217 (2013).
144. Budge, S., Parker, A. H., Hutchings, P. T. & Garbutt, C. Environmental enteric dysfunction and child stunting. *Nutr. Rev.* **77**, 240–253 (2019).
145. Robertson, R. C. *et al.* The gut microbiome and early-life growth in a population with high prevalence of stunting. *Nat. Commun.* **14**, 1–15 (2023).
146. Smith, M. I. *et al.* Gut microbiomes of Malawian twin pairs discordant for kwashiorkor. *Science* **339**, 548–554 (2013).
147. Meyer, A. M. & Caton, J. S. Role of the Small Intestine in Developmental Programming: Impact of Maternal Nutrition on the Dam and Offspring. *Adv. Nutr.* **7**, 169–178 (2016).
148. Kelly, P. *et al.* Histopathology underlying environmental enteric dysfunction in a cohort study of undernourished children in Bangladesh, Pakistan, and Zambia

- compared with United States children. *Am. J. Clin. Nutr.* **120 Suppl 1**, S15–S30 (2024).
149. ANDREW L. KAU, JOSEPH D. PLANER, JIE LIU, SINDHUJA RAO, TANYA YATSUNENKO, INDI TREHAN, MARK J. MANARY, TA-CHIANG LIU, THADDEUS S. STAPPENBECK, KENNETH M. MALETA, PER ASHORN, KATHRYN G. DEWEY, ERIC R. HOUP, CHYI-SONG HSIEH, AND JEFFREY I. GORDON. Functional characterization of IgA-targeted bacterial taxa from undernourished Malawian children that produce diet-dependent enteropathy. *Science* **7**, 276ra24 (2015).
150. Salameh, E. *et al.* Modeling undernutrition with enteropathy in mice. *Sci. Rep.* **10**, 15581 (12/2020).
151. Kotloff, K. L. *et al.* Burden and aetiology of diarrhoeal disease in infants and young children in developing countries (the Global Enteric Multicenter Study, GEMS): a prospective, case-control study. *Lancet* **382**, 209–222 (2013).
152. Sangiorgio, G., Calvo, M., Migliorisi, G., Campanile, F. & Stefani, S. The impact of *Enterococcus* spp. In the immunocompromised host: A comprehensive review. *Pathogens* **13**, 409 (2024).
153. Ong, K. K. *et al.* Insulin-like growth factor I concentrations in infancy predict differential gains in body length and adiposity: the Cambridge Baby Growth Study. *Am. J. Clin. Nutr.* **90**, 156–161 (2009).
154. Ahmed, S. *et al.* Association of Anti-Rotavirus IgA Seroconversion with Growth, Environmental Enteric Dysfunction and Enteropathogens in Rural Pakistani Infants. *Vaccine* **40**, 3444–3451 (2022).

155. Pruss, K. M. *et al.* Effects of intergenerational transmission of small intestinal bacteria cultured from stunted Bangladeshi children with enteropathy. *bioRxiv* 2024.11.01.621574 (2024) doi:10.1101/2024.11.01.621574.
156. Marume, A., Archary, M. & Mahomed, S. Predictors of stunting among children aged 6-59 months, Zimbabwe. *Public Health Nutr.* **26**, 820–833 (2023).
157. Abdulla, F., Rahman, A. & Hossain, M. M. Prevalence and risk predictors of childhood stunting in Bangladesh. *PLoS One* **18**, e0279901 (2023).
158. Lakshmy, R. Metabolic syndrome: role of maternal undernutrition and fetal programming. *Rev. Endocr. Metab. Disord.* **14**, 229–240 (2013).
159. Keats, E. C. *et al.* Effective interventions to address maternal and child malnutrition: an update of the evidence. *Lancet Child Adolesc. Health* **5**, 367–384 (2021).
160. Di Gesù, C. M. *et al.* Maternal gut microbiota mediate intergenerational effects of high-fat diet on descendant social behavior. *Cell Rep.* **41**, 111461 (2022).
161. Buffington, S. A. *et al.* Microbial reconstitution reverses maternal diet-induced social and synaptic deficits in offspring. *Cell* **165**, 1762–1775 (2016).
162. Iddrisu, I. *et al.* Malnutrition and Gut Microbiota in Children. *Nutrients* **13**, 2727 (2021).
163. Dang, H. *et al.* Maternal gut microbiota influence stem cell function in offspring. *Cell Stem Cell* **32**, 246-262.e8 (2025).
164. Bodenhofer, U., Bonatista, E., Horejš-Kainrath, C. & Hochreiter, S. msa: an R package for multiple sequence alignment. *Bioinformatics* **31**, 3997–3999 (2015).
165. Schliep, K. P. phangorn: phylogenetic analysis in R. *Bioinformatics* **27**, 592–593 (2011).

166. Wickham, H. Data Analysis. in *Use R!* 189–201 (Springer International Publishing, Cham, 2016).
167. Martinez, A. P. *PairwiseAdonis: Pairwise Multilevel Comparison Using Adonis*. (2020).
168. Reemst, K. *et al.* The role of the gut Microbiota in the effects of early-life stress and dietary fatty acids on later-life central and metabolic outcomes in mice. *mSystems* **7**, e0018022 (2022).
169. Guerrant, R. L., DeBoer, M. D., Moore, S. R., Scharf, R. J. & Lima, A. A. M. The impoverished gut—a triple burden of diarrhoea, stunting and chronic disease. *Nat. Rev. Gastroenterol. Hepatol.* **10**, 220–229 (4/2013).
170. Peterson, D. A., McNulty, N. P., Guruge, J. L. & Gordon, J. I. IgA response to symbiotic bacteria as a mediator of gut homeostasis. *Cell Host Microbe* **2**, 328–339 (2007).
171. Syed, S. *et al.* Serum anti-flagellin and anti-lipopolysaccharide immunoglobulins as predictors of linear growth faltering in Pakistani infants at risk for environmental enteric dysfunction. *PLoS One* **13**, e0193768 (2018).
172. Viladomiu, M. *et al.* IgA-coated E. coli enriched in Crohn's disease spondyloarthritis promote TH17-dependent inflammation. *Sci. Transl. Med.* **9**, eaaf9655 (2017).
173. Jackson, M. A. *et al.* Accurate identification and quantification of commensal microbiota bound by host immunoglobulins. *Microbiome* **9**, 33 (12/2021).
174. Serrano Matos, Y. A. *et al.* Colonization during a key developmental window reveals microbiota-dependent shifts in growth and immunity during undernutrition. *bioRxiv* 2023.07.07.547849 (2023) doi:10.1101/2023.07.07.547849.

175. Argaw-Denboba, A. *et al.* Paternal microbiome perturbations impact offspring fitness. *Nature* **629**, 652–659 (2024).
176. Vaughan, O. R., Sferruzzi-Perri, A. N. & Fowden, A. L. Maternal corticosterone regulates nutrient allocation to fetal growth in mice: Corticosterone regulates nutrient allocation to fetal growth. *J. Physiol.* **590**, 5529–5540 (2012).
177. Lopez-Tello, J. *et al.* Maternal gut microbiota Bifidobacterium promotes placental morphogenesis, nutrient transport and fetal growth in mice. *Cell. Mol. Life Sci.* **79**, 386 (2022).
178. Lopez-Tello, J. *et al.* Maternal gut Bifidobacterium breve modifies fetal brain metabolism in germ-free mice. *Mol. Metab.* **88**, 102004 (2024).
179. Malhotra, D., Burrack, K. S., Jenkins, M. K. & Frosch, A. E. Antigen-Specific CD4+ T Cells Exhibit Distinct Kinetic and Phenotypic Patterns During Primary and Secondary Responses to Infection. *Front. Immunol.* **11**, (2020).
180. Lieberman, J. Granzyme A activates another way to die: Granzyme A-mediated cell death. *Immunol. Rev.* **235**, 93–104 (2010).
181. Marques, R. E., Guabiraba, R., Russo, R. C. & Teixeira, M. M. Targeting CCL5 in inflammation. *Expert Opin. Ther. Targets* **17**, 1439–1460 (2013).
182. Mencarelli, A. *et al.* Highly specific blockade of CCR5 inhibits leukocyte trafficking and reduces mucosal inflammation in murine colitis. *Sci. Rep.* **6**, 30802 (2016).
183. van Gogh, M. *et al.* Next-generation IgA-SEQ allows for high-throughput, anaerobic, and metagenomic assessment of IgA-coated bacteria. *Microbiome* **12**, 211 (2024).

Appendix

Appendix A: Chapter 3 Supplemental Information

This section provides additional details on the analyses performed in Chapter 3, including results from PERMANOVA and pairwise comparisons.

| NMU VS MU (8W) | Df | SumOfSqs | R² | F | Pr(>F) | sig. |
|---|-----------|-----------------|----------------------|----------|------------------|-------------|
| Donor Microbiota | 1 | 1.1183831 | 0.8742 | 158.682 | 0.001 | ** |
| Maternal Undernutrition Status | 1 | 0.03285946 | 0.02569 | 4.66227 | 0.023 | * |
| Donor:Maternal Undernutrition Status | 1 | 0.01531157 | 0.01197 | 2.17248 | 0.197 | ns |
| Residual | 16 | 0.11276734 | 0.08815 | NA | NA | |
| Total | 19 | 1.27932147 | 1 | NA | NA | |

Table 3.1 PERMANOVA Analysis of NMU and MU animals at maturity

| Pairwise Comparisons (8W) | Df | SumsOfSqs | F.Model | R² | p.value | p.adjusted | sig |
|----------------------------------|-----------|------------------|----------------|----------------------|----------------|-------------------|------------|
| HD-NMU vs SD-NMU | 1 | 0.46393077 | 89.4354 | 0.91789 | 0.011 | 0.044 | * |
| HD-NMU vs HD-MU | 1 | 0.01363625 | 2.41498 | 0.23188 | 0.145 | 0.145 | |
| HD-NMU vs SD-MU | 1 | 0.61297434 | 109.097 | 0.93168 | 0.005 | 0.03 | * |
| SD-NMU vs HD-MU | 1 | 0.53826822 | 63.4954 | 0.8881 | 0.011 | 0.044 | * |
| SD-NMU vs SD-MU | 1 | 0.03453479 | 4.08725 | 0.33815 | 0.013 | 0.044 | * |
| HD-MU vs SD-MU | 1 | 0.6697639 | 75.1818 | 0.90383 | 0.006 | 0.03 | * |

Table 3.2. Pairwise Comparisons between NMU and MU animals at maturity.

| Variable | Df | SumOfSqs | R ² | F | Pr(>F) | sig |
|--------------------------------|----|------------|----------------|---------|--------|-----|
| Maternal Undernutrition Status | 1 | 0.03453479 | 0.33815 | 4.08725 | 0.009 | ** |
| Residual | 8 | 0.06759512 | 0.66185 | NA | NA | |
| Total | 9 | 0.1021299 | 1 | NA | NA | |

Table 3.3. PERMANOVA Analysis (SD-NMU and MU Animals 8W)

| Variable | Df | SumOfSqs | R ² | F | Pr(>F) | sig |
|--------------------------------|----|------------|----------------|---------|--------|-----|
| Maternal Undernutrition Status | 1 | 0.01363625 | 0.23188 | 2.41498 | 0.157 | ns |
| Residual | 8 | 0.04517222 | 0.76812 | NA | NA | |
| Total | 9 | 0.05880847 | 1 | NA | NA | |

Table 3.4. PERMANOVA Analysis (HD- NMU and MU Animals 8W)

| Variable | Df | SumOfSqs | R ² | F | Pr(>F) | sig |
|----------|----|------------|----------------|---------|--------|-----|
| Age | 3 | 0.84975642 | 0.91833 | 59.9677 | 0.001 | ** |
| Residual | 16 | 0.0755746 | 0.08167 | NA | NA | |
| Total | 19 | 0.92533101 | 1 | NA | NA | |

Table 3.5. PERMANOVA Analysis - Early Life Development - HD-MU

| Pairwise Comparisons (HD MU) | Df | SumsOfSqs | F.Model | R ² | p.value | p.adjusted (holm) | sig |
|------------------------------|----|------------|---------|----------------|---------|-------------------|-----|
| 2 vs 3 | 1 | 0.28254888 | 81.2693 | 0.91038 | 0.013 | 0.044 | * |
| 2 vs 4 | 1 | 0.50177614 | 275.738 | 0.97181 | 0.011 | 0.044 | * |
| 2 vs 8 | 1 | 0.74094133 | 154.811 | 0.95086 | 0.005 | 0.025 | * |
| 3 vs 4 | 1 | 0.03357787 | 7.20444 | 0.47384 | 0.012 | 0.044 | * |
| 3 vs 8 | 1 | 0.11432653 | 14.9896 | 0.65202 | 0.004 | 0.024 | * |
| 4 vs 8 | 1 | 0.02634208 | 4.41231 | 0.35548 | 0.044 | 0.044 | * |

Table 3.6. Pairwise Comparisons - Early Life Development - HD-MU

| Variable | Df | SumOfSqs | R ² | F | Pr(>F) | sig |
|----------|----|------------|----------------|---------|--------|-----|
| Age | 3 | 0.45913279 | 0.63513 | 8.70356 | 0.001 | ** |
| Residual | 15 | 0.26376134 | 0.36487 | NA | NA | |
| Total | 18 | 0.72289413 | 1 | NA | NA | |

Table 3.7. PERMANOVA Analysis - Early Life Development - SD-MU

| Pairwise Comparisons (SD-MU) | Df | SumsOfSqs | F.Model | R ² | p.value | p.adjusted (holm) |
|------------------------------|----|------------|---------|----------------|---------|-------------------|
| 2 vs 3 | 1 | 0.2968883 | 9.65323 | 0.57966 | 0.011 | 0.035 |
| 2 vs 4 | 1 | 0.1493437 | 7.15457 | 0.47211 | 0.008 | 0.035 |
| 2 vs 8 | 1 | 0.18575277 | 7.83922 | 0.49492 | 0.011 | 0.035 |
| 3 vs 8 | 1 | 0.15918264 | 11.5147 | 0.62192 | 0.005 | 0.03 |
| 3 vs 4 | 1 | 0.08704544 | 8.21196 | 0.53984 | 0.007 | 0.035 |
| 4 vs 8 | 1 | 0.0484511 | 7.9962 | 0.49988 | 0.012 | 0.035 |

Table 3.8. Pairwise Comparisons - Early Life Development - SD-MU

| Variable | Df | SumOfSqs | R ² | F | Pr(>F) | sig |
|-------------------------------|----|------------|----------------|---------|--------|-----|
| Donor Microbiota | 1 | 1.38590779 | 0.8186 | 143.51 | 0.001 | ** |
| Germ_free born/Cross-Fostered | 1 | 0.06528178 | 0.03856 | 6.75989 | 0.017 | * |
| Donor:Cross_foster | 1 | 0.08731767 | 0.05158 | 9.04169 | 0.007 | ** |
| Residual | 16 | 0.15451571 | 0.09127 | NA | NA | |
| Total | 19 | 1.69302294 | 1 | NA | NA | |

Table 3.9. PERMANOVA Analysis -HD-MU, SD-MU, GF-HD and GF-SD at maturity.

| Pairwise Comparisons | Df | SumsOfSqs | F.Model | R2 | p.value | p.adjusted (Holm) |
|----------------------|----|------------|---------|---------|---------|-------------------|
| HD-MU vs SD-MU | 1 | 0.6697639 | 75.1818 | 0.90383 | 0.007 | 0.036 |
| HD-MU vs GF-HD | 1 | 0.11043904 | 8.19181 | 0.50592 | 0.034 | 0.05 |
| HD-MU vs GF-SD | 1 | 0.85102614 | 145.209 | 0.94778 | 0.009 | 0.036 |
| SD-MU vs GF-HD | 1 | 0.60016343 | 44.6094 | 0.84794 | 0.01 | 0.036 |
| SD-MU vs GF-SD | 1 | 0.04216041 | 7.22814 | 0.47466 | 0.025 | 0.05 |
| GF-HD vs GF-SD | 1 | 0.80346156 | 77.2123 | 0.90612 | 0.006 | 0.036 |

Table 3.10. Pairwise Comparisons between HD-MU, SD-MU, GF-HD and GF-SD at maturity.

| Pairwise Comparisons (Fig 6) | Df | SumsOfSqs | F.Model | R ² | p.value | p.adjusted |
|------------------------------|----|------------|---------|----------------|---------|------------|
| HD-MU vs SD-MU | 1 | 0.6697639 | 75.1818 | 0.90383 | 0.008 | 0.042 |
| HD-MU vs SD-HD | 1 | 0.65275048 | 121.124 | 0.93804 | 0.01 | 0.042 |
| HD-MU vs HD-SD | 1 | 0.73805715 | 129.478 | 0.94181 | 0.007 | 0.042 |
| SD-MU vs SD-HD | 1 | 0.04171867 | 7.78155 | 0.49308 | 0.016 | 0.042 |
| SD-MU vs HD-SD | 1 | 0.03359757 | 5.92303 | 0.42541 | 0.016 | 0.042 |
| SD-HD vs HD-SD | 1 | 0.01094012 | 5.08158 | 0.38845 | 0.011 | 0.042 |

Table 3.11. Pairwise Comparisons between HD-MU, SD-MU, SD-HD and HD-SD at maturity.

| Variable | Df | SumOfSqs | R ² | F | Pr(>F) | sig |
|----------------------------|----|------------|----------------|---------|--------|-----|
| Birth Dam | 1 | 0.29363812 | 0.25272 | 53.092 | 0.001 | * |
| Cross-Foster Dam | 1 | 0.39270992 | 0.33799 | 71.0049 | 0.001 | * |
| Birth Dam:Cross-Foster Dam | 1 | 0.3870659 | 0.33313 | 69.9844 | 0.001 | * |
| Residual | 16 | 0.08849188 | 0.07616 | NA | NA | |
| Total | 19 | 1.16190582 | 1 | NA | NA | |

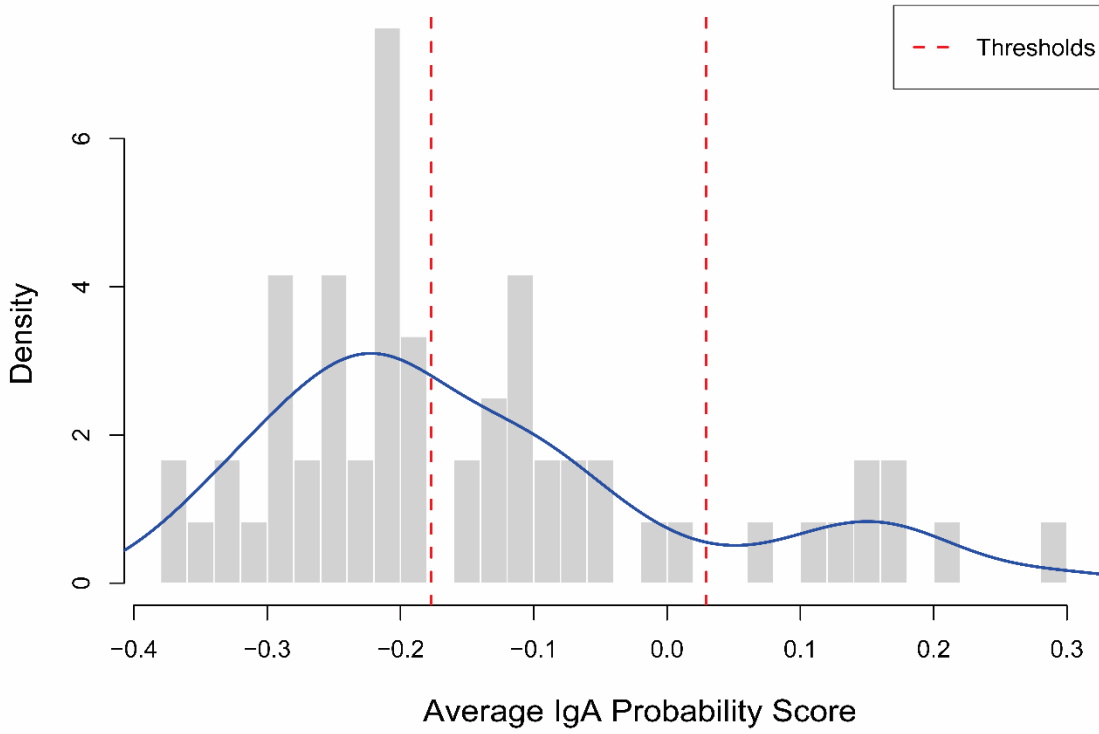
Table 3.12. PERMANOVA Analysis - In utero vs Postnatal Cross-Fostering Groups HD-MU and SD-MU, HD-SD. SD-HD

Appendix B: Chapter 4 Supplemental Information

This section provides additional details on the analyses performed in Chapter 4, including histograms of Gaussian mixture models applied to IgA Probability Score data to establish cutoff thresholds for identifying highly targeted and non-targeted microbes.

A.

Gaussian Mixture Model Fit For HD – Fecal BugFACs



B.

Gaussian Mixture Model Fit For HD – SI BugFACs

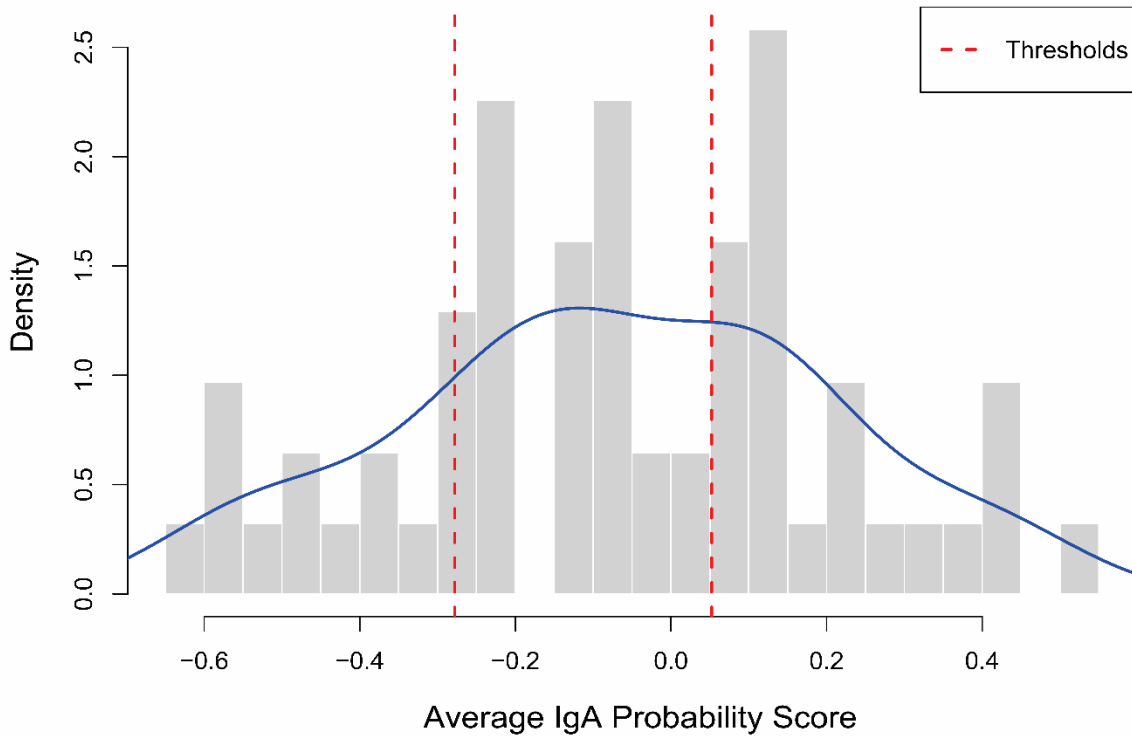
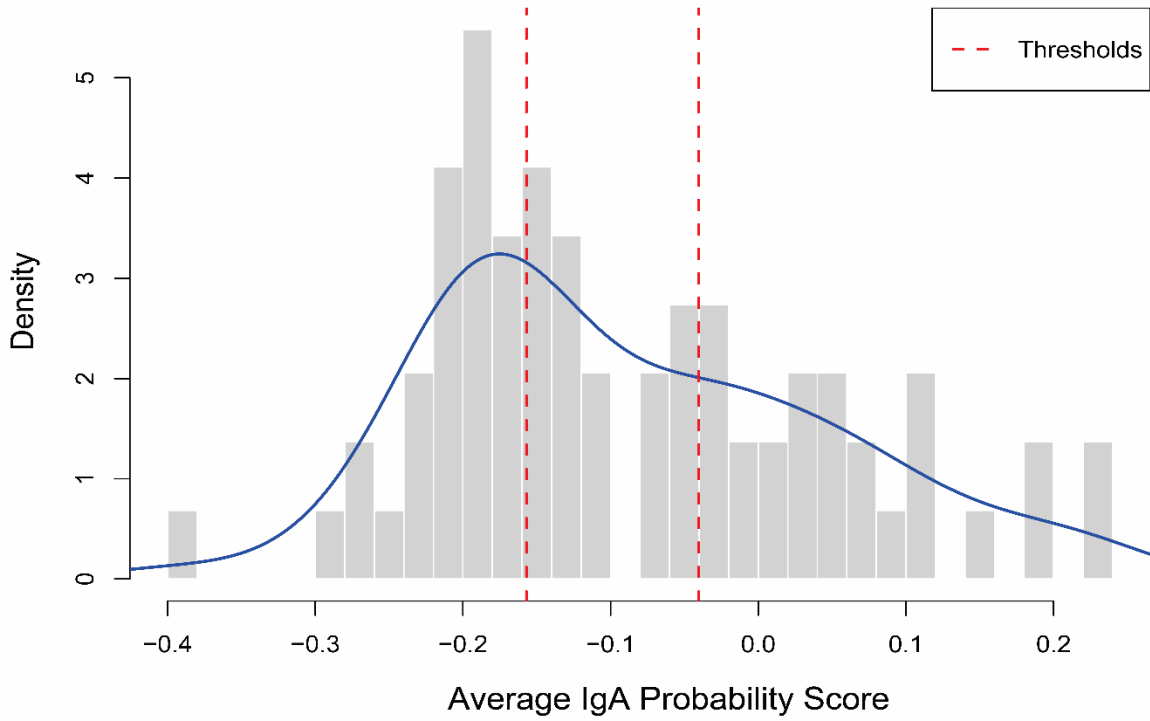


Figure 4.1B. Gaussian mixture model analysis for IgA Probability Ratio Scores in HD animals. (A) Histogram of the average IgA Probability Ratio Scores for each taxon identified in the feces and **(B)** small intestine (SI) contents of HD-MU animals at 8 weeks of age. The threshold for microbes highly likely to be targeted by IgA in the feces of HD-MU animals was ≥ 0.0076 , while the threshold for non-targeted microbes was ≤ -0.2014 . The threshold for microbes highly likely to be targeted by IgA in the small intestine of HD-MU animals was ≥ 0.1513 while the threshold for non-targeted microbes was ≤ -0.2506 . **(A-B)** $n=5/\text{group}$ [3 females and 2 males].

A.

Gaussian Mixture Model Fit For SD – Fecal BugFACs



B.

Gaussian Mixture Model Fit For SD – SI BugFACs

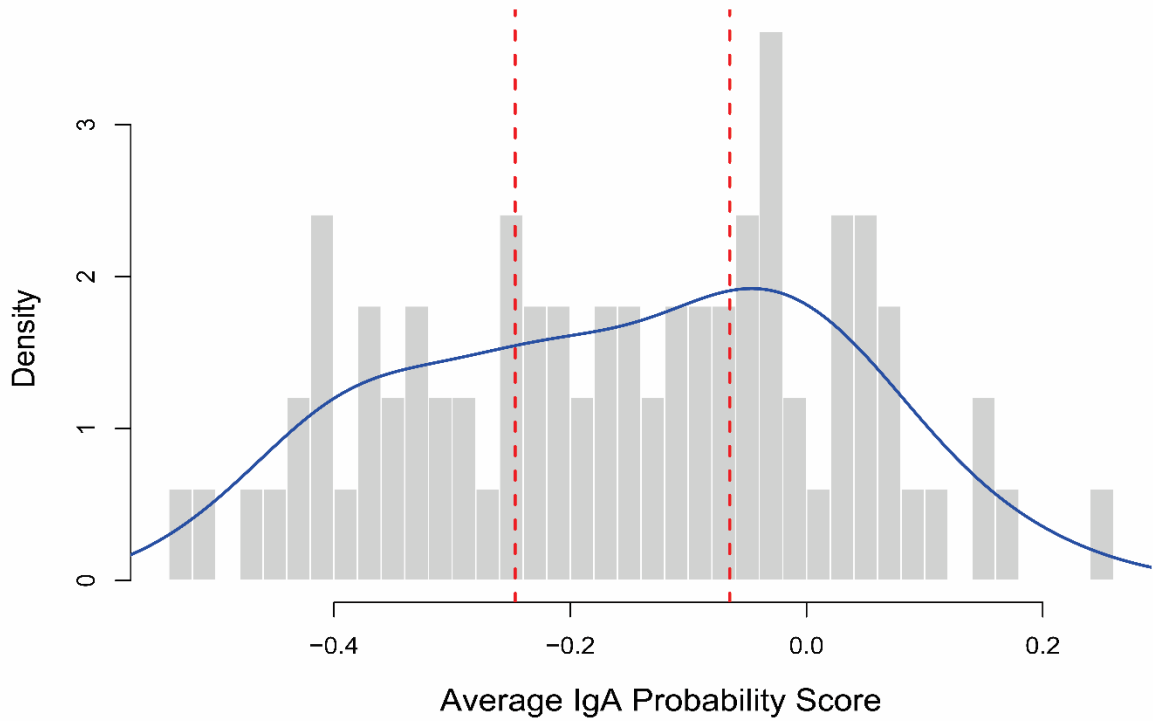


Figure 4.2B. Gaussian mixture model analysis for IgA Probability Ratio Scores in SD animals. (A) Histogram of the average IgA Probability Ratio Scores for each taxon identified in the feces and **(B)** small intestine (SI) contents of SD-MU animals at 8 weeks of age. The threshold for microbes highly likely to be targeted by IgA in the feces of SD-MU animals was ≥ 0.0072 , while the threshold for non-targeted microbes was ≤ -0.2907 . The threshold for microbes highly likely to be targeted by IgA in the small intestine of SD-MU animals was ≥ 0.1071 while the threshold for non-targeted microbes was ≤ -0.2061 . **(A-B)** $n=5/\text{group}$ [3 females and 2 males].

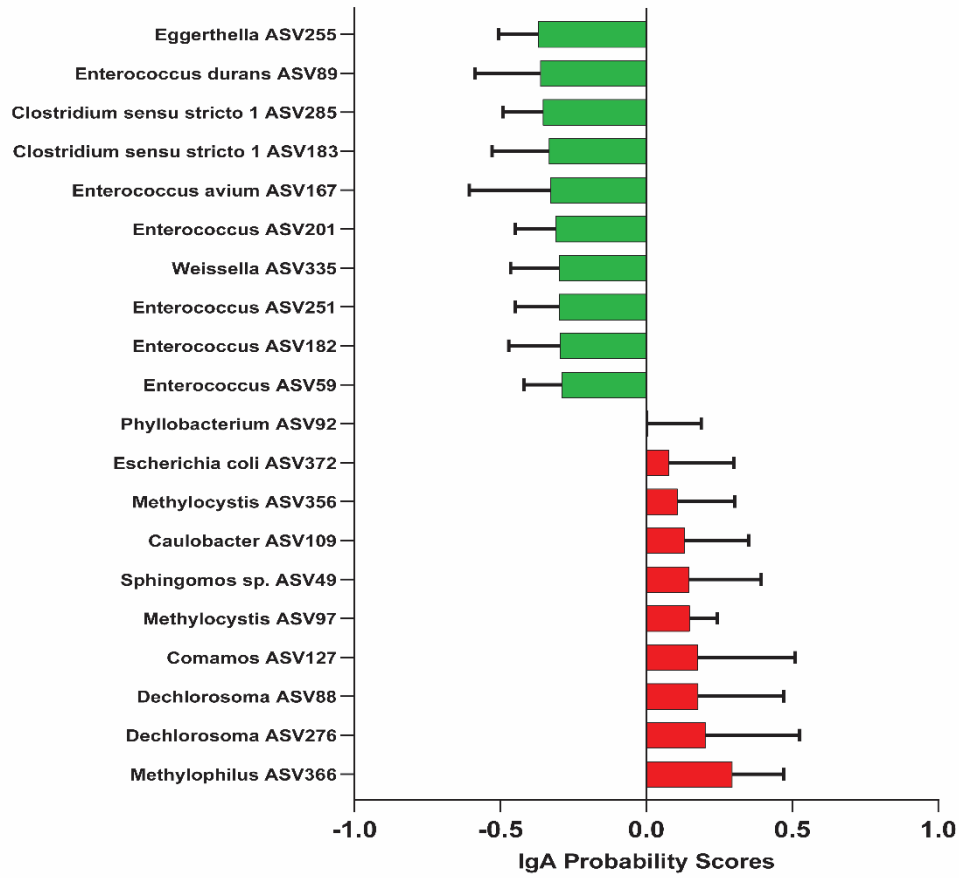
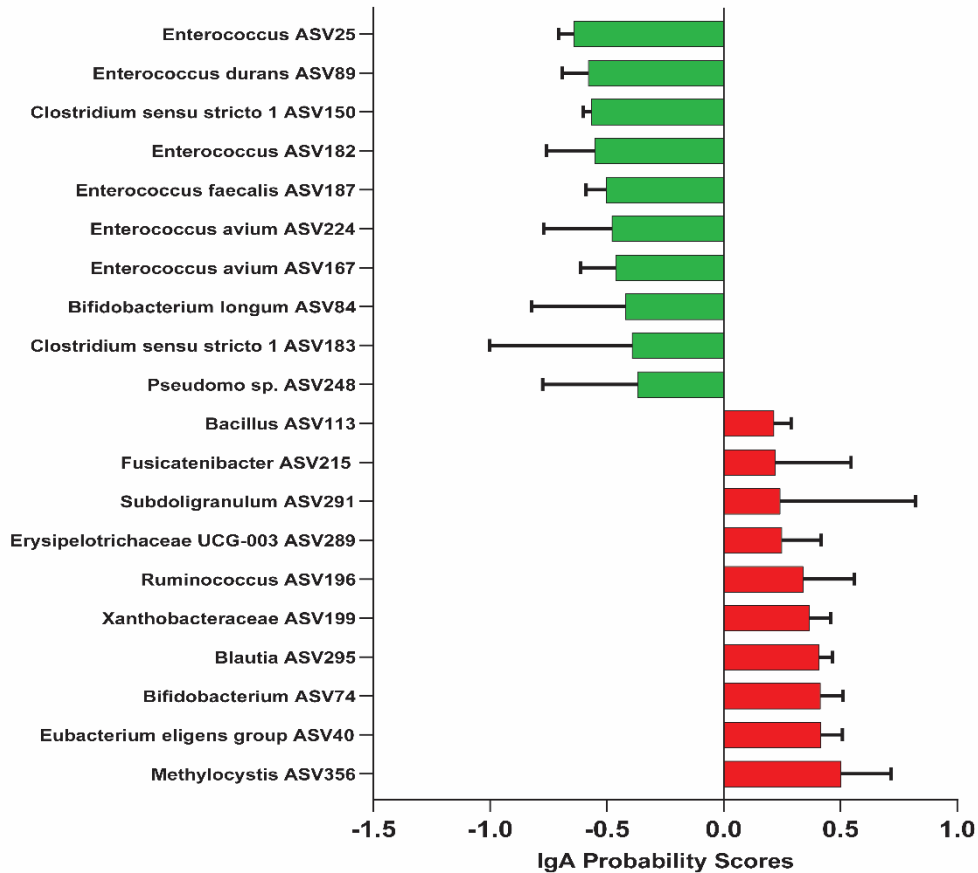
A.**Feces****B.****Small Intestine**

Figure 4.3B. HD-MU animals have an increased likelihood of having *Escherichia coli* sp. targeted by IgA in both feces and small intestine. (A) IgA Probability Ratio Score for fecal and (B) intestinal microbes from HD-MU at 8 weeks of age. (A-B) Each bar represents the average IgA Probability Ratio Score calculated for a microbial taxon that had a score in at least three animals. (A-B) n=5/group [3 females and 2 males].